Electron Transport in Confined Structures in Very High Mobility GaAs in Perpendicular Magnetic Fields

by

Iuliana Radu

MSc. in Physics, University of Bucharest, 2000

Submitted to the Department of Physics
in partial fulfillment of the requirements for the degree of

Doctor of Philosophy

at the

MASSACHUSETTS INSTITUTE OF TECHNOLOGY

February 2009

Author .....
Department of Physics
January 5, 2009

Certified by .....
Marc A. Kastner
Donner Professor of Physics and Dean of the School of Science
Thesis Supervisor

Accepted by .....
Thomas J. Greytak
Professor and Associate Department Head for Education

Electron Transport in Confined Structures in Very High Mobility GaAs in Perpendicular Magnetic Fields

by

Iuliana Radu

Submitted to the Department of Physics
on January 5, 2009, in partial fulfillment of the
requirements for the degree of
Doctor of Philosophy

Abstract

In this thesis we study properties of two-dimensional electron transport through constrictions in perpendicular magnetic fields. We present two sets of experiments, one focusing on properties in the integer quantum Hall effect the second looking at properties in the fractional quantum Hall effect at filling fraction $\nu = 5/2$. Both sets of experiments employ electrostatically defined quantum point contacts (QPCs) fabricated on a high mobility GaAs/AlGaAs two-dimensional electron gas (2DEG).

In the first set of experiments, we study the suppression of the spin splitting of the Landau levels in QPCs compared to the bulk 2DEG. By using QPCs with different lithographic widths and varying the voltage applied on the gates, we can control the width of the conduction channel from ~3000 to ~100 nm. The width of the channel is estimated from the low magnetic field dependence of the conductance through the QPC. We study the suppression of the spin-splitting of the Landau levels as a function of the effective width of the QPC and measure the number of channels of conduction N_S, above which the spin-splitting is no longer observed. We find that N_S is approximately half of the number of quantized channels in the QPC for all widths less than approximately 1200 nm. For the same width range, we show that the cyclotron diameter at the lowest magnetic field where the spin splitting is resolved is half of the effective width of the QPC.

In the second set of experiments, in the fractional quantum Hall regime at $\nu = 5/2$, QPCs are used to bring counter-propagating edge states close enough that quasiparticles can tunnel between them. Weak quasiparticle tunneling has been long proposed as a method to study the properties of these quasiparticles, because the tunneling conductance depends on both the charge of the tunneling quasiparticles and the modified Coulomb interaction that characterizes their interactions. Several models have been proposed to describe the state at $\nu = 5/2$; some predict non-abelian statistics, while others predict the more mundane abelian properties. Although all models predict the same quasiparticle charge $e^* = 1/4$, they predict different values of the interaction parameter, thus allowing us to potentially discriminate between them. We study the temperature and dc bias dependence of the tunneling conductance, while preserving

the same filling fraction in the constriction and the bulk of the sample. The data show scaling of the bias-dependent tunneling over a range of temperatures, in agreement with the theory of weak quasiparticle tunneling, allowing us to extract values for the effective charge and interaction parameter of the quasiparticles. The ranges of values obtained are consistent with those predicted by the anti-Pfaffian and the $U(1) \times SU_2(2)$ models, making these non-abelian states more likely than abelian ones.

Thesis Supervisor: Marc A. Kastner
Title: Donner Professor of Physics and Dean of the School of Science

Acknowledgments

I have to admit that I probably have never read anybody's thesis from cover to cover, but I always read the acknowledgements. They tell the story behind the research and in many instances the story of the person writing the thesis. In my case, these acknowledgments reflect the tortuous path I took to get here. I started my PhD in Seattle at University of Washington and only later moved to MIT. Many great people have touched my life in both places, and I wish to mention a few of them.

First and foremost my gratitude goes to my PhD adviser, Marc Kastner. He took me in his group in a time of trial and trouble in my life and gave me courage to believe in myself. Marc says that the only thing he is good at is to find good people and delegate. He is certainly far too modest, but people working with him or for him enjoy a lot of freedom in solving problems and in many a case even finding problems worth solving. Marc gave me freedom to explore and that in turn gave me confidence in my capabilities as a researcher. I have enjoyed talking physics with him because Marc has a deep understanding of all phenomena and always challenged me to think in simple terms and try to explain even the most esoteric of phenomena in a simple way. The summer he spent in his research office, while his office in the Physics Headquarters was being renovated, was the most enjoyable time in my stay at any university. And during those months I learned more physics and how to think of physics than in the many years before. Marc's enthusiasm about physics research kept us all going and his keen insight and good eye for finding the interesting bit in gigabytes of boring data has kept us on the right track.

Before coming to MIT, while at University of Washington, I was fortunate enough to meet Dr. Yael Hanein, dear friend and mentor. She helped me become an experimentalist and taught me a great deal about cryogenics, how to fab, and how to do so many things that I cannot possibly list all off them here. At times, she had more confidence in me than I had myself. When I went through the biggest slump in my life, she encouraged me to pursue my dream and helped me achieve it. This took me to MIT in Marc Kastner's group. She is also a good friend and together with

her partner Gabi Steinhardt and my husband Andreas we have spend many holidays together and visited many islands around Seattle.

While at MIT, I had the chance to interact with many interesting and smart people. I am indebted to the other two members of my thesis committee: Ray Ashoori and Xiao-Gang Wen. Ray and I had many interesting conversations, many of them about physics and recently about babies, as his son is only a few months older than mine. I have enjoyed them all! Xiao-Gang is not only a member of my thesis committee but is also the main theorist with whom I have collaborated over the course of my PhD. He gave us great physical insight into complicated theoretical issues. Together with his graduate student Bas Overbosch and his former student Claudio Chamon, professor at Boston University, we have spent many hours hunched over data. Bas not only offered me my first introduction to non-abelian anyons, but has also prepared for me many theoretical models with which to fit our data. He is also a trusted friend. Claudio has the ability to explain in very simple words the most complicated oh theories and it was pleasure to discuss physics with him.

Marc Kastner has a knack for attracting not only very bright but also very friendly people in his group, who collaborate with and help each other. Sami Amasha is one of the most dedicated physicists I know. He is also very generous with his time and help, so generous that many times I worried that he helped me in detriment of his sleep. We have spend many long hours in the lab together while I was doing temperature dependence measurements and he was tuning his stubborn dot. I have enjoyed our heated physics discussions and our careful liquid helium planning and I miss our helium transfer conversations. He taught me many things in the lab and also many outside, for example how to appreciate American football. I miss his Superbowl parties and I miss his friendship. Sami was also brave enough to eat our first attempts at a traditional Thanksgiving meal with turkey cooked by a vegetarian. Ghislain Granger was the senior graduate student on the project as I started in the Kastner Lab. He took me under his wing and showed me many things about the dilution refrigerator. His attention to detail was unparalleled and he taught me how to be patient when running an experiment. Tamar Mentzel and I shared an office for

a few years and we became good friends. One of the few women studying for a PhD in physics, Tamar was the person to go and chat with when trying to figure "things American" and my resource for Judaica. We also shared the many ups and downs of grad school. Tamar is very excited about physics and I admire her determination to get her project working. Kenny Maclean used to work together with Sami on real time charge detection experiment for which I had provided the samples. He is always glad to lend a hand when needed and it was interesting talking physics with him as he always surprises me with his very insightful understanding of phenomena. I am sure his project with Tamar will give great results. Ian Gelfand kept us all entertained with his fabulous stories, many of which have been, surprisingly, corroborated by other people. He is the clean-room wizard in residence and as I was making samples a great source for very detailed clean-room advice. Colin Dillard joined our lab as an undergraduate student and worked to set-up the current measurement system. After a short experience at Harvard, he decided to come back here for his PhD and is currently taking over the project I was working on. It is great fun to work with Colin and it was interesting to see him grow into the very good experimentalist he is now. I am sure that he will get many interesting results out of the project. I have enjoyed getting to know Jingshi Hu, Laurie Calvet, Maria Schriver, Dirk Weiss, Andreai Kogan, Fumiaki Toyama, Kaiwing Fung and Sophie Charpentier.

Last but certainly not least of the Kastner group, I would like to acknowledge Dominik Zumbuhl. He started as a postdoc in the lab at the same time I started as a graduate student and we worked on the same project. Everything that Dominik works on comes out great, just enforcing my stereotype about the Swiss. He taught me many things, ranging from very neat soldering and GaAs processing, to Igor programming and dot tuning. He always challenged me to do things better in the lab and in my presentations. I am grateful for learning from him. Through Dominik, or maybe because of Dominik, the collaboration with Charlie Marcus and his group started and brought me on-board the most interesting project: looking for non-abelian statistics signatures at the 5/2 fractional quantum Hall effect state. The original owner of this project was Jeff Miller who needed a great short last project for the end of his PhD.

It turns out that the project is still going four years later, but it has produced many interesting results along the way. Jeff is probably the person with whom I have spent the most time working. First of all, Jeff is a funny guy and that makes working with him really pleasant and never boring. Jeff not only excels in physics but also has many other talents: he is great at writing and photography, and really good at making illustration. His great aesthetic sense shows in the figures of the articles we have published together. And when it comes to writing, he has taught me to not use too fancy words (such as evince) in my papers. Jeff is full of energy: he does not mind transferring helium in the small hours of the morning or doing temperature dependence until late in the night, all this with a small baby. Jeff and his wife Manjari became good friends and gave me and Andreas a crash course in parenting and caring for baby. Their wonderful baby Neer, a big and very tall boy now, made me realize that I wanted a baby of my own. Jeff, thank you for a few great years working with you!

Charlie Marcus has an enormous amount of energy and a sheer joy for physics. He is great at finding very interesting projects and bringing together the people that would make those projects work. He welcomed me in his lab in the summer of 2008 when the experiment at MIT stopped working and we were waiting for a replacement dewar. I found his comments on my writing and presentations to be very helpful. From the Marcus lab, I have also collaborated with Eli Levenson-Falk a very bright and hard-working undergraduate. I am sure great things are ahead of him. I have also enjoyed talking physics and learning many new things from Doug McClure, Yiming Zhang, Ferdinand Kuemeth, Jimmy Williams and Alex Johnson from the Marcus lab.

The search for non-abelian statistics has brought me in touch with many great scientists. I am grateful to Loren Pfeiffer for providing the heterostructure on which Jeff made the samples used in the experiments presented in this thesis. Loren has helped me understand some of the materials science behind the heterostructure and I have enjoyed our conversations about tree planting and politics. I have also enjoyed learning physics from and having many conversations with some of the greatest theorists: Bert Halperin, Bernd Rosenow, and Michael Levin from Harvard, Ady Stern

from Weizmann Institute in Israel, Steve Simon from Bell Labs, Nick Read from Yale, Michael Freedman from Microsoft, Matthew Fisher from UCSB, Chetan Nayak and his student Waheb Bishara from Station Q of Microsoft/UCSB, Alexei Kitaev from Caltech, Shankar Das Sarma from University of Maryland, Ed Rezayi from California State, Vito Scarola at University of Maryland at the time, and many others. Bernd Rosenow also became our good friend, being a European ex-pat just like my husband and me. Michael Levin is also one of our friends and we spent together many Fourth of July celebrations and many Superbowls. I have also benefited from discussions with some great experimentalists: Horst Stomer from Columbia, Jim Eisenstein from Caltech, Moty Heiblum from Weizmann, Amir Yacoby from Harvard and Weizmann. Their questions and insights helped me better understand our experiment. I am also grateful to David Goldhaber Gordon for introducing me to Marc Kastner and suggesting that I consider MIT for grad school. I have enjoyed discussing physics with him.

While at MIT, I have benefited a lot from the camaraderie and friendship, and many times good food, from the Women in Physics. This group has a great tradition of reciprocal support through the tough times of a PhD and in many instances of childbearing and childcare while in graduate school. I am especially grateful to Bonna Newman who has invested an incredible amount of time in creating a spirit of community in the Physics department.

Jei Lee Freeman, Jessica Landry, Dianne Brooks and Susan Rosevear, the ladies down the hall, have given me clerical support for various things around CMSE but most importantly, they have given me their friendship. Thank you for your encouragements and for all the great advice on child rearing. You made my life at MIT a much more pleasurable and down to earth experience. John Jordan from Airgas, Paul and Don from Cryolab found liquid helium for my experiments even though the whole world was going through a severe shortage. They delivered the 300 liters needed every week for my experiment to run and cheered me up when things were slumping. On the administrative side, Heather Williams has ensured that everything runs smoothly, efficiently and that we would get everything we needed for our re-

search. Also on the administrative side, I would like to acknowledge Gil Cordova, Brian Canavan, Sean Robinson, Jacqueline Blair Carota, Claudia LaBollita-James, Crystal Young, Ed Kruzel, and Gretchen Poehlman and thank them for their kind support. While doing sample processing in the MIT clean-rooms I have learned a lot from Vicky Diadiuk, Kurt Broderick, Mark Mondol, and Ariel Nava.

My life while at MIT was made more pleasant by having great friends, many of which I have met through Sami. I will miss spending Fourth of July watching the fireworks with Peter Bermel, Cody Nave and his wife Kathy, Neville Sanjana, Bas Overbosch and his lovely wife Elske, Michael Levin and for my first year in Boston also Ghislain. My friend Claudiu Stan, whom I had know for many years, well before coming to MIT or even knowing that I want a PhD in physics, has provided wonderful insight into all things MIT and life in the USA.

To my parents, Ioana and Paul Prvulescu, for their constant support, love and confidence in me, thank you. For helping me follow my dream and becoming who I am today, thank you. There are not enough words to describe my gratitude for you coming here and taking care and loving Alex while I was busy writing this thesis. My son Alex was and is a constant source of joy and delight since learning that I am pregnant a year ago. Your birth was the most humbling and exhilarating experience in my live. Having you puts things in perspective and keeps me grounded. You have even helped with some of the computer work and I am sure you would have loved to help more.

Coming to the US was the best decision of my life and it seems that I am getting a PhD. But most importantly, I have found here my beloved husband, partner and friend Andreas Klust. We both had to travel half-way around the world to find each other. Having you in my life fills it with joy and warmth. You helped me in so many ways and I am grateful for so many things! I am grateful for all those days when you came to my lab and stayed with me while I was working, such that we can still spend some time together that day. I am grateful for all those midnight helium transfers you helped me with and for coming with me to MIT to check on the experiment at the oddest hours. I am grateful for cooking all that great food and making sure that

I ate sensibly even when I was too stressed out to care about it myself. Thank you for your constant love and support. Thank you for all the things I don't remember right now to thank you for. I look forward to many more years together with you!

Contents

1 Introduction **19**

2 Brief theoretical overview of quasiparticle tunneling at $\nu = 5/2$ **25**

2.1 Classical Hall effect 26

2.2 Integral quantum Hall effect 26

2.3 Fractional quantum Hall effect 28

2.4 The fractional quantum Hall state at $\nu = 5/2$ 31

2.5 Anyons 33

2.6 Quasiparticle tunneling in the fractional quantum Hall effect 34

2.7 Relating the tunneling conductance to directly measurable quantities 39

2.8 Energy scales in a magnetic field 41

2.9 Summary 42

3 Suppression of Spin Splitting in Narrow Channels **43**

3.1 Introduction 43

3.2 Sample 45

3.3 Measurement details 46

3.4 Width estimates 49

3.4.1 Sharvin Formula 50

3.4.2 Square-well potential with perpendicular magnetic field 51

3.4.3 Parabolic potential with perpendicular magnetic field 52

3.5 Evaluating 2D electron density in the QPC 55

3.6 Experimental data and discussion 57

3.7 Discussion and conclusions 63

4 Quasiparticle Tunneling in the Fractional Quantum Hall Effect at $\nu = 5/2$ — experimental **67**

4.1 Introduction 67

4.2 Sample 69

4.3 Measurement details 70

4.4 Annealing 71

4.5 Bias and temperature dependence 72

4.6 Extracting g and e* 77

4.7 Strong tunneling 82

4.8 Conclusions 85

5 Estimating Electron Temperature **87**

5.1 Coulomb blockade as electron thermometer 88

5.2 Estimating temperature using the Hall effect 93

5.3 Conclusion 96

A Fabrication of lateral quantum dots on GaAs **97**

A.1 Mesa Isolation 98

A.2 Ohmic Contacts 99

A.2.1 Traditional Recipe 99

A.2.2 E-beam writer recipe 100

A.3 Small Gates 101

A.4 Large Gates 102

A.4.1 Traditional Recipe 103

A.4.2 E-beam writer recipe 103

List of Figures

2-1 Schematic of the tunneling current in the weak tunneling picture. . . 36

2-2 Schematic of the tunneling current in the strong tunneling picture. . . 38

2-3 Schematic of the currents in the weak tunneling regime in a single drain measurement set-up. 40

3-1 Optical and SEM images of the devices 45

3-2 Sketch of a Hall bar with a QPC: edge states in the bulk and QPC . 46

3-3 Sketch of a Hall bar with a QPC illustrating 4-terminal measurements 47

3-4 Comparison of fits to the longitudinal resistance vs magnetic field for several confining potential models 53

3-5 Comparison of conduction channel widths at several gate voltages, and for several lithographic QPCs 54

3-6 Magnetic field dependence of the diagonal resistance from QPC of various lithographic width 56

3-7 Diagonal conductance vs. magnetic field for the 300 nm QPC at various gate voltages 58

3-8 Diagonal conductance vs. magnetic field for the 200 nm QPC at various gate voltages 60

3-9 Number of spin-split Landau levels vs width and vs. the total number of Landau levels 61

3-10 B_{spin} vs. width and the cyclotron diameter at B_{spin} vs width 62

4-1 SEM images of the devices used 70

4-2 Magnetic field dependance of R_D and R_{xy} illustrating "annealing" . . 72

4-3 Differential tunneling conductance as a function of magnetic field and dc bias at several temperatures 73
4-4 Differential tunneling conductance as a function of gate voltage and dc bias at several temperatures 75
4-5 Weak tunneling 76
4-6 Fits to the weak tunneling data: best fit, fit with the K8 state, fit with the Pfaffian 78
4-7 Fits to the weak tunneling data: fit with the 331 state, fit with the anti-Pfaffian, fit with the composite fermion model 80
4-8 Map of the fit quality 81
4-9 Strong tunneling 83
4-10 Best fit to the strong tunneling data 85

5-1 Coulomb blockade peak used to determine electron temperature . . . 90
5-2 No dc bias applied 91
5-3 Conversion of gate voltage into energy 92
5-4 R_{xx} as a function of magnetic field around $\nu = 3$ at several mixing chamber temperatures 93
5-5 Temperature dependence of the position in magnetic field of the $\nu = 3$ gap corner 94
5-6 Temperature dependence of the peak height in R_{xx} around $\nu = 3$ . . . 95

A-1 SEM micrograph of small gates 102

List of Tables

3.1 Estimates of the conductance channel width 54

Chapter 1

Introduction

The quantum Hall effect has proven to be a very fertile ground for physics research, and the discovery of its two forms, the integer [88] and the fractional quantum Hall effects [87], has brought two Nobel prizes. Of the fractional states, the one at filling fraction $\nu = 5/2$ has attracted much interest from theoretical physicists because it holds promise to have excitations that are non-abelian. In most cases, when we interchange the position of two identical quantum particles, the interchange only modifies the phase of the wavefunction. This normal behavior is called "abelian". However, in the case of non-abelian particles, the interchange can modify their nature in more profound ways. The publication in 2005-2007 [18, 80, 11, 36, 24] of a series of articles proposing a scheme of how to experimentally probe the non-abelian nature of these particles has broadened the interest in the $\nu = 5/2$ state, and several groups of experimental physicists have embarked on the quest to find evidence for non-abelian particles. The possibility of finding non-abelian particles is interesting in itself from a physicist's standpoint. However, discovering them could also make possible the most arcane form of quantum computing, topological quantum computing [46]. Our group, in collaboration with the Marcus group at Harvard, has been investigating the state at $\nu = 5/2$ since 2005, when nothing was known about its behavior in confined structures. Although we have not proven that the state has non-abelian particles, we have found evidence suggesting that this might be the case and a few other interesting things along the way.

We have started our quest by investigating how the 5/2 state can be preserved in confined structures, structures needed to probe the non-abelian nature of the state. We have found that confinement reduces the energy gap of the state (and the likelihood that the state is preserved in the structure) in a non-trivial fashion [56]. While trying to understand how confinement affects the 5/2 state, we started investigating how confinement affects other states as well. In particular, we studied how it suppresses the spin-splitting of the Landau levels in the integer quantum Hall effect, a study which we present in Chapter 3. Although, apparently, a different system altogether, the spin-splitting of the Landau levels is a result of many-body physics, as is the stability of the 5/2 state. Having understood how to preserve the 5/2 state in confined structures we have performed quasiparticle tunneling experiments, which, short of directly probing their non-abelian nature, have forced them to reveal their properties.

In physics, most single-particle properties have been investigated and understood already, so the challenge lies in understanding many-particle properties. Phil Anderson said in 1972 that "More is different!" [3] and he was right. When many particles come together and interact the result is not a simple sum of the parts and the fractional quantum Hall effect is a brilliant example of why this is the case. In this effect, the electrons in a two-dimensional sea come together and create quasiparticles with effective charge e^* which is just a fraction of the electron charge. Intuitively, when several items are put together they form a bigger item not a smaller one. However, finding this smaller object happens every time at low enough temperatures (in a dilution refrigerator), at high enough magnetic field and in clean enough samples.

Indeed, one very important ingredient in these experiments is the very special material used as a sample. This material is a layered structure of two semiconductors (GaAs and AlGaAs). A two-dimensional electron gas (2DEG) forms at the interface between these two materials, where the electrons are confined to this interface but virtually free to move in the plane of this interface. For the experiment to work, a very clean and smooth interface is needed, such that the electrons can move for very large distances virtually unperturbed. Loren Pfeiffer and Ken West are crystal

growers at Alcatel-Lucent Bell Labs. They specialize in the growth of this material with a very smooth and clean interface, the best quality material in the world.

Among the very strange and special states in the fractional quantum Hall effect the one at $\nu = 5/2$ is quite unique. It is one of the few, maybe even the only one (although the jury is still out on this question), that forms at a fraction with an even denominator. For this reason, standard models designed for odd-denominator fractional states cannot describe it. Instead, several other models have been proposed, some with abelian and some with non-abelian statistics. All models predict the same effective charge, but they predict different values of the interaction strength. Based on a theory developed originally by X. G. Wen [95], we have designed an experiment that probes the effective quasiparticle charge and the strength of interaction between these quasiparticles, g.

We start with a very clean semiconductor sample with the 2D electron system at the interface between the GaAs and AlGaAs layer. We place the sample in a high enough magnetic field that the filling fraction 5/2 is achieved and cool it to very low temperatures, only a few hundredths of a degree above absolute zero. By applying a negative voltage to metallic gate electrodes on top of the sample, the electrons in the 2D system are repelled from the region immediately under the gates. This results in a constriction in the 2DEG, called a quantum point contact (QPC), with a voltage controllable size. To probe the sample we pass a very small current through it. Because of the magnetic field, the current will flow mostly close to the edges of the sample. The constriction forces the quasiparticles to reveal themselves by tunneling in the region of the constriction from one edge to the opposite one. This tunneling process is the strongest at the lowest temperature and lowest currents. It also shows clear signatures which help us determine the values of e^* and g. Based on these values, we find that the theoretical models most consistent with the experimental data are the ones with non-abelian quasiparticles.

This experiment is the first one to probe the parameters that characterize the state at filling fraction 5/2 and to show control over the tunneling process. The most interesting conclusion is that we find indirect evidence for non-abelian states.

However, to prove beyond doubt that this is the case, further experiments are needed. These experiments would involve two constrictions, similar to the single one used in this experiment, creating a device that would reveal interference of the quasiparticles.

This thesis is organized as follows. In Chapter 2 we introduce the Hall effect, focusing on the fractional quantum Hall effect. In this context, we explain the concepts of edge states, of composite fermions and of anyons. Our presentation of the fractional quantum Hall effect leads to the introduction of the $\nu = 5/2$ state and the models proposed to describe it. One of the methods that helps experimentally discriminate between these models is the weak quasiparticle tunneling. We discuss the theory behind this method and how the tunneling conductance depends on temperature and dc bias. We derive how the tunneling conductance can be determined from two directly measurable resistances. Finally we provide some numbers for the energy scales in the quantum Hall effect.

In Chapter 3 we investigate the suppression of spin splitting of the Landau levels in QPCs relative to the bulk 2DEG. We present transport measurements in a perpendicular magnetic field through QPCs of various lithographic widths and various gate voltages. We discuss several techniques to estimate the effective width of the conduction channel in these QPCs, and apply them to our measurements. By varying the applied gate voltage we can control the width of the conduction channel continuously from $\sim$ 3000 nm to $\sim$ 100 nm. We use this capability to measure the number of the spin-split Landau levels as a function of conduction channel width. We find that the lowest magnetic field where the spin splitting is still resolved gives a cyclotron diameter equal to half the width of the conduction channel. In this Chapter, we also include a description of the measurement set-up used in all experiments presented in this thesis and of the quantities measured.

In Chapter 4 we present experimental studies of quasiparticle tunneling at $\nu = 5/2$, in which approximately the same filling fraction is maintained in the QPC and the bulk of the sample. Maintaining the same filling fraction is a prerequisite for preserving the edge states through the QPC. We outline the method used to maintain the same filling fraction and the steps taken to insure that the same edge state is present

in both QPC and the bulk of the sample. We study the dc bias and temperature dependence of the tunneling data and find that the data from various temperatures can be collapsed onto a single curve, in agreement with the theory for weak tunneling [95, 10, 26]. In the framework of weak tunneling theory we extract an effective quasiparticle charge e^* and an interaction parameter g, and, based on the value of g, we observe that two non-abelian states, the anti-Pfaffian [51, 52] and the $U(1)\times SU_2(2)$ [92] are most consistent with our data.

In Chapter 5 we measure the electron temperature in our system. We measure electron temperature using Coulomb blockade peaks in laterally gated quantum dots, and use this temperature to place a upper bound on electron temperature in our quantum Hall measurements. Since the samples in the quantum Hall regime have significantly lower resistance than the quantum dot samples, we expect that the electron temperature in this case will also be lower. However, there are no absolute thermometers in the quantum Hall regime. For this reason, we empirically estimate the electron temperature by tracking the temperature dependence of two quantum Hall features and find values which are lower than those measured in the Coulomb blockade regime.

The Appendix provides information about sample fabrication. Since the largest part of this recipe has been handed down through several generations of graduate students, we only outline the steps we have used without much explanation, and rather focus on the innovative part of the recipe, the fabrication of very narrow gates.

Chapter 2

Brief theoretical overview of quasiparticle tunneling at $\nu = 5/2$

In this chapter we outline the concepts used in the interpretation of the experiments presented in the later chapters. We start by introducing the Hall effect, the classical and both realizations of the quantum effect, integer and fractional. We introduce the concepts of composite fermion and anyon and provide a brief overview of abelian and non-abelian anyons. Our presentation of the fractional quantum Hall effect (FQHE) is geared towards the introduction of the $\nu = 5/2$ state. We survey some of the proposed models to describe this state and review previous experiments characterizing it. Next we introduce the weak quasiparticle tunneling between edges as a means of investigating the properties of FQHE states in general, and the one at $\nu = 5/2$, in particular.

For excellent books on the quantum Hall effect, both integer and fractional, see, for example, Refs. [16], [68] and [76]. For an experimentalist's view of the Hall effect see the absolutely wonderful Nobel lecture given by Horst Stormer [82]. For an introduction to non-abelian anyons and their proposed application—topological quantum computing—see Nayak *et. al.* in [63]. A beautiful pedagogical review of anyons in the quantum Hall effect can be found in Ref. [79].

2.1 Classical Hall effect

E. Hall, while a graduate student, discovered what we refer to now as the classical Hall effect in 1879 in a sheet of gold. He observed that by placing the gold leaf in a perpendicular magnetic field and passing a current through it he could measure a voltage perpendicular to the direction of the current. This is called now a Hall voltage and it can be explained entirely using classical electrodynamics. When the electrons in the sample move in a perpendicular magnetic field B, the Lorentz force pulls them perpendicular to the direction of the motion and that of the magnetic field. This gives rises to charge accumulation on one side of the sample and hence a voltage drop perpendicular to the direction of the current. It can be shown that the Hall resistance—the resistance associated with this perpendicular voltage drop—is $R_{xy} = eB/n$ where e is the electron charge and n is the sheet density of the charge carriers in the sample. If the sample is 3-dimensional, then n is the carrier density (per unit of volume) multiplied by the thickness of the sample. R_{xy} is independent of the shape of the sample, making it the method of choice for determining carried density in materials, especially semiconductors.

2.2 Integral quantum Hall effect

Slightly more than a hundred years later, in 1980, K. von Klitzing, discovered that for a 2-dimensional electron gas at low temperatures and high magnetic field, instead of the linear dependence we might have expected, R_{xy} has a step-like dependence on magnetic field, with the resistance quantized at very specific values $R_{xy} = \frac{1}{n}h/e^2$ where n are integers [88]. This is called integer quantum Hall effect (IQHE) and as the name implies, its explanation relies on quantum mechanics.

In the absence of magnetic field, the density of states of a two-dimensional electron gas (2DEG) is independent of energy. When placed in a magnetic field, energy gaps open in the spectrum, which consists of highly degenerate discrete energy levels, called Landau levels, at $E_n = (n - 1/2)\hbar\omega_c$, where $\omega_c = eB/m$ is the cyclotron frequency

at the field B. Only a very specific number of states can be accommodated in a Landau level, reflecting the number of electron orbits that can be fitted into the sample: $d = eB/h$. Temperature and disorder broaden the discrete Landau levels; disorder also creates a finite density of localized states between the Landau levels. The presence of disorder is crucial to the formation of plateaus in R_{xy}. When the chemical potential lies in a delocalized state associated with a Landau level, the sample behaves like a metal, scattering is possible, the magnetoresistance R_{xx} takes finite values and R_{xy} varies with magnetic field. This is called a *compressible state* because the charge density can fluctuate. However, if the chemical potential is pinned by the localized states between Landau levels, varying the potential slightly only adds or removes localized states which do not contribute to conduction. In this situation, charge fluctuations cannot occur, $R_{xx} = 0$, R_{xy} takes the quantized values noted above and the system is in a *incompressible state.*

In the IQHE in an incompressible state, the current in the sample is carried by edge states, which are extended states at the border of the sample where the charge carriers move freely without encountering scattering. The bulk of the sample is insulating and does not contribute to conduction. The picture of edge states was first introduced by Halperin in Ref. [33]. An intuitive way to understand edges is to think of them in a classical picture where, under the pull of the Lorentz force, the electrons move in circular orbits. In the center (bulk) of the sample, this movement keeps them localized, however, within one magnetic length $\ell = (\hbar/eB)^{1/2}$ of the edge of the sample, the orbits skip off the edge and the electrons effectively move in one direction. In these edges, electrons can move in only one direction and are not backscattered, which makes the resistance along the edge zero. When measuring, only the 1D resistance arising in the Landauer formalism (h/e^2) is obtained for each edge state (see for example [7]). Hence, the Hall resistance is quantized because only the edge states carry current and behave like 1D channels.

One can define a quantity called filling number ν, which is not necessarily an integer or a rational fraction, as the ratio between the number of electrons N_e and the number of magnetic flux quanta N_Φ in the sample. $\nu = N_e/N_\Phi$. Obviously, the

magnetic field through the sample is not quantized, but its quantization is a good approximation. For integer Landau levels, this number is an integer.

It should be noted that the energy quantization of the Landau levels is not present in 3D because motion in the third dimension, parallel to the magnetic filed, eliminates the energy gaps that are specific to 2D systems. Such 2D systems have several experimental incarnations: the silicon MOSFET and the GaAs/AlGaAs heterostructure, the strained silicon samples, the Si/SiGe heterostructure and recently graphene sheets. The silicon MOSFET is the type of sample used for the first IQHE experiments. In these samples, a 2DEG forms at the interface between silicon and silicon dioxide. The electron density can be tuned via a top metallic gate. One of the main disadvantages of this type of sample is the low mobility. Mobility is a measure of the distance electrons can move without scattering off of lattice imperfections, impurities etc and is the proportionality number between the drift velocity of electrons in an external electric field and the electric field. The GaAs/AlGaAs heterostructure is the type of sample most widely used nowadays for experiments in the quantum Hall regime because specimens with mobility as high as 4×10^7 cm^2/Vs, which gives a mean free path of ~ 0.3 mm, can be grown by molecular beam epitaxy (MBE). In these samples the 2DEG resides at the interface between GaAs and AlGaAs, on the GaAs side, usually in a narrow quantum well.

2.3 Fractional quantum Hall effect

A short two years after the discovery of the IQHE, in 1982, Tsui, Stormer and Gossard reported the presence of a quantized plateau at $R_{xy} = 3h/e^2$ accompanied by a zero in R_{xx} at the same field [87]. This is consistent with quantum Hall effect at $\nu = 1/3$ and the phenomenon is referred to as the fractional quantum Hall effect (FQHE). Subsequently, many more fractions have been discovered experimentally (more than 50 in the region with $\nu < 1$ alone [67]). Unlike the IQHE, a single particle phenomenon, the FQHE arises from interactions between electrons, which are enhanced by the suppression of kinetic energy in magnetic field. For $\nu = 1/m$ a trial

wavefunction proposed by Laughlin [49] for $\nu = 1/m$) accounts for the experimental observations:

$$\Psi_{Laughlin} = \prod_{j<k}(z_j - z_k)^m \prod_j e^{-|z_j|^2/4}, \tag{2.1}$$

where z is the position of the electron in units of magnetic length ℓ and m is an odd integer. The requirement that m is odd arises from the fact that $\Psi_{Laughlin}$ is a wavefunction for fermions and it needs to be antisymmetric upon particle exchange. $\Psi_{Laughlin}$ has two factors. The first factor describes the many-body nature of the state with electrons repelling each other while the second factor is a typical single particle Landau level wavefunction, which localizes every electron within a radius of one magnetic length ℓ. It is interesting to note that the first factor describes the incompressibility of the state; FQHE states, just like IQHE states, are incompressible. The picture of edge states, associated with the incompressibility of the state, has been extended to the fractional states [91], with the caveat that composite edges can now exist, with current flowing in both directions.

We can treat the electrons and the magnetic field as one interacting system and visualize every flux quantum as a vortex in the sea of electrons. Inside such a vortex, the electrons are displaced and the flux quantum behaves like a lack of charge or a hole. Correlation of such a hole with an electron could lower the energy of the system. The vortices are fermions, just like the electrons, and their behavior is governed by the Pauli exclusion principle. At filling number 1, when the numbers of electrons and vortices are equal, we can picture the overall system as being formed of electrons and vortices paired, one electron on top of each vortex and no room for variation since the Coulomb repulsion pushes the electrons in the sea as far away from each other as possible. Alternatively, the combination of an electron and a vortex, both fermions, generates a composite boson. Bosons can condense and form an energy gap, the energy gap associated with the Landau level. This way of of thinking can be generalized to describe the formation of the FQHE. Consider, for example, $\nu = 1/3$. In this case there are 3 flux quanta for each electron. We can consider the composite particle (CP) formed by an electron and 3 vortices. This particle is again a boson and the

bosons thus formed can condense and create an energy gap, the energy gap associated with FQHE at $\nu = 1/3$. This can be extended to any state at $\nu = 1/m$ where m is an odd number. The requirement that m is odd arises from the necessity that the CPs formed by one electron and m flux quanta are bosons. It is interesting to note that by increasing the magnetic field by enough to add one flux quantum generates an additional vortex and this is equivalent to removing a charge of e/m from the system. The effective charge e^* of the quasihole thus generated is just a fraction of the electron charge. The fractional charge of the quasiholes/quasiparticles has been observed in several experiments either by noise correlation measurements [19, 21, 75] or interferometric measurements [30]. It is expected that the quasiparticles formed this way have also special statistical properties, called fractional statistics. The fractional statistics is a complicated property, and we dedicate a section below to the concepts of anyons and fractional statistics. So far, no direct experimental verification of the fractional statistics exists, although experiments showing indications of fractional statistics have been reported [14, 15].

An alternate picture describing the FQHE was proposed by Jain [40]. He proposed a new particle called the *composite fermion* (CF) which is a bound state of an electron and an even number of vortices. Electrons minimize their energy by capturing an even number of vortices, and the remaining interaction between CFs is negligible. Hence, the problem of a strongly interacting electron liquid is mapped onto that of a noninteracting gas of CFs. Since a large part of the magnetic field is incorporated into the CFs, the CFs experience a lower magnetic field than the external field. In this picture, at $\nu = 1/2$ all the magnetic field is incorporated into the CFs themselves, the CFs experience no magnetic field. At zero magnetic field, no Landau levels form, which explains why no Hall quantization is observed at $\nu = 1/2$. As the magnetic field is varied from $\nu = 1/2$, the CFs start to experience a magnetic field and Landau levels form with the CFs as particles. It is straightforward to see that these integer plateaus for CFs correspond to fractional plateaus for electrons at $\nu = \frac{m}{2m+1}$, where m are integers. The picture presented above for excitations with fractional charge also holds in the CF model.

2.4 The fractional quantum Hall state at $\nu = 5/2$

Most of the FQHE plateaus occur at filling fractions with an odd denominator, but at least one exception has been observed experimentally: $\nu = 5/2$[1]. The quantization at $\nu = 5/2$ has been first observed by Willett *et al.* [98]. When modeling this state, the two full Landau levels are ignored and presumed to be inert, and only the half-filled Landau level contributes to the properties of the state. It is obvious that the 5/2 state is not a typical FQHE state, and the Laughlin wavefunction cannot describe it. For the 5/2 state, if we follow the thinking behind the Laughlin state, $m = 2$. An even m makes the Laughlin wavefunction symmetric, and thus does not obey the Pauli exclusion principle.

Moore and Read have proposed what is now called the Pfaffian wavefunction [60] to describe the 5/2 state starting from the Laughlin wavefunction and ensuring that it is antisymmetric under exchange, even though it has an even m:

$$\Psi_{Pfaf} = \mathcal{A}\left(\frac{1}{z_1 - z_2}\frac{1}{z_3 - z_4}\cdots\right)\prod_{j<k}(z_j - z_k)^2 \prod_j e^{-|z_j|^2/4} \tag{2.2}$$

where $\mathcal{A}\left(\frac{1}{z_1-z_2}\frac{1}{z_3-z_4}\cdots\right)$ represents the antisymmetric sum over all pairs of electron positions. This antisymmetric sum is called a Pfaffian. The Pfaffian wavefunction, just like the Laughlin wavefunction, accounts for many body effects and Coulomb repulsion, but, via the antisymmetric sum, it lowers the repulsion between pairs of electrons. This is similar to the BCS theory of superconductivity. The lowering of the repulsion gives rise to an effective attraction allowing the CFs to form weakly coupled Cooper pairs (bosons) which can condense and form an energy gap. However, unlike for standard superconductors with s-wave pairing ($S_z = 0$), the pairing here is p-wave ($S_z = 1$). This makes the overall state spin polarized. A less obvious consequence of the p-wave pairing is the non-abelian nature of the state [70]. We discuss below what non-abelian means.

[1]Quantization at $\nu = 19/8$ has been reported in a single article [101] but has not been observed again since. As I am writing this chapter, an article on the arXive reports the observation of a plateau at $\nu = 1/4$ [53].

Several other proposals for wavefunctions have been put forth: the 331 state, the anti-Pfaffian, the $U(1) \times SU_2(2)$ state and the $K8$. The so-called 331 state [34, 35] can be thought of as s-wave pairing ($S_z = 0$) of a spin-down CF at z_j with a spin-up CF at w_j:

$$\Psi_{331} = \prod_{j<k}(z_j - z_k)^3 \prod_{j<k}(w_j - w_k)^3 \prod_{j<k}(z_j - w_k) \prod_j e^{-(|z_j|^2+|w_j|^2)/4} \qquad (2.3)$$

It is interesting to note that the 331 state, with s-wave pairing has abelian statistics. The anti-Pfaffian [52, 51], another model, is the particle-hole conjugate of the Pfaffian model. Both the anti-Pfaffian and the $U(1) \times SU_2(2)$ [92] models rely on CFs forming Cooper pairs that condense. Both wavefunctions also predict non-abelian statistics. The $K8$ state [94] is also a paired state, however the CFs forming the pairs are strongly coupled. This state is expected to have abelian properties.

All these models rely on CFs forming Cooper pairs, which are bosons and can condense, thus opening up a gap in the energy spectrum. The flux quantum for Cooper pairs, $h/2e$, is only half a flux quantum ϕ_0. This means that the magnetic flux associated with a vortex is only $\phi_0/2$, which in turn translates into a quasihole charge of half of the expected $e/2$. For all proposed models for the $\nu = 5/2$ state, $e^* = e/4$. Using shot noise measurements in a QPC, Dolev *et al.* reported a charge $e^* = e/4$ in the vicinity of the $\nu = 5/2$ plateau [21]. However, charge measurements alone cannot distinguish between the models. Experimental work using tilted magnetic fields [22] and variable-density samples [66] have investigated whether the state is spin polarized or not. Their results indicate that the 5/2 state is probably spin polarized, suggesting that some of the models can be excluded. Later we address quasiparticle tunneling between edge states as a means of investigating which models best describes the $\nu = 5/2$ state. Numerical calculations [61, 71] indicate that the Moore-Read state is the best candidate model to describe the $\nu = 5/2$ state.

2.5 Anyons

In three dimensions, identical particles are either fermions or bosons with very distinct and special properties. Fermions, upon interchange, acquire a minus sign in their wavefunction (or a phase of π). They obey the Pauli exclusion principle, which means that no two fermions can have the exact same set of quantum numbers. Bosons, upon interchange, acquire no phase. They can also condense, which means that many of them can have the same set of quantum numbers. This translates into an energy gap in their spectrum, between the condensate and the rest of the particles in the system.

In two dimensions, things are a lot more complicated since interchange is in this case a topologically nontrivial operation. In three dimensions, two interchange operations (on the same set of two particles) give an identity transformation—a trivial operator. In two dimensions, two interchange operations are the equivalent of a full rotation of one particle around the other. This means that the acquired phase from a single interchange operation can take **any** value between 0 and π, hence the name **anyon** [97]. Moving one anyon around another results in a nontrivial phase change in the wavefunction. This is called braiding.

Anyons are thought to be of two different types: abelian anyons and non-abelian anyons. In group theory, a group is said to be abelian if is has commutativity. For anyons, a simple way to think of abelian properties is to consider the phase change arising from interchange as a matrix rather than a number. If the matrix is diagonal then anyons are abelian and it does not matter which particle is rotated around the other. If the matrix is nondiagonal, it matters which particle is rotated and which one is fixed. In reality, the abelian or non-abelian nature of these quasiparticles is given by their fusion rules. Fusion rules describe what happens when two quasiparticles are brought together and combined. In this context, anyons are non-abelian if the fusion of a pair can have more than one result.

For example, the Moore-Read Pfaffian state has two types of particles: ψ represents the CF and σ is the quasihole excitation of charge $e/4$. $\mathbb{I}$ represents the

condensate, or vacuum. The fusion rules are:

$$\psi \times \psi = \mathbb{I} \tag{2.4}$$

$$\sigma \times \sigma = \mathbb{I} + \psi \tag{2.5}$$

$$\psi \times \sigma = \sigma \tag{2.6}$$

Their meaning is very simple. If two CFs are fused together, a Cooper pair results and joins the condensate. If two quasihole excitations are fused, the result can be either a CF (σ) or they could annihilate each other and the result is identical to the condensate $\mathbb{I}$. This second fusion rule gives the Moore-Read model its non-abelian properties, because by fusing two identical quasiholes there can be two outcomes. The third rule is just the associativity of the other two rules.

Most FQHE states with an odd denominator are believed to have anyonic quasiparticles with abelian statistics. As we have seen above, some of the models proposed to describe the $\nu = 5/2$ state have abelian quasiparticles, while others have non-abelian quasiparticles.

2.6 Quasiparticle tunneling in the fractional quantum Hall effect

Having introduced anyons, we can now focus on a method that could allow us to differentiate between several models proposed to describe the $\nu = 5/2$ state. This method relies on quasiparticle tunneling between the counter-propagating edges at the given filling number. Initially developed for fractional states with odd denominator with abelian statistics) [95], the theory of weak quasiparticle tunneling between edge states has been extended to non-abelian states [10, 26, 59, 93, 96]. The weak quasiparticle tunneling theory takes a perturbative approach to determining the tunneling current between counter-propagating edges. A non-perturbative solution, based on the thermodynamic Bethe ansatz for Laughlin states at filling fraction $\nu = 1/m$ has been presented in Ref. [25]. However, this non-perturbative solution cannot be extended

to quasiparticles with non-abelian statistics as it cannot account for quasiparticle braiding of more than 2 particles.

In the quantum Hall effect, the gap in the bulk prohibits excitations [33], while the edge states have no gap. Wen has shown that the gapless edge excitations of a FQHE state are "chiral" Luttinger liquids [91]. A Luttinger liquid is an interacting 1-dimensional electron system, a non-Fermi-liquid system. The chirality comes from the magnetic field, which separates the left and the right moving particles to different sides of the sample.

In general, a Luttinger liquid is characterized by an interaction parameter g, which depends on the ratio of the Coulomb energy in the system U_C to the Fermi energy in the absence of interactions, reflecting the interaction strength between left and right-moving electrons:

$$g = 1/\sqrt{1 + \frac{U_C}{E_F}} \tag{2.7}$$

For non-interacting particles, $U_C = 0$, which gives $g = 1$. In superconductors $g = 0$ because the kinetic energy is suppressed by the Cooper pair formation. These Cooper pairs are bosons and condense, leaving $E_F = 0$. In an edge state, electrons move in a single direction and g becomes a topological invariant [95] determined by the Hall state of the bulk[2]. For simple FQHE states, such as the one at $\nu = 1/3$, $g = \nu$. For more complex states, the interaction parameter g reflects the structure of the edge associated with the state in a non-trivial manner. It is interesting to note that most of the models at $\nu = 5/2$ have different g parameters, depending on the number of modes the edge is expected to have. The K8 model [94] is expected to have $g = 1/8$, the Moore-Read Pfaffian state has $g = 1/4$ [60, 96], the 331 state has $g = 3/8$ [34, 35], while the last two states the anti-Pfaffian and the $U(1) \times SU_2(2)$ have $g = 1/2$ [52, 51, 10, 92]. The weak tunneling theory predicts that the tunneling rate depends on g. Therefore one could use tunneling to determine which model most closely describes the 5/2 state. However, this method does not provide direct evidence whether the state is non-abelian or not.

[2]This makes it crucial that in experiments the same state exists in the bulk of the sample and the constriction. See our work in Chap. 4 describing how this can be achieved experimentally.

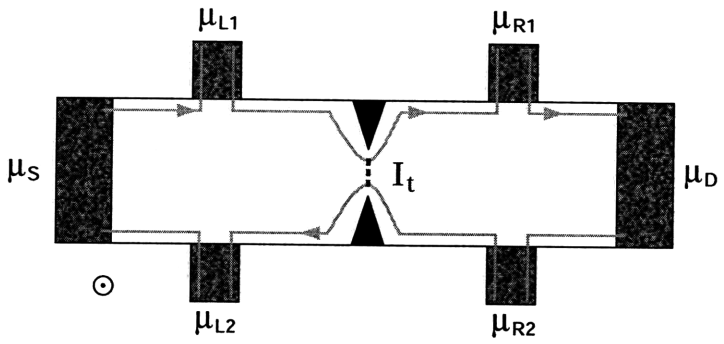

Figure 2-1: Weak tunneling picture. Counter-propagating edges states are brought close together at a QPC and charges can tunnel from one edge to the other. For weak tunneling most of the edge current continues to flow through the QPC. Quasiparticles, not electrons, tunnel through the bulk, illustrated by the dashed line inside the QPC. Electron tunneling is suppressed.

Electrons in edge states encounter no backscattering, but when the counter-propagating edges are brought close enough together quasiparticles can tunnel from one edge to the other through the bulk of the sample. Experimentally, the edges can be brought close together using a constriction patterned on the Hall bar, called a quantum point contact (QPC). In the weak tunneling regime there is low probability of tunneling between the edges, so that most of the current flows through the QPC unaffected (see Fig. 2-1). The tunneling current in this case is computed via perturbation theory, in which a quasiparticle is created at one of the edges, tunnels through the bulk and is annihilated at the counter-propagating edge [95]. It turns out that the lowest order non-zero term is the second order term, a two particle process, in which a quasiparticle-quasihole pair is created out of vacuum (or condensate) in the bulk of the sample and the quasiparticle tunnels to one of the edges while the quasihole tunnels to the other [10]. In this picture, the higher order terms, which can be thought of as particles with larger effective charge e^*, or multiple pair processes, will have significantly lower amplitudes and the calculations are generally limited to the first non-zero term. It is interesting to note that the two-particle tunneling process can be treated as a correlation problem of the two edges. One of its consequences is

the qualitative temperature dependence: the lower the temperature, the higher the degree of correlation between the two edges, hence the higher is the tunneling conductance. In the extreme case of $T = 0$ this leads to a singularity at zero bias, with the tunneling current diverging. It should be pointed out that this is not a physical result, but rather just a consequence of the breakdown of perturbation theory. As the correlation between edges increases so does the number of quasiparticles that tunnel, which means that at some point the perturbative approach to treating the problem can no longer be applied. This is the limit of strong tunneling, and it can be achieved either by lowering the temperature of the system or by increasing the probability that quasiparticles tunnel. Experimentally, the latter is achieved by either bringing the counter-propagating edges closer together by applying a more negative voltage on the gates defining the QPC, or, as we discuss in Chapter 4, by using a long constriction. As the tunneling becomes strong, most of the electrons in the edges are backscattered and only a small fraction continue moving in the original direction of the edge state. In this limit the tunneling can be thought of as electrons tunneling in the forward direction between the fractional edges through vacuum or through bulk at a different (lower) filling number as depicted in Fig. 2-2. Although perturbation theory breaks down and cannot be applied, qualitative expectations for this regime exist. First and foremost, the singularity at zero bias in the $T = 0$ limit is eliminated. We expect that the tunneling conductance is limited to the value it would take when the edge of the top, highest energy occupied, is backscattered and the underlying edge passes through the QPC unperturbed. For example, if the top edge is $\nu = 5/2$ and the underlying edge is $\nu = 7/3$ then we expect that the tunneling conductance g_T is limited to $(5/28)e^2/h$. If the underlying edge is $\nu = 2$ then g_T would be limited to $(5/8)e^2/h$. In the regime between weak and strong quasiparticle tunneling we expect that the accuracy of the prediction using perturbation theory could be improved by summing over higher order terms. However, for non-abelian states no such summation can be performed. The higher order terms would have to account for the braiding of the quasiparticles, which becomes very difficult for more than 2 particles.

In the weak tunneling regime, the tunneling conductance as a function of temper-

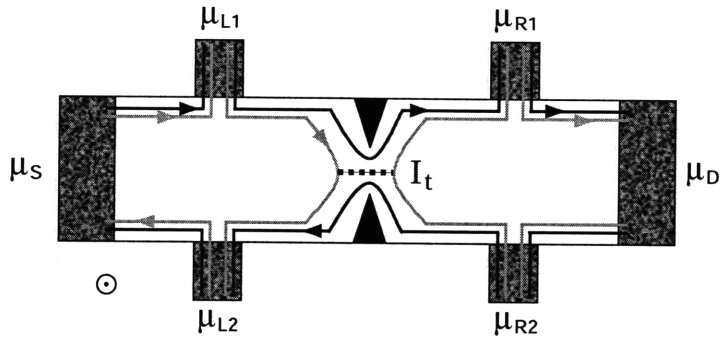

Figure 2-2: Strong tunneling picture. Counter-propagating edges states are brought close together at a QPC and charges can tunnel from one to the other. The edge in which the tunneling happens is strongly back-scattered by the QPC , so that it can no longer pass through the QPC. In this case, electrons rather than quasiparticles tunnel through "vacuum".

ature and applied dc bias is given by [95, 64]

$$g_T(T, I_{dc}) = AT^{(2g-2)} F\left(g, \frac{e^* I_{dc} R_{xy}}{kT}\right), \tag{2.8}$$

with

$$F(g,x) = B\left(g + i\frac{x}{2\pi}, g - i\frac{x}{2\pi}\right)\left\{\pi\cosh(x/2) - 2\sinh(x/2) Im\left[\Psi\left(g + i\frac{x}{2\pi}\right)\right]\right\} \tag{2.9}$$

where e^* is the charge of the quasiparticle expressed in units of e (charge of the electron) and k is the Boltzmann constant. $B(x,y)$ represents the Euler beta function and $\Psi(x)$ is the digamma function. This formula allows us to extract not only a g parameter but also e^*.

The above formula predicts that at zero dc bias the tunneling conductance varies with temperature as a power law T^{2g-2}, typical behavior for Luttinger liquids. At zero dc bias, the tunneling current varies with temperature as T^{2g-1}. In the zero temperature limit, the tunneling current depends on dc bias also as a power law: V^{2g-1}. In both cases the exponent depends on the interaction parameter g. For the integer states $g = 1$ which makes the tunneling conductance independent of dc bias

and temperature — ohmic behavior consistent with the Fermi liquid nature of the IQHE states. For $g < 1/2$, the tunneling conductance has negative values above a certain dc bias. The position of the zero in the tunneling conductance is well approximated by $\frac{e^* V_{dc}}{2\pi kT} = g$ for small g. This negative differential conductance indicates that the tunneling current is non-monotonic in dc voltage. The tunneling current has a maximum at a value of the dc bias voltage given by $e^* V_{dc}^0 = \pi kT arctanh(2g)$. An intuitive physical explanation for this is that at low dc bias voltage, the applied bias helps particles tunnel across the bulk and increases the tunneling current, while at voltages larger than the temperature of the system, the voltage acts to effectively heat up the system and decreases the tunneling current by reducing the degree of correlation between edges. It is also interesting to note that e^* and g are not truly independent parameters, and when fitting data with eq. 2.8 one finds pairs of (e^*, g) rather than independent numbers.

2.7 Relating the tunneling conductance to directly measurable quantities

When investigating quasiparticle tunneling between edge states, there are two possible experimental set-ups that can be used to determine the tunneling conductance g_T or the tunneling current I_t. The one-drain set-up discussed here and used in the experiments presented in this thesis, is the typical Hall measurement set-up. A schematic is presented in Fig. 2-3.

In this set-up the tunneling current is not drained separately and becomes part of the injected current. One can think that the source injects $I_{SD} + I_t$, where I_{SD} is the externally imposed current, and at the same time drains I_t. The relations between currents and voltages in this set-up are:

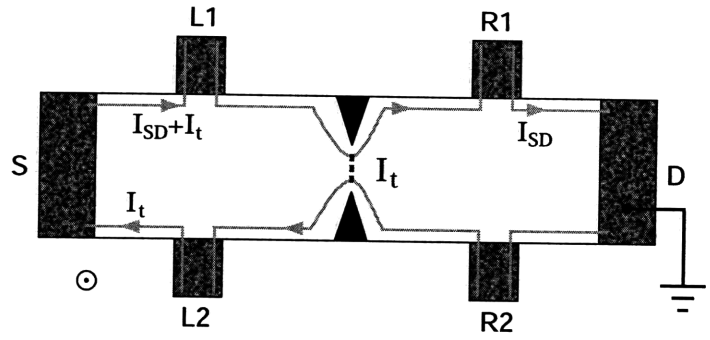

Figure 2-3: Weak quasiparticle tunneling in a single drain set-up. Counter-propagating edges states are brought close together at a QPC and charges can tunnel from one edge to the other. The source injects $I_{SD} + I_t$ and at the same time drains the tunneling current I_t. The drain of the sample, held at virtual ground, drains I_{SD}. The voltage drop across the QPC depends on the tunneling current.

$$V_{L1L2} = V_{R1R2} = R_{xy} I_{SD} \tag{2.10}$$

$$V_{L1R1} = V_{L2R2} = R_{xy} I_t \tag{2.11}$$

$$V_{L1R2} = R_{xy}[I_{SD} + I_t(V_{L1R2})] \tag{2.12}$$

where R_{xy} is the Hall resistance and the voltage drops between various ohmics are marked with the respective names of the ohmics. For example, the voltage drop between the ohmics L1 and R1 is V_{L1R1}. The diagonal resistance R_D is measured with the voltage probes placed not only on opposite sides of the Hall bar, but also on either side of the QPC. For the direction of field depicted in Fig. 2-3, R_D is measured between the contacts marked L1 and R2. In a differential measurement, the diagonal resistance R_D is given by:

$$R_D = \frac{\partial V_{L1R2}}{\partial I_{SD}} \tag{2.13}$$

Expressing I_{SD} as a function of V_{L1R2} and performing the derivative in eq. 2.13, gives:

$$R_D = \frac{R_{xy}}{1 - R_{xy}\left(\frac{\partial I_t}{\partial V}\right)_{V=V_{L1R2}}} \tag{2.14}$$

In the weak tunneling limit, the tunneling current is much smaller than the total current through the sample $I_t \ll I_{SD}$ and that $V_{L1R2} \simeq R_{xy} I_{SD}$. Using these two approximations in eq. 2.14, the tunneling conductance g_T is:

$$g_T = \left(\frac{\partial I_t}{\partial V}\right)_{V=R_{xy}I_{SD}} = \frac{R_D - R_{xy}}{R_{xy}^2} \tag{2.15}$$

This equation shows that it is sufficient to measure two four-probe resistances in order to determine the tunneling conductance. The second measurement set-up, the two drain set-up, not presented here, is used by the Heiblum group at Weizmann Institute in their shot noise measurements [21]. The tunneling conductance in this second set-up is similar to the set-up with a single drain.

2.8 Energy scales in a magnetic field

It is interesting to put a few numbers behind some of the physical quantities and energy scales associated with a magnetic field. For example, at a typical magnetic field for the 5/2 state to form, $B \simeq 4.5$ T, the magnetic length, which the length associated with the width of the edge states is:

$$\ell = \sqrt{\frac{\hbar}{eB}} \simeq 12 \text{ nm} \tag{2.16}$$

The Coulomb repulsion energy between electrons a magnetic length apart, in GaAs is:

$$U_C = \frac{e^2}{4\pi\varepsilon\ell} \simeq 110 \text{ K} \tag{2.17}$$

The cyclotron energy at the same magnetic field is:

$$E_C = \hbar\omega_C \simeq 90 \text{ K}, \tag{2.18}$$

while the Zeeman energy in GaAs is:

$$E_Z = g^* \mu_B B \simeq 1.2 \text{ K}. \tag{2.19}$$

Note that the largest energy scale is the electron repulsion.

The activation gap for the 5/2 state in the experiments presented in the following chapters is $\sim$ 130 mK, although gaps as large as 500 mK have been reported [101].

2.9 Summary

In this chapter we have introduced the Hall effect, both classical and quantum and concepts pertaining to the Hall effect, composite fermions and anyons. We have presented several models describing the FQHE state at $\nu = 5/2$ and a method that helps discriminate between these models, weak quasiparticle tunneling. We have also outlined how the tunneling conductance can be derived from two directly measurable resistances. Finally we have provided some numbers for the energy scales in the quantum Hall effect.

Chapter 3

Suppression of Spin Splitting in Narrow Channels

3.1 Introduction

In the early 1990's studies of QPCs [90] in magnetic fields began to explore the problem of how the confinement of a two-dimensional electron gas (2DEG) influences the integer quantum Hall effect. For an overview of the topic see Ref. [7]. In this chapter we continue this work and investigate how the width of the sample influences the spin splitting of the Landau levels.

In transport measurements in 2D systems, Landau level quantization is observed as plateaus in the Hall conductance in steps of $2e^2/h$, or in the Hall resistance at even filling numbers. The spin splitting manifests itself as extra plateaus at odd filling numbers. The minimum magnetic field where the splitting is observed is higher than the field where the Landau level quantization starts, because the energy gap associated with the spin splitting is smaller than the cyclotron energy which governs the gaps at even filling numbers. The Landau level quantization is observed at even filling numbers when the cyclotron energy is larger than the temperature and disorder broadening [50, 99]. The gap associated with the spin splitting of the Landau levels Δ_s is larger than the single-electron Zeeman energy $g_0\mu_B B$, where g_0 is the Landé g-factor in bulk GaAs, μ_B is the Bohr magneton and B is the magnetic field [23,

50, 99]. This is because the kinetic energy is reduced by the orbital quantization in magnetic field and the exchange interaction then results in a polarization of the electron spins [41]. Since in one-dimensional systems, the effect of the Coulomb interaction is expected to be stronger than in 2D, confinement is expected to increase Δ_s and to decrease the minimum magnetic field B_{spin} at which spin splitting of the Landau levels is observed [78]. However, it is found experimentally that in confined structures such as QPCs, the spin splitting is suppressed compared to corresponding bulk 2DEG [44, 62, 100]. In Si, the valley splitting is also suppressed [44]. Several theoretical articles have investigated this effect for the first Landau level [45, 4, 5] or the first two Landau levels [102]. Using magnetocapacitance measurements, Pallechi et al. [65] have measured the spin gap of the first Landau level as a function of confinement and have found that it decreases with increasing confinement. Their data are reproduced quite accurately by a self-consistent Hartree-Fock calculation [83]. By using samples with very high mobility and using an assortment of QPCs of several widths, we investigate this phenomenon over a large range in Landau level number and magnetic field.

The samples are QPCs of several lithographic widths, in a split-gate geometry, patterned on a high mobility GaAs/AlGaAs heterostructure. The effective width of the conduction channel depends both on the lithographic width and also on the gate voltage V_g applied. The width can be estimated from the low-field dependence of resistance on magnetic field. Using this combination of variation of gate voltage and lithographic width we have access almost continuously to effective widths between 100 and 3000 nm. In this width range the number of spin-split Landau levels N_S varies from 1 to 42 while in bulk this number is ~ 70. One of the possible clues for understanding the dependence of N_S on confinement comes from the fact that for width less than ~ 1200 nm, N_S is approximately half of the number of the conduction channels through the QPC at magnetic field. We also find that the cyclotron diameter at the lowest magnetic field, for which the spin splitting is observed, B_{spin} is approximately half of the effective width of the QPC.

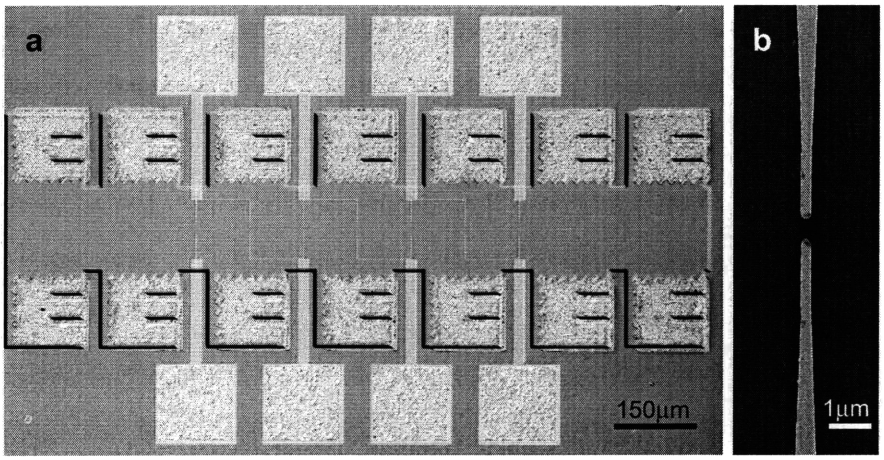

Figure 3-1: (a) Optical micrograph of the entire device (the outline of the wet-etched Hall bar has been enhanced for clarity) Darker yellow pads are the gates, while the faint yellow-gray pads are the ohmic contacts. (b) SEM micrograph of the 500nm QPC.

3.2 Sample

The sample used the experiments presented in this chapter consists of a high mobility GaAs/AlGaAs heterostructure, with the 2DES 200 nm below the surface and two Si δ-doping layers positioned symmetrically 100 nm on each side of the 2DES. The mobility of the 2DES is estimated to be 2000 m^2/Vs and the carrier density 2.5×10^{15} m^{-2}. A 150 μm wide Hall bar is patterned on this heterostructure using optical lithography and wet etching. On the Hall bar, metallic (Cr/Au) gates which form the QPCs have been pattered using e-beam lithography and lift-off. The QPCs have a split-gate geometry. An SEM micrograph of the gate geometry of the 500 nm QPC is presented in Fig. 3-1b. There are 7 such QPCs on a chip with nominal lithographic widths of 3000, 2000, 1200, 775, 500, 300 and 200 nm (the 2000 nm QPC is not used for the experiment presented in this chapter). The layout of the sample is presented in Fig. 3-1a. The combination of multiple ohmic pads and gate placement allows the formation and measurement of any one of the QPCs mentioned above, individually.

The sample is mounted on a cold finger attached to the mixing chamber of a dilution refrigerator with a base temperature of less than 10 mK in a magnetic field oriented perpendicular to the plane of the 2DES. The actual electron temperature is

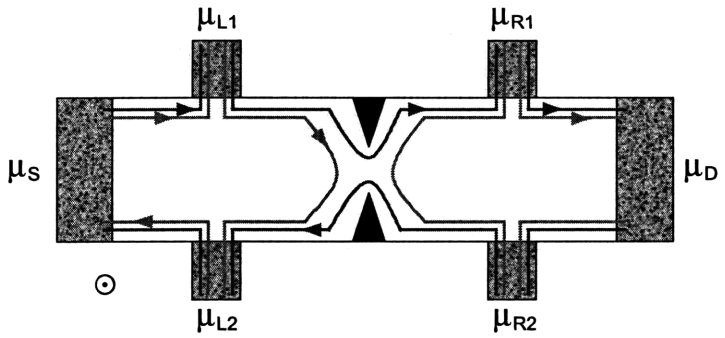

Figure 3-2: Sketch of a six terminal Hall bar with a constriction. The current flow in the edges of two quantum Hall states is sketched close to sample boundary. The constriction reflects one of the edges while a second one passes unperturbed. The local electrochemical potentials are labeled for each contact.

higher than the mixing chamber temperature (see Chapter 5).

When using the QPCs, we apply the same voltage V_g to the pair of lithographic gates forming them. Because of the depth of the 2DES, the electrons under the gates deplete at voltages $V_g < -1.8$ V, which are more negative than for heterostructures usually used for gated devices. All measurements presented here are performed with the gates depleted.

The heterostructure was grown at Bell Labs by Loren Pfeiffer and Ken West. Jeff Miller from the Marcus lab patterned the QPC devices on this heterostructure at Harvard. Measurements were done at MIT in the Kastner Lab. Details covering sample preparation can be found in Ref. [57].

3.3 Measurement details

Measurements in the quantum Hall effect (QHE) are typically performed in a four-terminal configuration, where the voltage probes are assumed ideal; that is, they do not carry current. In this scenario, the contact resistance does not influence the measurement. In the QHE, the current in the sample is carried by edge states, which are close to the edges of the sample. When measuring the four-terminal Hall resistance

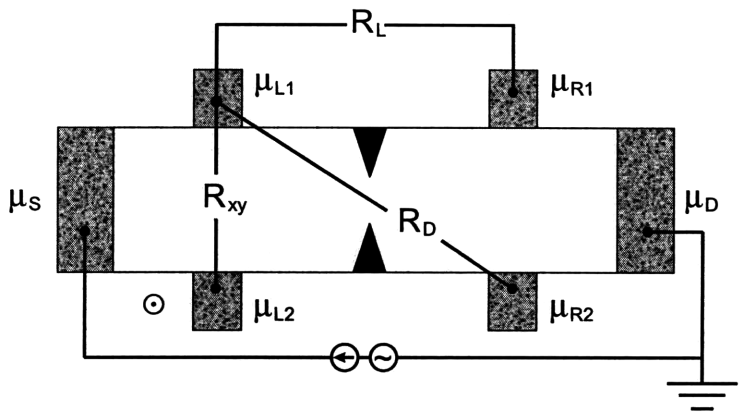

Figure 3-3: Sketch of a Hall bar with a constriction illustrating the three four-terminal measurements we make: R_{xy} is the traditional Hall resistance, R_L is the longitudinal resistance across the QPC and R_D is the diagonal resistance. The drain contact is held at local ground.

at high magnetic field, in fact one counts the number of edge states present in the sample.

$$R_{xy} = \frac{h}{2e^2}\frac{1}{N_{bulk}}, \tag{3.1}$$

where N_{bulk} represents the number of (spin-degenerate integer) edges in the sample. This equation can be generalized for any filling number (integer or fractional).

When a constriction is created on the Hall bar some of the edge states are reflected back (see Fig. 3-2), and two other resistances can be measured (see Fig. 3-3). The longitudinal resistance through the QPC R_L, measured with both voltage probes placed on the same side of the Hall bar, is the four-terminal version of a two-probe resistance measurement of the sample. The diagonal resistance R_D, where the voltage probes are placed not only on either side of the QPC but also on opposite sides of the Hall bar, is, roughly speaking, the equivalent of the Hall resistance in the QPC.

In Fig. 3-3 we show the measurement contacts for a Hall bar on which a QPC has been created. There are two current probes, a source and a drain (typically one of them is virtual ground), and four voltage probes which allow simultaneous measurement of all three resistances mentioned above. To determine how these resistances relate to the number of edge in the sample at high field, following Ref. [7],

we perform a Landauer-Büttiker calculation [12]. Assuming that the voltage probes are ideal (they carry no current) then the current at the source and the current at the drain obey $I_S = -I_D = I$. Let us also assume that the drain is held at virtual ground: $\mu_D = 0$. Then the Landauer formula gives:

$$N_{bulk}\,\mu_S - (N_{bulk} - N_{QPC})\,\mu_{L1} = \frac{h}{2e} I \tag{3.2a}$$

$$N_{bulk}\,\mu_{L1} = N_{bulk}\,\mu_S \tag{3.2b}$$

$$N_{bulk}\,\mu_{R1} = N_{QPC}\,\mu_{L1} \tag{3.2c}$$

$$N_{bulk}\,\mu_{R2} = N_{bulk}\,\mu_D \tag{3.2d}$$

$$N_{bulk}\,\mu_{L2} = N_{QPC}\,\mu_{L1}, \tag{3.2e}$$

where N_{QPC} represents the number of conduction channels (two-fold degenerate because of spin) that pass through the QPC. Since:

$$R_L = \frac{\mu_{L1} - \mu_{R1}}{eI} \tag{3.3}$$

and

$$R_D = \frac{\mu_{L1} - \mu_{R2}}{eI} = R_L + R_{xy}, \tag{3.4}$$

then using Eqs. 3.2a one finds:

$$R_L = \frac{h}{2e^2}\left(\frac{1}{N_{QPC}} - \frac{1}{N_{bulk}}\right) \tag{3.5}$$

and

$$R_D = \frac{h}{2e^2}\frac{1}{N_{QPC}} \tag{3.6}$$

It is obvious then that R_L reflects the combined effects of bulk and QPC behavior while R_D is the equivalent of the Hall resistance in the QPC. It is worth noting that the Hall resistance in the bulk of the sample, given by

$$R_{xy} = \frac{\mu_{L1} - \mu_{L2}}{eI} = \frac{h}{2e^2}\frac{1}{N_{bulk}}, \tag{3.7}$$

is unaffected by the presence of the QPC. At zero magnetic field $R_{xy} = 0$, hence $R_L = R_D$. Both these last two facts are confirmed experimentally.

Although all the above equations have been derived in the Landauer-Büttiker formalism, which requires high magnetic field and the existence of edge states to be applicable, they still hold in the low field range. In this field range (when the cyclotron radius is greater than the width of the QPC) N_{QPC} represents the number of 1D magneto-electric subbands within the QPC rather than the number of edge states that are transmitted through it [7]. Throughout this chapter, in addition to the directly measured quantities outlined above, we also use the related conductances $G_D = 1/R_D$ and $G_L = 1/R_L$.

Data presented in this chapter are acquired in a four probe configuration by applying a small ac current and measuring voltages with a lock-in technique. In all measurements the excitation current is chosen small enough that the voltage is proportional to the current. For the 200 nm QPC, because of wiring constraints, only a three-probe measurement could be performed, meaning that one of the voltage probes coincides with a current probe. In the analysis carried out for the data from this QPC, a small constant value of resistance is subtracted, consistent with the resistance of one of our measurement wires (650 Ω).

3.4 Width estimates

In analyzing and comparing data from various QPCs, one of the important quantities is the degree of confinement at the QPC in the direction perpendicular to the current flow. The effective width of the electron gas in the QPC cannot be measured directly. Furthermore, the shape of the confining potential is not known. We therefore compare the data with several solvable models that have been proposed. The easily solvable models for the confining potential are the square well and the harmonic oscillator. For each of these we can estimate an effective width of the QPC, and throughout this chapter we use the effective width to characterize the confinement. To estimate the effective width, we use three different methods based on the different models of the

confining potential and theoretical assumptions about transport. For all of them, we ignore the finite length of the QPC, and treat the potential associated with the gates as one-dimensional. As we shall see, all three models return approximately the same numbers for the estimated width.

3.4.1 Sharvin Formula

In the Landauer formalism, at zero magnetic field, the current in the sample is equally distributed among 1D subbands which are the transversal (propagating) modes of the confining potential in the constriction. As a consequence, the conductance is proportional to the number of propagating modes at the Fermi level,

$$G = \frac{2e^2}{h} N_{QPC}. \tag{3.8}$$

Assuming a hard-wall confining potential, each 1D subband has a width of half of a Fermi wavelength $\lambda_F/2$. Then for a QPC of width W, the number of 1D subbands participating in conduction is:

$$N_{QPC} = \text{Int}\left[\frac{W}{\lambda_F/2}\right] \tag{3.9}$$

This gives for ballistic electron transport at zero magnetic field a resistance:

$$R(B=0) = \frac{h}{2e^2}\frac{\lambda_F/2}{W} \tag{3.10}$$

This formula is the 2D analog [90] of the resistance through a 3D QPC [77]. To estimate the Fermi wavelength we use the 2D electron density in the QPC estimated as explained below. By measuring the resistance at zero magnetic field we can thus estimate the width of the QPC.

Whereas this method to estimate the width relies on the zero-field resistance of the sample, similar information can be obtained from the magnetic field dependance of the resistance. The 1D transport subbands discussed above can be depleted by reducing the width of the QPC,by modifying the Fermi energy, or by applying a magnetic

field perpendicular to the plane of the sample. The corresponding subbands in the presence of a magnetic field are called magneto-electric subbands, and the increase in magnetic field will depopulate them. In the following, we outline the effect of the magnetic field on resistance for two confining potentials: a square-well potential and a parabolic potential.

3.4.2 Square-well potential with perpendicular magnetic field

Assuming a square-well lateral confinement potential and using a Bohr-Sommerfeld quantization [89], the number of conduction channels through the QPC is found to be

$$N_{QPC}(B) \approx \mathrm{Int}\left[\frac{2}{\pi}\frac{E_F^{QPC}}{\hbar\omega_c}\left(\arcsin\frac{W}{2\ell}+ +\frac{W}{2\ell}\left[1-\left(\frac{W}{2\ell}\right)^{1/2}\right]\right)\right], \text{if} \quad \ell > W/2 \tag{3.11a}$$

$$N_{QPC}(B) \approx \mathrm{Int}\left[\frac{1}{2}+\frac{E_F^{QPC}}{\hbar\omega_c}\right], \text{if} \quad \ell < W/2 \tag{3.11b}$$

where $\ell = \hbar k_F/eB$ represents the classical cyclotron radius at the given field. Detailed derivations of the Eqs. 3.11 may be found in Ref. [7]. These complicated formulas describe the transition from electrical conduction channels to Landau levels as the magnetic field increases. At zero field the nature of the 1D conduction channels is strictly electrostatic. As the magnetic field increases, they become magnetoelectric subbands and at very high field, where the effect of the confinement is negligible, they can be treated as Landau levels. The magnetic field and the confinement play equal roles when the width of the QPC and the cyclotron diameter are equal. Let B_0 be the field at which $\ell = W/2$. At fields lower than B_0, electrostatic effects dominate and N_{QPC} does not change significantly with increasing magnetic field while the number of the Landau levels in the bulk of the sample decreases rapidly. This makes R_L decrease with increasing magnetic field (see Eq. 3.5). At fields higher than B_0, the electrostatic effects become less important and the change in the Hall resistance will

dominate making R_L increase approximately linearly with magnetic field.

To extract the width of the QPC we perform a one parameter fit to the R_L data using N_{QPC} from Eqs. 3.11 in Eq. 3.5, ignoring the discreteness of the number of conduction channels. The Fermi energy E_F^{QPC} is determined from the 2D electron density in the QPC, in the same way that λ_F is extracted above.

3.4.3 Parabolic potential with perpendicular magnetic field

Assuming a parabolic lateral confining potential $V(x) = \frac{1}{2}m\omega_0^2 x^2$, the number of conduction channels is found to be [9, 8]:

$$N_{QPC} = \text{Int}\left[\frac{1}{2} + \frac{E_F^{QPC}}{\hbar\sqrt{\omega_c^2 + \omega_0^2}}\right], \tag{3.12}$$

where ω_c is the cyclotron frequency at a given magnetic field. Following Ref. [7] we define the effective width of the conduction channel to be the separation between the equipotentials at the Fermi energy: $W_{para} = 2\hbar k_F/m\omega_0$. Although the equation defining the number of conduction channels no longer has two branches, all the considerations presented above about R_L's dependence on magnetic field still hold in this case. And just as for a square-well potential, we fit R_L data using N_{QPC} from Eq. 3.12 while ignoring the discreteness of the number of conduction channels.

Using these last two methods to evaluate the width, we perform fits to the R_L as shown on Fig. 3-4. The square-well approximation works better for the wider QPCs, while the parabolic potential provides a better approximation for the narrower QPCs. For all QPCs however, the square-well approximation underestimates R_L in the region where $\ell = W/2$ (where the red and green lines intersect). In the same region, the parabolic approximation overestimates the data. These facts signal that the shape of the potential at the QPCs is neither parabolic nor square-well, but rather somewhere between the two.

In Table 3.1, width estimates from all three methods are presented for each QPC used in the study at the gate voltages in Fig. 3-4. All methods return approximately the same results. However, the Sharvin method and the square-well potential method

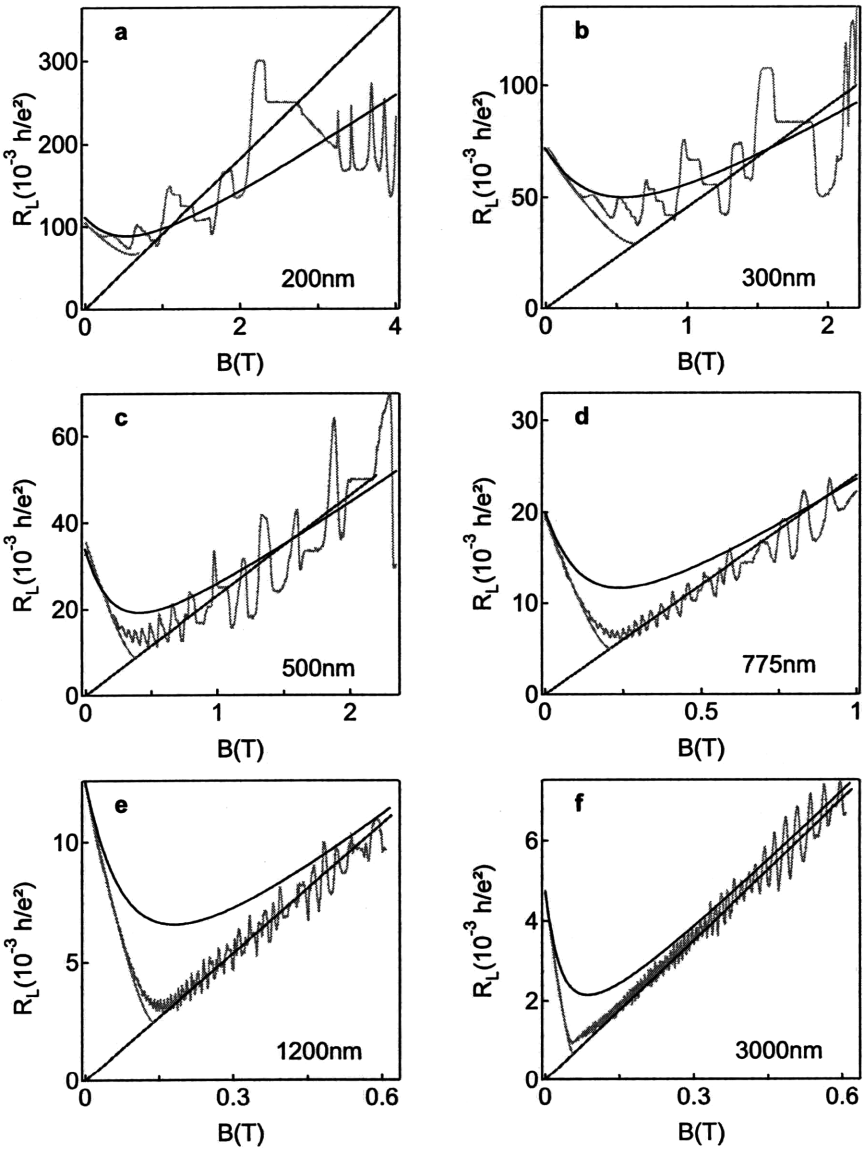

Figure 3-4: (a)-(f) Longitudinal resistance across QPCs of six different lithographic widths. The orange (light traces) are the longitudinal resistance. The black trace in each panel is the best fit to the data assuming a parabolic confining potential in the constriction. The green and red traces are best fit to the data assuming a square-well confining potential. All data are taken at $V_g = -3$ V, except for the 200 nm QPC where data are taken at $V_g = -2.8$ V.

W_{litho}	$W_{Sharvin}$	W_{SW}	W_{para}
3000	2800	2751	3350
1200	1084	1092	1264
775	697	701	790
500	419	407	474
300	211	215	221
200	160	164	142

Table 3.1: Conductance channel width estimates for the data in Fig. 3-4. W_{litho} represents the nominal lithographic width, $W_{Sharvin}$, W_{SW}, W_{para} represent the width estimated using the Sharvin formula, the square-wall potential approximation and the parabolic potential approximation, respectively.

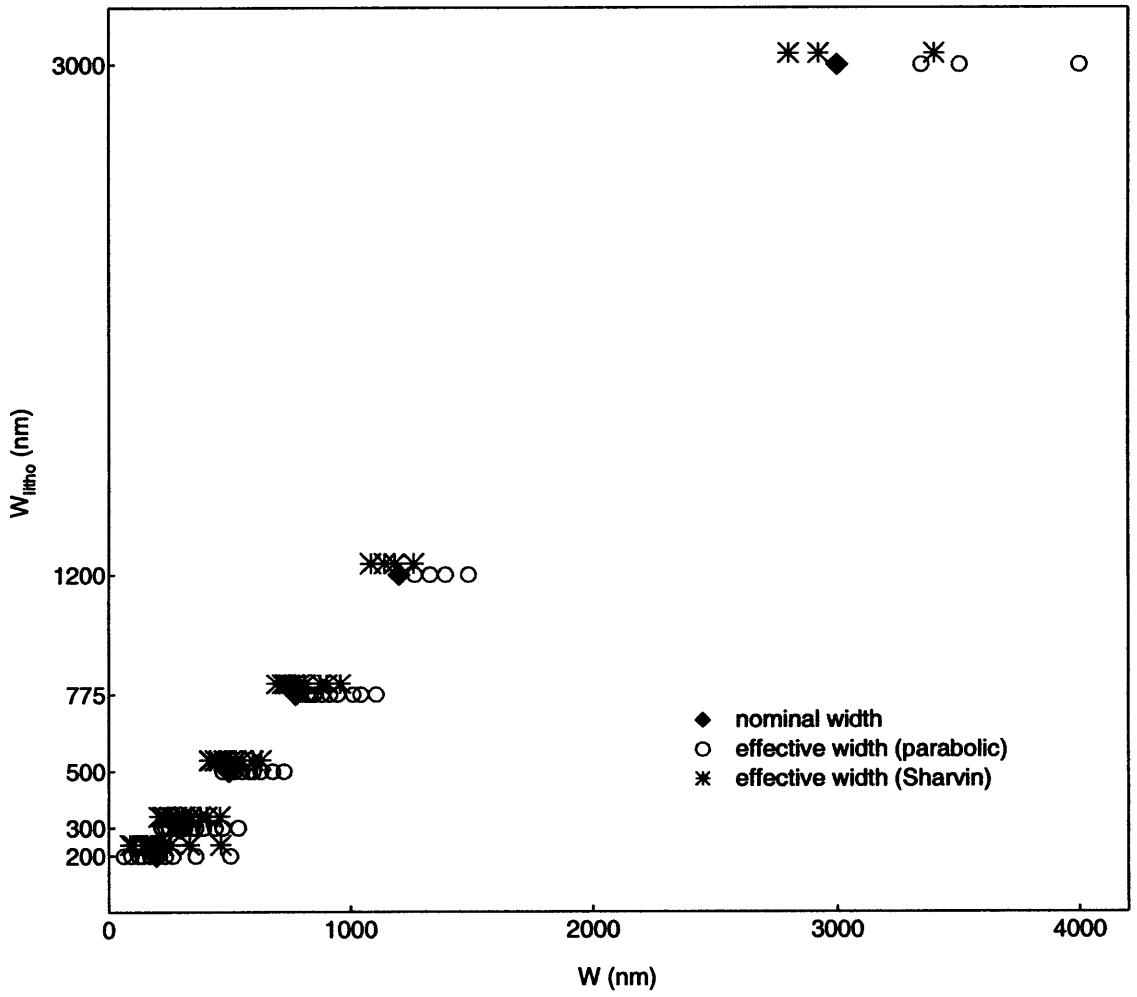

Figure 3-5: Effective width of the conduction channel W estimated assuming parabolic confinement (red open circles) and the Sharvin formula (blue stars) at various gate voltages. For comparison, the lithographic width of the QPCs is also included as a black diamond.

return results which are virtually the same. This is not surprising, since both methods assume a square-well potential, one at zero magnetic field and the second in a finite perpendicular magnetic field. A detailed comparison of the estimates with the Sharvin formula and the parabolic potential are presented in Fig. 3-5. The nominal (lithographic) size of the QPCs has been also included. For a given lithographic width, the effective width decreases as the applied gate voltage is made more negative. By employing these 6 QPCs and varying the gate voltage, we have almost continuous control over the width of the conduction channel from 100 to 1200 nm. Note that in many cases, the fits return numbers which are larger than the nominal width of the QPC. This could be explained by inaccuracies in the electron microscope measurement of the devices. Alternatively, it is possible that the simplest picture of gate depletion, in which a region around the gates approximately equal to the depth of the 2DEG is depleted [29], is not valid for this sample. It is also conceivable that the narrowest part of the metallic gates does not deplete the electrons in the 2DEG until very negative voltages and this is reflected in apparently wider QPCs. If the simple picture of gate depletion were to hold, no conduction would be observed through 200 and 300 nm QPCs, while as presented in Figs. 3-7 and 3-8, finite conduction is recorded for these QPCs. Similar observations of conduction higher than expected have been reported in the literature [86] in a similar heterostructure.

3.5 Evaluating 2D electron density in the QPC

Inside the QPC, because of confinement, the electrons can no longer be modeled as a 2D electron gas. However, we extend the 2DEG concept and define an 2D electron density (n_S) nonetheless. Taking into account the finite length of the constriction, we model the electrostatic potential in the vicinity of the QPC as a saddle potential [13, 27, 55]. Let the potential energy at the saddle point be V_0 [37, 13, 27]. V_0 is expected to depend on gate voltage and on the geometry of the gates. We define the Fermi energy at the QPC to be $E_F^{QPC} = E_F - V_0$. Based on this local Fermi energy, we

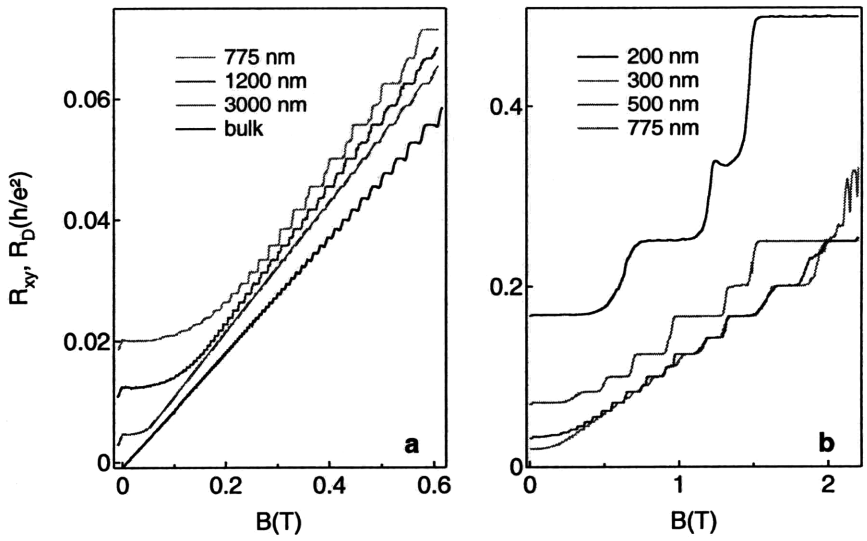

Figure 3-6: Diagonal resistance as a function of magnetic field in QPCs with different lithographic width illustrating the change in local electron density as a function of the width of the QPC. For comparison we also plot the Hall resistance in the bulk. Quantized resistance values are quoted in h/e^2. (a) Diagonal resistance in QPCs with lithographic width of 3000, 1200 and 775nm. (b) Diagonal resistance in QPCs with lithographic width of 775nm (same as in (a)), 500nm, 300nm and 200nm, respectively. Data are taken at $V_g = -3$ V.

define the electron density at the QPC by analogy with a 2D system:

$$n_S = \frac{E_F^{QPC} m}{\pi \hbar^2} \tag{3.13}$$

Note that no assumption about the shape of the confining potential is needed to estimate this electron density in this way.

In analogy with the two dimensional system, we assume that electron density is proportional to the slope of R_D as a function of magnetic field. To determine these electron densities in the QPC, by analogy to the standard method of determining density in a 2DEG from the Hall resistance, we perform linear fits to the high field region of the R_D data, averaging over quantized plateaus. By doing this, we find electron densities in the QPCs that depend on the effective width. The density decreases dramatically with decreasing lithographic width (see Fig.3-6).

3.6 Experimental data and discussion

As seen from the measurements of the diagonal resistance as a function of magnetic field (Fig. 3-6) decreasing the width of the QPC increases the resistance at zero magnetic field. When the field is increased from zero, the diagonal resistance is approximately constant until the magnetic field begins to deplete the quasi-1D electrical bands. However, at high field, R_D increases with the magnetic field in a way similar to the Hall resistance of the 2DEG.

In Figs. 3-7 and 3-8 we present the diagonal conductance (G_D) of the 300 and 200 nm QPCs, respectively, at various gate voltages. The change in gate voltage significantly changes the conductance at zero magnetic field. For example, for the 300 nm QPC, the conductance at zero field varies from $\approx 34\ e^2/h$ to $14\ e^2/h$ when V_g varies from -2 to -3 V. In the 200 nm QPC, the conductance varies from $\approx 23\ e^2/h$ to $4\ e^2/h$ when V_g varies from -2.3 to -3.1 V. Although the 2DEG has very high mobility we do not always observe conductance quantization at zero and low magnetic field: the conduction at zero magnetic field is not quantized until $V_g < -2.2$ V for the 300 nm QPC, or until $V_g < -2.1$ V for the 200 nm QPC, even though there is depletion under the gates at less negative voltages. However, at higher fields, the magnetic field acts to induce conductance quantization. For example, the data for $V_g = -2$ V in Fig. 3-7 show a zero field conductance $G_D(0) = 34e^2/h$, but the first visibly quantized conductance step in magnetic field occurs at $G_D(0) = 28e^2/h$. On the other hand, at a more negative gate voltage, for example $V_g = -3$ V, the quantized conductance steps are visible even at zero magnetic field. The number of observed quantized steps of $2e^2/h$, the number of Landau levels (when the quantization is first observed in a magnetic field), is labeled N_L.

The lack of conductance quantization at zero field can be understood assuming that the potential in the QPC is a saddle [13, 27, 55], where both the direction along the conduction channel and the one across it are parabolas. The potential is then $V(x,y) = V_0 + \frac{1}{2}m\omega_0^2 x^2 - \frac{1}{2}m\omega_y^2 y^2$, where x is the direction along the conduction channel. The Hamiltonian for an electron moving in this potential can be separated

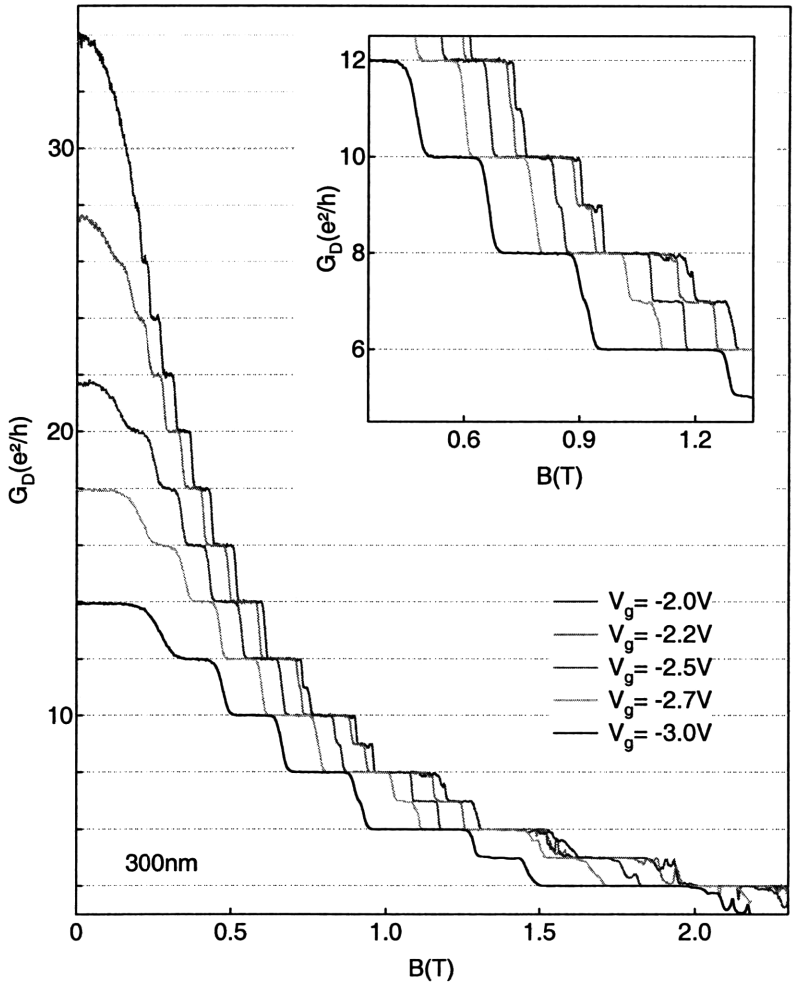

Figure 3-7: Diagonal conductance as a function of magnetic field for the 300nm QPC at various gate voltages. The dashed horizontal lines mark steps of $2e^2/h$. More negative gate voltage reduces the number of channels of conduction through the QPC at zero field. The inset is an expansion of the region where the spin splitting of the Landau levels disappears with decreasing magnetic field. The number spin-split Landau level decreases with more negative gate voltage.

into a transverse part with the energy levels of a harmonic oscillator $\hbar\omega_0(n+\frac{1}{2})$ with $n = 0, 1, 2, \ldots$, and a longitudinal part corresponding to conduction in an effective potential $V_0 + \hbar\omega_0(n+\frac{1}{2}) - \frac{1}{2}m\omega_y^2 y^2$, giving rise to the quasi-1D conduction bands (Landauer's conduction channels). In this context, the conductance can be thought of as a transmission problem of the individual bands over a barrier of height V_0. Each band scatters off of a barrier in the y direction, thus acquiring an intrinsic width equal to ω_y. The quantized conductance steps are visible if the gap between nearby states is larger than the broadening of the state $\omega_0 \geq \omega_y$ [13]. The applied magnetic field contributes to quantization and the condition is relaxed $\omega_c + \omega_0 \geq \omega_y$. Both ω_0 and ω_y are expected to depend on gate voltage, explaining why we observe conductance quantization at zero field only in certain QPCs and only for some gate voltage (see Figs. 3-7, 3-8).

At high enough magnetic field, at all values of V_g, the conductance quantization takes place in steps of e^2/h instead of $2e^2/h$, the signature of spin splitting. The magnetic field where the spin splitting of the Landau levels is first observed depends on the width of the QPC, occurring at higher field for narrower QPCs. In the insets of Figs. 3-7 and 3-8 we present expand the regions in field where the spin splitting is first observed in the 300 and 200 nm QPCs. The dashed horizontal lines mark multiples of $2e^2/h$, so the presence of a plateau half-way between these lines is a sign of spin splitting. The number of spin-split Landau levels is labeled N_S. In the bulk of the sample, signatures of spin splitting can be observed down to magnetic fields as low as 80 mT, corresponding to $N_S = 70$. The presence of the QPC reduces N_S to 42 for the widest QPC investigated and to only 1 for the narrowest one at $V_g = -3.1$ V. N_S depends on gate voltage: for example, in Fig. 3-7, at $V_g = -2$ V $N_S = 6$ ($G_D = 11e^2/h$) while at $V_g = -3$ V a spin-split plateau appears only at $G_D = 7e^2/h$, corresponding to $N_S = 4$. N_S also depends on the lithographic width of the QPC: in Fig. 3-8 at $V_g = -3$ V spin splitting is observed at $G_D = 3e^2/h$, corresponding to $N_S = 2$

We now analyze the aggregate data for all QPCs at all accessible gate voltages. In Fig. 3-9a the number of Landau levels N_L and the number of the spin-split Landau

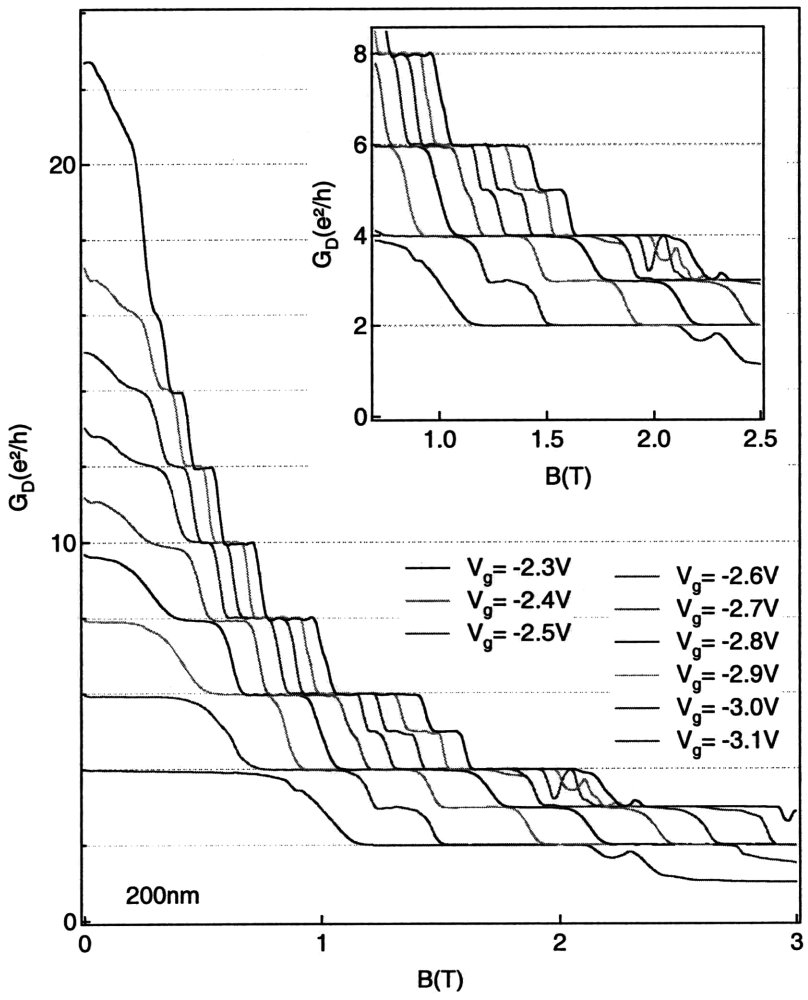

Figure 3-8: Diagonal conductance as a function of magnetic field for the 200nm QPC at various gate voltages. Dashed horizontal lines mark steps of $2e^2/h$. More negative gate voltage reduces the number of channels of conduction through the QPC at zero field. The inset is an expansion of the region where the spin splitting of Landau levels disappears with decreasing magnetic field. The number spin-split Landau level decreases with more negative gate voltage.

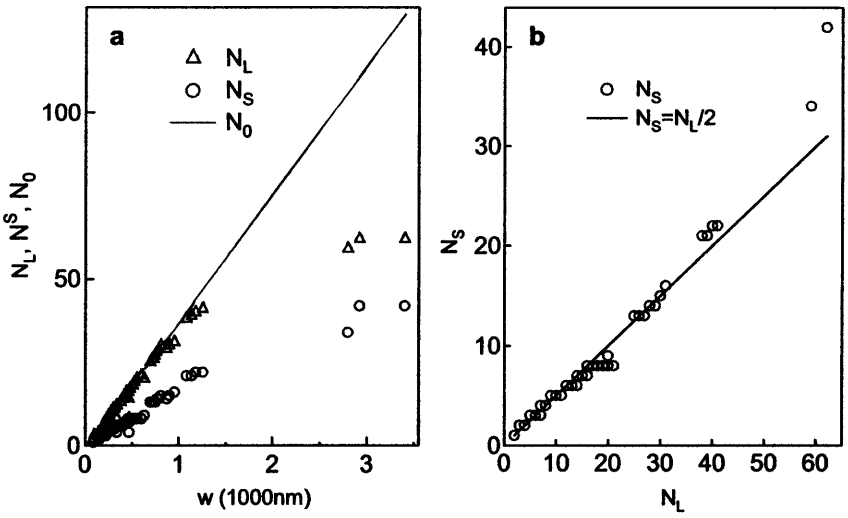

Figure 3-9: (a) The number of spin-split Landau levels N_S (red open circles) and the total number of Landau levels N_L (blue open triangles), for all QPCs at all the gate voltages measured, plotted against the effective width of the conduction channel W obtained using the parabolic potential approximation. For comparison, we show also the number of conduction channels at zero field N_0 (green solid line). (b)N_S plotted against N_L (red open circles). The black solid line is N_S=$N_L/2$.

levels N_S is plotted as a function of estimated QPC width. For reference, the number of conduction channels at zero magnetic field $N_0 = G_D(0)h/2e^2$ is also shown. The width is estimated using the parabolic approximation. As explained above, N_L and N_0 are not always the same; conductance quantization at zero field is present only for narrow enough lithographic width and negative enough gate voltage. It appears that both N_L and N_S level off at the largest widths. The number of Landau levels coincides with N_0 for $N_L < 32$. The number of spin-split Landau levels changes smoothly from 42 for the widest conduction channel (estimated to have a width $W \sim 3500$ nm) to only one for the narrowest conduction channel ($W \sim 70$ nm).

In Fig. 3-9b we plot the number of spin-split Landau levels versus the total number of quantized Landau levels. The black line represents $N_S = N_L/2$. The number of spin-split Landau levels is approximately half the total number of Landau levels for QPCs with effective width less than about 1200 nm, or $N_L < 32$. It is interesting to note that below this number of levels the conduction at zero field becomes quantized and $N_L = N_0$, suggesting that the two phenomena are related. Conductance quan-

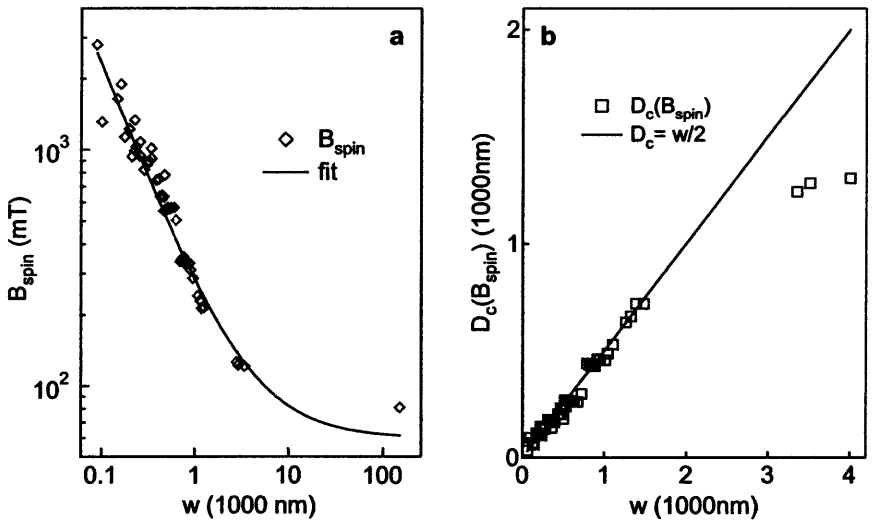

Figure 3-10: (a) Magnetic field where the first spin-split Landau level occurs B_{spin} vs effective width (obtained assuming a parabolic potential). The data point at 150000 nm (the width of the Hall bar) represents the bulk, where the onset of spin splitting occurs at 80 mT with $N_S = 70$. The black line is a fit to a power law with saturation at large width: $B_{spin} = 45.8 + 230890/\mathrm{W}$, with B_{spin} expressed in mT and the width in nm. (b) Cyclotron diameter at the magnetic field where the spin splitting first appears vs. effective width. The black solid line is $D_c = \mathrm{W}/2$.

tization at zero magnetic field ($N_L = N_0$) can be understood, as explained above, in terms of level broadening caused by scattering from the electrostatic potential of the gates.

The magnetic field where the first spin-split Landau level occurs B_{spin} is plotted as a function of effective QPC width in Fig. 3-10a. The data point at the largest width (150 μm, the lithographic width of the Hall bar) corresponds to the bulk of the sample. For all other data points, the width is identical to the one in Fig. 3-9a. B_{spin} increases with decreasing QPC width W, and it is interesting that this dependance can be fit very well by a power law with a saturation at large W. The black line in Fig. 3-10a is the best fit to the data with a power law: $B_{spin} = B_\infty + a/\mathrm{W}$, with B_{spin} expressed in mT and the width in nm. $B_\infty = 45.8$ mT and $a = 230890$ mTnm. A nonzero B_∞ means that spin-splitting is suppressed even in the absence of confinement. Possible sources of suppression could be sample disorder or temperature. The proportionality between B_{spin} and the inverse of the width suggests a simple relation between the cyclotron radius at B_{spin} and the width. Using the electron sheet density estimated as

explained above, we estimate the cyclotron diameter D_c associated with B_{spin}. This is plotted versus effective width in Fig. 3-10b. For width less than ~1500 nm, the cyclotron diameter at B_{spin} is half of the width of the QPC. This fact is in accordance with a possible intuitive explanation for the disappearance of spin splitting: the spin splitting disappears when the wavefunctions on opposite sides of the QPC start to overlap [103].

3.7 Discussion and conclusions

The suppression of spin splitting in Landau levels is difficult to explore because we have no direct access to the energy gaps associated with it. Whereas in 2DEGs or QPCs in parallel magnetic field [85, 84] the gaps associated with Landau and spin-split Landau levels can be estimated using temperature activation measurements, no such method can be applied for measuring energy gaps in QPCs in perpendicular magnetic fields. The conductance through the QPC in perpendicular magnetic field does not reflect solely the properties of the electron system in the QPC but also, partially, the properties of the surrounding 2DES. This happens because the carrier density associated with the QPC is lower than the 2DEG density (as seen above). Similarly, we expect that measurements using a finite source-drain bias do not provide information on the energy gaps associated with the QPC alone. The lack of access to direct energy measurements limits the information that can be obtained about spin splitting to noting the field where the splitting first appears, or to counting the number of the spin-split Landau levels.

Ihnatsenka and Zozoulenko [38, 37, 39] have calculated the transmission of QPCs in a magnetic field and investigated the disappearance of the spin splitting below a critical field, B_{spin}. In their calculations, they assume an infinitely long channel where the total potential is calculated self-consistently assuming that the bare electrostatic confinement induced by the gates is a parabolic potential. Some of their numerical calculations are performed for one of our QPCs. For a channel with zero-field conductance $G(0) = 50e^2/h$ they find quantized conductance at zero magnetic field

($N_L = 26$) and $N_S = 11$ [39]. The calculated conductance is similar to that of our 500 nm QPC at gate voltage -2.0 V (see Fig. 6 in Ref. [39]), which has $G(0) = 46e^2/h$ and $N_S = 9$. However, while the latter QPC has $G(0) = 46e^2/h$, close to the theoretical one, it has only $N_L = 17$ quantized channels. Ihnatsenka and Zozoulenko argue that the odd conductance steps disappear when the extent of the wave function describing the states becomes much larger than the width of a compressible strip [17] in the center of the wire. This compressible strip arises from the competition between the spin excitation energy, the Coulomb interaction and the confinement potential. Based on a strictly electrostatic calculation, an analytical formula giving the width of the compressible strip has been proposed by Chklovskii *et al.* [17]. Its width is proportional to the energy gap of the spin-split state. Comparison with the current experiment are difficult since, as mentioned above, no direct information about the size of the energy gap associated with the spin-split Landau levels can be obtained in a transport measurement in a QPC in perpendicular magnetic field.

We can attempt to estimate the width of the central compressible strip using the bulk 2DEG value of the spin-splitting energy. It is well known that for the 2DEG the bare Zeeman gap ($E_Z = g_0\mu_B B$) is not large enough to account for the spin-splitting energy. Instead the gap for spin flips is given by $\Delta_s = E_Z + E_{ex}$, where E_{ex} is the exchange energy. Δ_s can be estimated from the thermal activation measurements of R_{xx} near its minima, assuming that R_{xx} is limited by the density of quasiparticles thermally excited across the gap we are estimating. It has been proposed that in transport measurements the spin gap at constant density is linear[1] in magnetic field [50]. Then one can define an effective g factor g^*, such that

$$\Delta_S = g^*\mu_B B. \tag{3.14}$$

For our system, $g^* = 3.35$, approximately 8 times larger then the bare g_0 factor for GaAs. Assuming that the spin gap in the QPC is given by the same formula (3.14), where the magnetic field is given by B_{spin}, then we can estimate the width of the

[1]Capacitance measurements [20] have found that the exchange energy is proportional to $B^{3/2}$.

central compressible strip. Following this recipe, we do not find agreement between our data and the proposed origin of the spin splitting disappearance [39].

To conclude, in this chapter, we have presented transport measurements in a perpendicular magnetic field through QPCs formed by gates of various lithographic widths on a very high mobility 2DEG. By varying the applied gate voltage we can control the width of the conduction channel continuously from $\sim$ 3000 nm to $\sim$ 100 nm, corresponding to a range of quantized conductance channels at low field from 62 to 2. Surprisingly, we find that the number of spin-split Landau levels is approximately equal to half the number of visibly quantized conductance steps at low field for effective QPC widths less than $\sim$1200 nm. We also find that the cyclotron diameter at the magnetic field where the spin splitting first appears is approximately half of the effective width of the QPC. This seems to indicate that the spin splitting of the Landau levels disappears when the wavefunctions at the opposite sides of the QPC start to overlap.

Chapter 4

Quasiparticle Tunneling in the Fractional Quantum Hall Effect at $\nu = 5/2$ — experimental

4.1 Introduction

As we have seen in Chapter 2, the fractional quantum Hall effect (FQHE) [87] results from the formation of novel states in a two-dimensional electron system (2DEG) at high magnetic field and low temperature, in which electron-electron interactions lead to gaps in the bulk excitation spectra. Because of these gaps, current can only flow via extended states that propagate around the edges of the 2DEG [33]. Theory predicts that if two such counter-propagating edges are brought together close enough, then quasiparticles that form in these FQHE states can tunnel between them. Experimentally, this can be realized with a quantum point contact (QPC) patterned on the 2DEG. If the tunneling probability is small, known as the weak tunneling regime [95], the tunneling current is predicted by theory to depend strongly on the voltage difference between the edges (or, because of the Hall effect, the overall current through the QPC) and to scale with temperature in a way that provides a measurement of the effective charge, e^*, of the quasiparticles and the strength of the Coulomb

interaction, g. Since both e^* and g are specific to the wavefunction describing the FQHE state, tunneling can be used to gain insight into the properties of FQHE wavefunctions. In Chapter 2, we have also pointed out that several wavefunctions have been proposed to describe the state at $\nu = 5/2$ and although all predict the same $e^* = 1/4$ [32, 60, 92, 52, 51, 34, 35, 94], they have different values of the interaction parameter g [96, 10, 26, 52, 51]. Thus tunneling can be used to discriminate between possible $\nu = 5/2$ wavefunctions, although tunneling alone does not provide direct evidence about the non-abelian statistics of the quasiparticles.

Using shot noise techniques [19, 75], recent experiments have investigated the quasiparticle charge for $\nu = 5/2$ [21] and have found values consistent with theoretical predictions. Previous experiments have investigated qualitatively quasiparticle tunneling using gated devices in the regime where the filling fraction in the QPC and the bulk are not equal at $\nu = 5/2$ [56] and at $\nu < 1$ [73, 72, 74]. The process where electrons, not quasiparticles, tunnel between edge states at $\nu = 1/3$ through vacuum, has been studied in Ref. [58]; for these experiments the authors have extracted $g = 3$ consistent with theoretical predictions.

In this chapter we present experimental studies of quasiparticle tunneling at $\nu = 5/2$, in which approximately the same filling fraction is maintained in the QPC and the bulk of the sample. Maintaining the same filing fraction is a prerequisite for preserving the edge states through the constriction. Previous studies of tunneling in the FQHE regime have employed QPCs with significantly different filling fractions in the vicinity of the QPC with respect to the bulk [73, 72, 74, 56] thus making any comparison to existing theoretical predictions difficult. The tunneling conductance in our QPCs exhibits a zero-bias peak that scales with temperature in quantitative agreement with the theory for weak tunneling [95, 10, 26], demonstrating that interedge tunneling of quasiparticles can be achieved. We extract e^* and g, and, based on the value of g, we observe that two non-abelian states, the anti-Pfaffian [51, 52] and the $U(1) \times SU_2(2)$ [92] are most consistent with our data. A version of this chapter has been published in the journal Science [69].

4.2 Sample

The samples used in the experiments presented in this chapter consist of a high mobility GaAs/AlGaAs heterostructure (same as the one used in Chap. 3), with the 2DEG 200 nm below the surface and two Si δ-doping layers positioned symmetrically 100 nm on each side of the 2DEG. The mobility of the 2DES is estimated to be 2000 m^2/Vs and the carrier density 2.5×10^{15} m^{-2}. The energy gap at $\nu = 5/2$ is estimated to be $\sim$ 130 mK [56]. Hall bars with a width of 150 μm are patterned on this heterostructure using optical lithography and wet etching. A micrograph of such a Hall bar is presented in Fig. 3-1. On the Hall bar, metallic (Cr/Au) gates which form the QPCs have been pattered using e-beam lithography and lift-off. When a negative gate voltage V_g is applied to these gates, the 2DEG underneath is depleted, creating constrictions tunable with V_g. The measurements presented in this chapter are performed on devices with two different gate geometries, as shown in Fig. 4-1. Device 1 is a simple QPC, one of those used in Chapter 3, with gate separation of $\sim$800 nm. Device 2 is a channel $\sim$1200 nm wide, formed by energizing the gates marked G1, G2, G3 and G4 (gates A1 and A2 are held at ground and not used in this experiment). When forming the constrictions, we apply the same voltage V_g to all lithographic gates defining the device. The electrons under the gates are eliminated at voltages $V_g < -1.8$ V. For this reason, data have been acquired at $V_g < -2.0$ V to insure that the gates are fully depleted.

The sample is mounted on a cold finger attached to the mixing chamber of a dilution refrigerator with a base temperature of less than 10 mK in a magnetic field oriented perpendicular to the plane of the 2DES. The actual electron temperature is higher than the mixing chamber temperature for temperatures lower than $\approx$ 20 mK. Temperatures below 20 mK have been estimated using a combination of resonant electron tunneling in lateral quantum dots and by tracking several quantum Hall effect features as a function of temperature as detailed in Chapter 5. In the data analysis presented below, we use the electron temperature.

The heterostructure has been grown at Bell Labs by Loren Pfeiffer and Ken West.

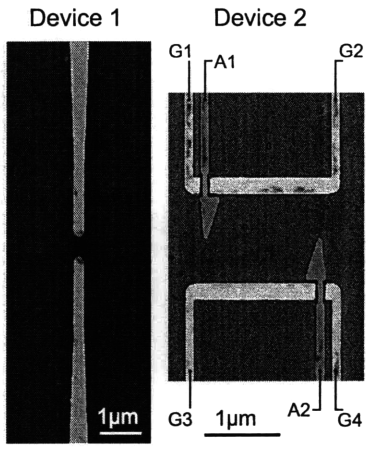

Figure 4-1: SEM micrograph of devices similar to those used in the experiments presented in this chapter. Device 1 is a simple QPC with a split-gate geometry. Device 2 is channel $\sim$ 1200 nm wide, formed by applying a negative voltage to gates G1, G2, G3 and G4. The gates marked A1 and A2 (greyed out) are held at ground.

Jeff Miller from the Marcus Group has patterned the QPC devices on this heterostructure at Harvard. Measurements have been made at MIT in the Kastner Lab. Details of the sample preparation can be found in Ref. [57].

4.3 Measurement details

Measurements were performed in a four-terminal configuration, similar to those described in Chapter 3 in section 3.3. We employed a lock-in technique with the ac current excitation ranging from 100 to 400 pA and in certain cases a dc bias current of up to 20 nA.

The significant quantity for these tunneling experiments is the tunneling current (or the tunneling conductance), however, no measurement probes it directly. To determine the tunneling conductance g_T, we simultaneously measure the Hall resistance R_{xy} and the diagonal resistance R_D (voltage probes on opposite sides of the Hall bar and also opposite sides of the QPC) [7, 56]. Details of these measurements are given in Chapter 3. In the weak tunneling regime [95], when the bulk of the sample is at a quantum Hall plateau, the tunneling voltage is the same as the Hall voltage, while

g_T is related to R_D by:

$$g_T = \frac{R_D - R_{xy}}{R_{xy}^2} \tag{4.1}$$

Note that R_{xy} is independent of dc bias when the bulk of the sample is at a FQHE plateau.

4.4 Annealing

One of the key differences between the experiments presented in this chapter and those in Chapter 3 is the electron density in the constriction relative to that in the bulk. In the former, when the gates are energized, the density in the QPC is significantly smaller than in the bulk of the sample. For example, for device 1 the difference in density is ~15%. In the experiments presented below, we are able to eliminate the electrons under the gates and induce inter-edge tunneling without changing the density and hence the filling number in the constriction significantly. To achieve this we energize the gates at 4 K, by applying the most negative gate voltage we plan to use in the experiments (usually -3 V). We allow the system to relax at this relatively high temperature for a few hours, then cool the sample to base temperature and while at low temperature we limit V_g to the range -2 to -3 V.

To verify that the same state forms in the QPC and bulk we take magnetic field sweeps encompassing several integer plateaus (as shown in Fig. 4-2a). The integer plateaus in bulk and QPC overlap almost perfectly and are quantized in both cases at the expected values. At the fractional plateaus, in the QPC, extra resistance consistent with tunneling in the QPC is observed. Additional evidence that the densities are the same in the QPC and bulk comes from low magnetic field data (Fig. 4-2b): the slopes of R_{xy} and R_D as a function of field are virtually identical, which requires the same electron density in the QPC and bulk within 2%. For comparison, we also show a data trace taken with a QPC where the gate voltage has been applied at base temperature (not annealed): in this case the slope of R_D as a function of field is significantly higher, implying that the electron density in the QPC is lower by $\sim$ 15% than the bulk. For clarity, this last trace has been offset vertically by

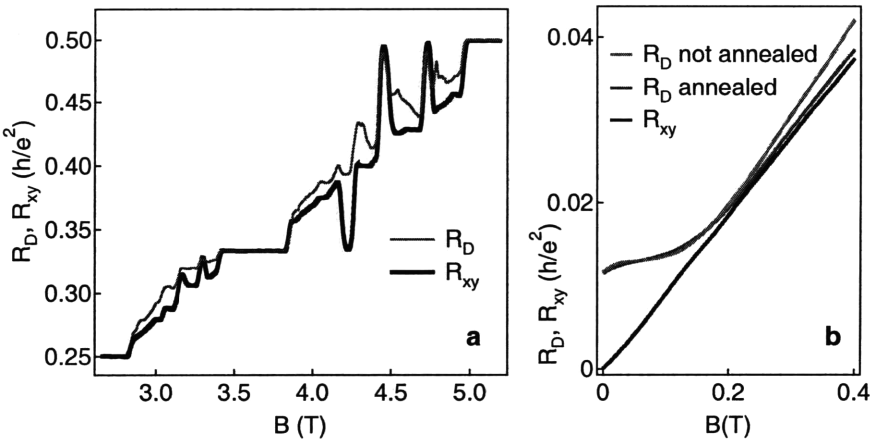

Figure 4-2: (a) Magnetic field dependence of the diagonal (R_D) and Hall (R_{xy}) resistance for device 2 at fixed gate voltage from $\nu = 2$ to $\nu = 4$ illustrating that both the QPC and the bulk are at the same filling fraction. (b) Low-field data from the same device (device 2) emphasizing that the carrier density in the annealed QPC is nearly the same as that of the bulk (red and black traces with almost matching slopes), while in the non-annealed QPC (green trace) the density shifts significantly. For clarity, the non-annealed data has been offset vertically by 0.003 h/e^2.

0.003 h/e^2 so that the traces have approximately the same value of resistance as the data with the annealed constriction at zero magnetic field. Keeping the same filling number in the QPC and the bulk of the sample facilitates the comparison with the theory of quasiparticle tunneling, and it is one of the fundamental differences between this work and previous tunneling experiments [73, 72, 74, 56].

4.5 Bias and temperature dependence

We present the dependence of g_T on both the current through the QPC I_{dc} and the magnetic field in Fig. 4-3 at four different temperatures. When applying a dc current bias, g_T shows a zero-bias peak above fractional plateaus while R_{xy} is independent of dc bias, for the investigated range in dc bias. At base temperature (Fig. 4-3a) when scanning the magnetic field the reentrant integer quantum Hall states (RIQHS)[1] cause the dc bias dependence to be more complicated. At the RIQHS, the bulk of the

[1]RIQHS, as the name says, are integer Hall effect states which form (R_{xy} is quantized at some integer value) at filling numbers that are not integers (re-enter). These states are usually observed in the second Landau level and only in very high mobility samples.

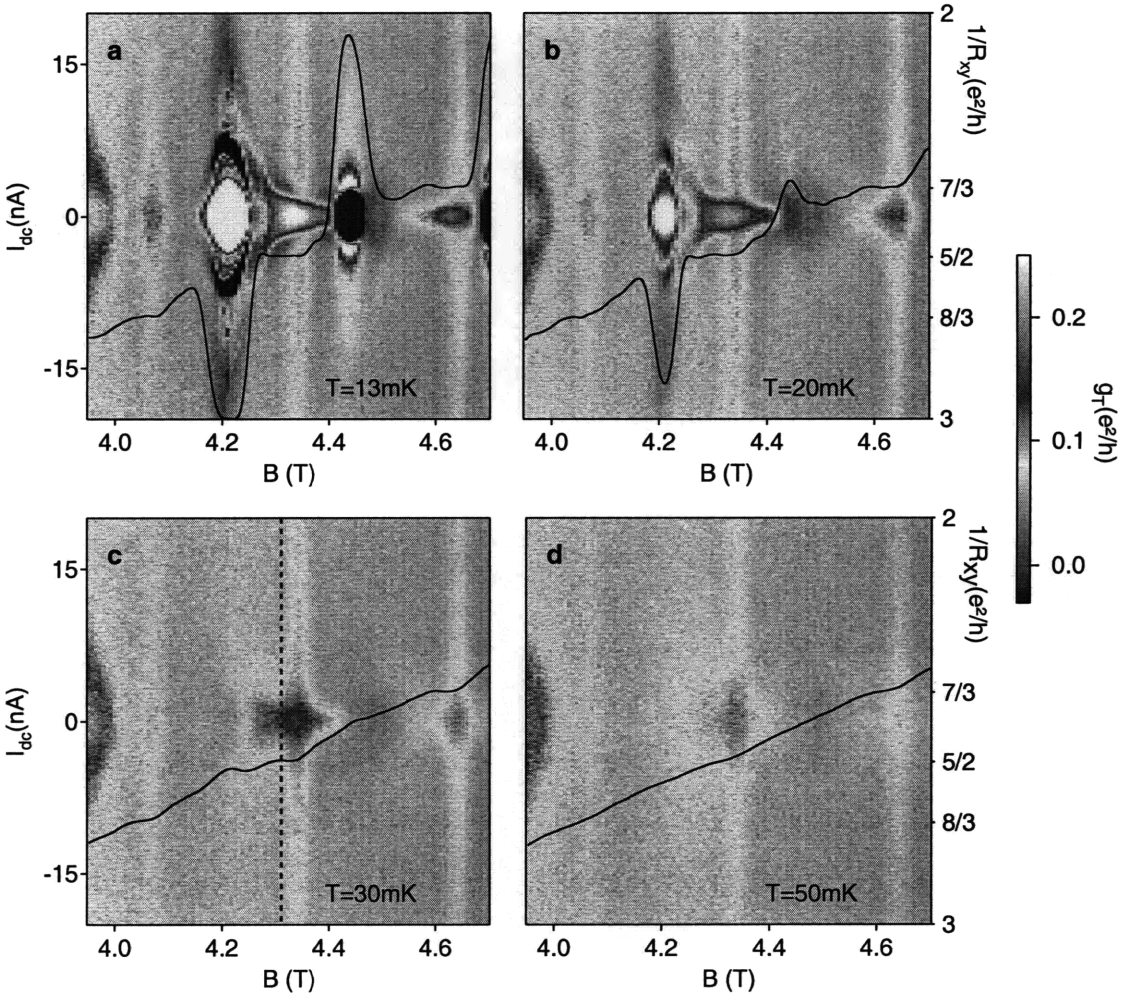

Figure 4-3: Differential tunneling conductance g_T (device 2) as a function of magnetic field and dc bias current at several temperatures: (a) T=13 mK, (b) T=20 mK, (c) T=30 mK, (d) T=50 mK. On each graph, the zero-dc-bias R_{xy} trace from the same temperature is superimposed (right axis). The field range encompasses the FQHE states 7/3, 5/2 and 8/3. At the higher temperatures, dc bias non-linearities exist only at the fractional plateaus. All other features, such as those from the re-entrant quantum Hall effect, disappear at $\sim$ 30 mK. The vertical red line in panel c marks the center of the $\nu = 5/2$ plateau in bulk.

sample exhibits dc bias dependence (not shown) whereas it shows no bias dependence at any other fields. Despite this complexity, identifying the region where quasiparticle tunneling can be studied is fairly simple. As the temperature increases from Fig 4-3a to Fig. 4-3d, the zero dc bias peaks above FQHE states decrease in height but do not disappear completely even at the highest temperature. Over the same temperature range, the dc bias dependence associated with the RIQHS disappears above 20 mK. The bulk of the sample, represented here by black curves superimposed on the QPC dependence, shows a similar behavior as a function of temperature, with the RIQHS disappearing completely above 20 mK, while the fractional plateaus are still present even at 50 mK (Fig. 4-3d). The data shown in Fig. 4-3 are for device 2. However, qualitatively similar results are obtained for device 1.

To study quasiparticle tunneling at a FQHE state we set the magnetic field to the center of the corresponding bulk plateau. For $\nu = 5/2$, the magnetic fields are $B = 4.31$ T for device 2, the position of the vertical dashed line in Fig. 4-3, and $B = 4.3$ T for device 1. Although the two devices are fabricated on the same heterostructure, the chips come from different parts of the wafer and because of a small electron density gradient in the wafer, the $\nu = 5/2$ forms at slightly different magnetic fields in the two devices.

With the field set at the center of the fractional plateau in the bulk (red dashed line in Fig. 4-3c), we maximize the effect of tunneling with the aid of the applied gate voltage by measuring g_T as a function of both V_g and I_{dc}, at various temperatures (see Fig. 4-4). At the lowest temperatures (Fig. 4-4a), the zero-bias peak persists throughout the V_g range. At higher temperatures, a peak in both dc bias and V_g is observed, centered near $V_g = -2.5$ V (Fig. 4-4d and e). To study quasiparticle tunneling, we set V_g to the center of this peak (marked with a dashed line in Fig. 4-4), the feature that persists to the highest temperature, because theory predicts that tunneling decreases slowly, as a power law, with temperature.

After we follow this recipe for finding the region where quasiparticle tunneling is most likely, we fix both the magnetic field and V_g at those values and acquire dc bias data at various temperatures (see Fig. 4-5). These data have been acquired at

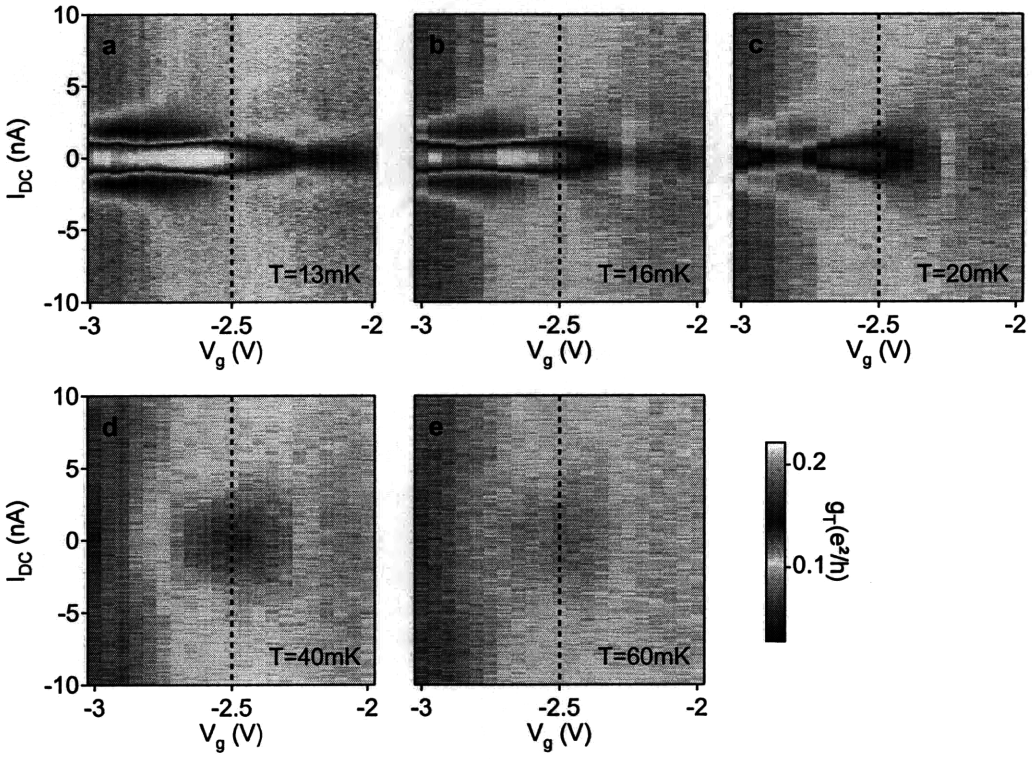

Figure 4-4: Differential tunneling conductance g_T (device 1) as a function of V_g and dc bias current at several temperatures: (a) T=13 mK, (b) T=16 mK, (c) T=20 mK, (d) T=40 mK, (e) T=60 mK. A peak in both dc bias and V_g becomes visible at T=40 mK. The vertical dashed line marks the center of this resonance.

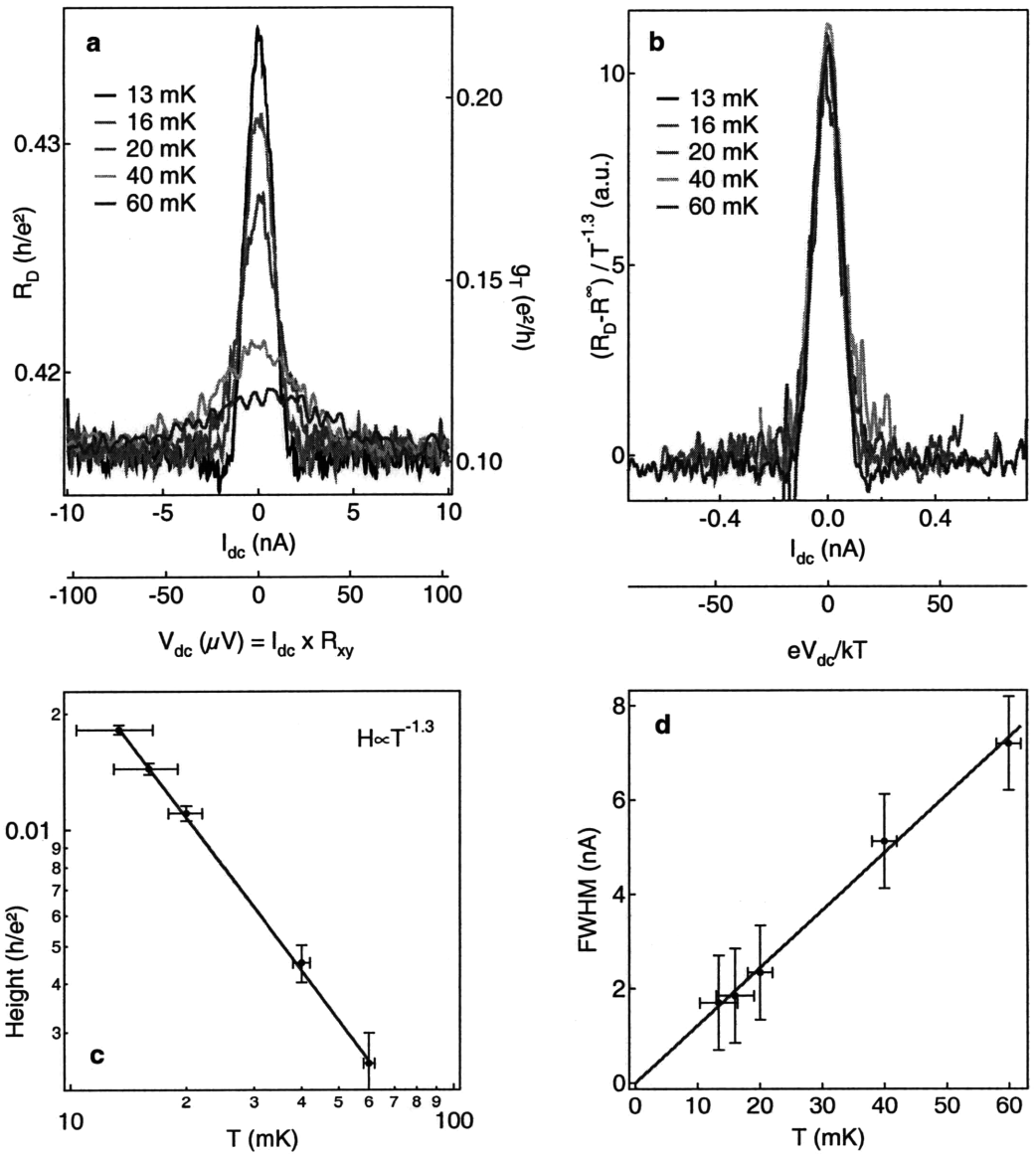

Figure 4-5: (a) R_D (device 1) as a function of dc bias at fixed magnetic field (B=4.3 T, middle of $\nu = 5/2$) and fixed gate voltage (V_g=-2.5 V) at several temperatures. R_{xy} is independent of dc bias over the range of I_{dc} (not shown), which makes the bias dependence of R_D proportional to that of g_T (right axis) up to a constant (0.4 h/e^2). (b) Data collapsed onto a single curve using a power law of -1.3. (c) Zero dc bias peak height as a function of temperature. The red line is the best fit with a power law where the power is -1.3. (d) The peak full width at half maximum (FWHM) as a function of temperature. The red line is best fit with a line going through zero.

B=4.3 T and V_g = -2.5 V (dashed red line in Fig. 4-4) using device 1. We present the data as both R_D plotted against the left axis and in units of g_T on the right axis. Since in the weak tunneling picture the voltage drop between the two counterpropagating edge states in the QPC is the dc current multiplied by the Hall resistance, we have labeled the horizontal axis with both the current and the dc voltage, using $R_{xy} = 0.4\ h/e^2$ [95]. Traces representing individual temperatures saturate at high dc bias at a common value R^{∞}, higher than the expected 0.40 h/e^2. It is worth noting that the height of the zero bias peak (measured from R^{∞}) decreases with increasing temperature — a clear non-Fermi liquid signature. The peak height follows a power law as a function of temperature with a power of -1.3 (Fig. 4-5c), while the peak width expressed here in terms of full width at half maximum (FWHM) (measured from the common high bias background) increases linearly with temperature (see Fig. 4-5d) and extrapolates to zero at zero temperature, consistent with a zero intrinsic line-width. The data can be collapsed onto a single curve (Fig. 4-5) when the horizontal axis is scaled by T and the vertical axis is scaled by $T^{-1.3}$ (after subtracting the common background R^{∞}), indicating once more that weak tunneling theory can be applied to these data. In this case, the horizontal axis is also labeled by a dimensionless measure of energy difference between opposite edges: eV_{dc}/kT.

4.6 Extracting g and e*

Both the power law dependance of peak height and the zero intrinsic line-width of the zero bias peak are consistent with theoretical predictions for weak quasiparticle tunneling between fractional edge states [95, 10, 26]. In the weak tunneling theory, the zero bias peak height is expected to vary with temperature as T^{2g-2}, where g is the measure of the interaction strength. This would produce $g = 0.35$ for the data in Fig. 4-5. The theoretical calculations give a functional form for the combined dc bias and temperature dependence.

$$g_T(T, I_{dc}) = AT^{(2g-2)} F\left(g, \frac{e^* I_{dc} R_{xy}}{kT}\right), \tag{4.2}$$

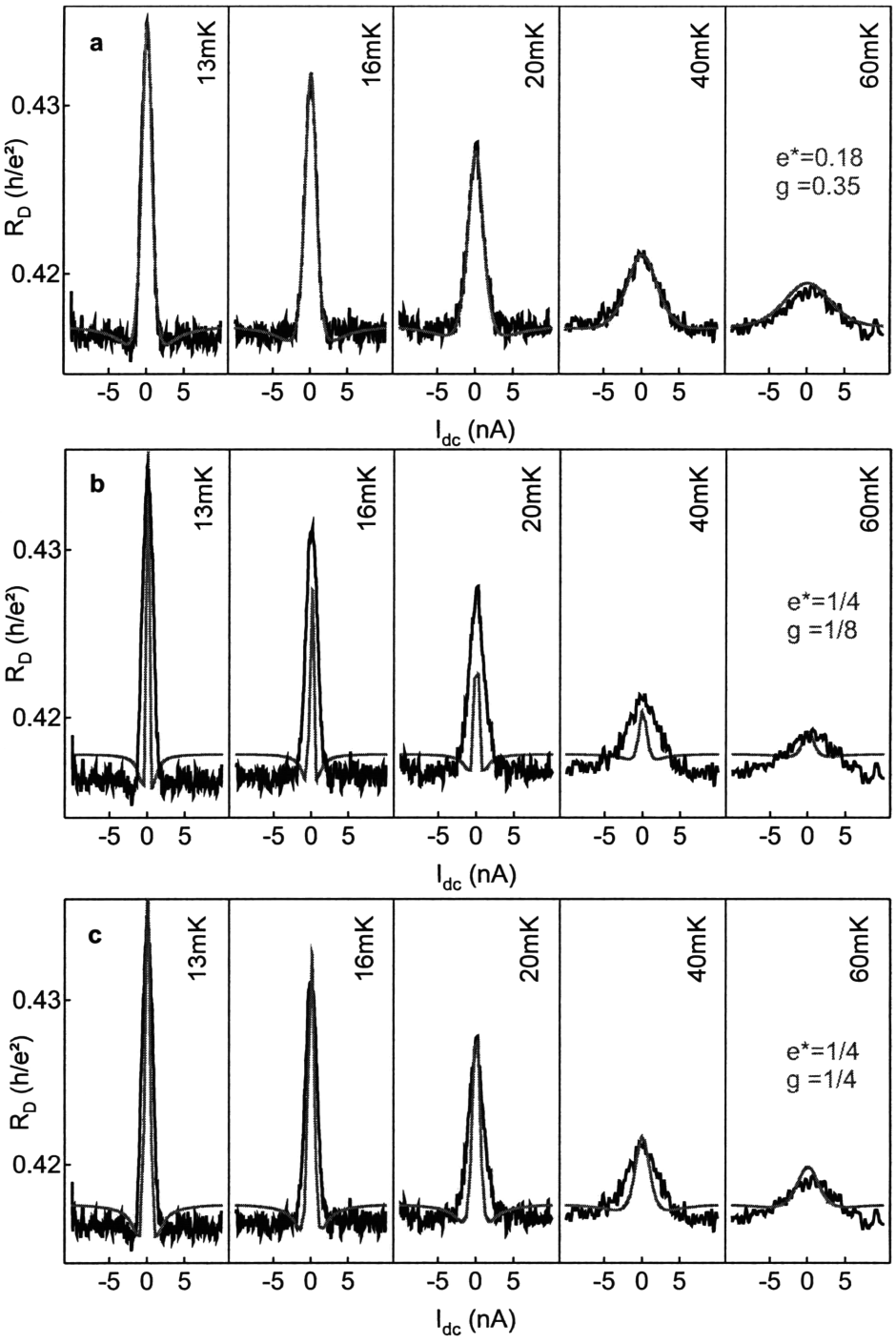

Figure 4-6: (a) Best fit of all the data in Fig.4-5 with the weak tunneling formula (eq. 2) returns $e^* = 0.18$ and $g = 0.35$. (b) Fit to the data holding $e^* = 1/4$ and $g = 1/8$ as predicted for the K8 state [94]. (c) Fit to the data holding $e^* = 1/4$ and $g = 1/4$ as predicted for the Pfaffian state [60, 96].

with

$$F(g,x) = B\left(g + i\frac{x}{2\pi}, g - i\frac{x}{2\pi}\right)\left\{\pi\cosh(x/2) - 2\sinh(x/2)Im\left[\Psi\left(g + i\frac{x}{2\pi}\right)\right]\right\} \tag{4.3}$$

where e* is the charge of the quasiparticle expressed on units of e (charge of the electron) and k is the Boltzmann constant. $B(x,y)$ represents the Euler beta function and $\Psi(x)$ is the digamma function. This formula, which reduces to the power-law temperature dependence at zero bias, allows us to extract not only a g parameter but also e^*.

Eqs. 4.2 and 4.3 yield an excellent fit as seen in Fig.4-6a. All five temperatures are fit simultaneously with four free parameters: a vertical offset corresponding to R^∞, an amplitude A, and the two quantities g and e^* that characterize the tunneling quasiparticle. The best fit returns $g = 0.35$, the same value found from the power law fit of the peak heights (Fig. 4-5c), and $e^* = 0.18$, which is within error of the predicted $e^* = 1/4$, as discussed below. These results show that the data are consistent with quasiparticle tunneling. Similar analysis performed on data from a different device (device 2 with only gates G1 and G4 biased) yields quantitatively similar results.

Placing error bars on our fits is a delicate matter since the conductance follows a power law in temperature, but the accessible temperature range is limited on the low side by the experimental apparatus and on the high side by the disappearance of the 5/2 state in the QPC. This gives us access to less than a decade in temperature. Therefore, rather than fitting only the peak height as in Fig. 4-5c, to reduce the error bars we fit the entire dc bias range with the functional form 4.2 as in Fig. 4-6a. For a visually compelling way of looking at the quality of the fit, we perform a matrix of fits with fixed pairs (e^*,g), leaving only A and R^∞ as free fit parameters. To assess the quality of each fit we define a normalized fit error which is given by the residual of the fit per point divided by the noise of the measurement (0.0005 h/e^2). When this parameter is ≤ 1, it indicates that the fit is consistent with the data within the noise of the measurement. Higher values indicate worse fits, with values ≥ 1.5 indicating fits with discrepancies clearly larger than the noise. The fit matrix, along with several

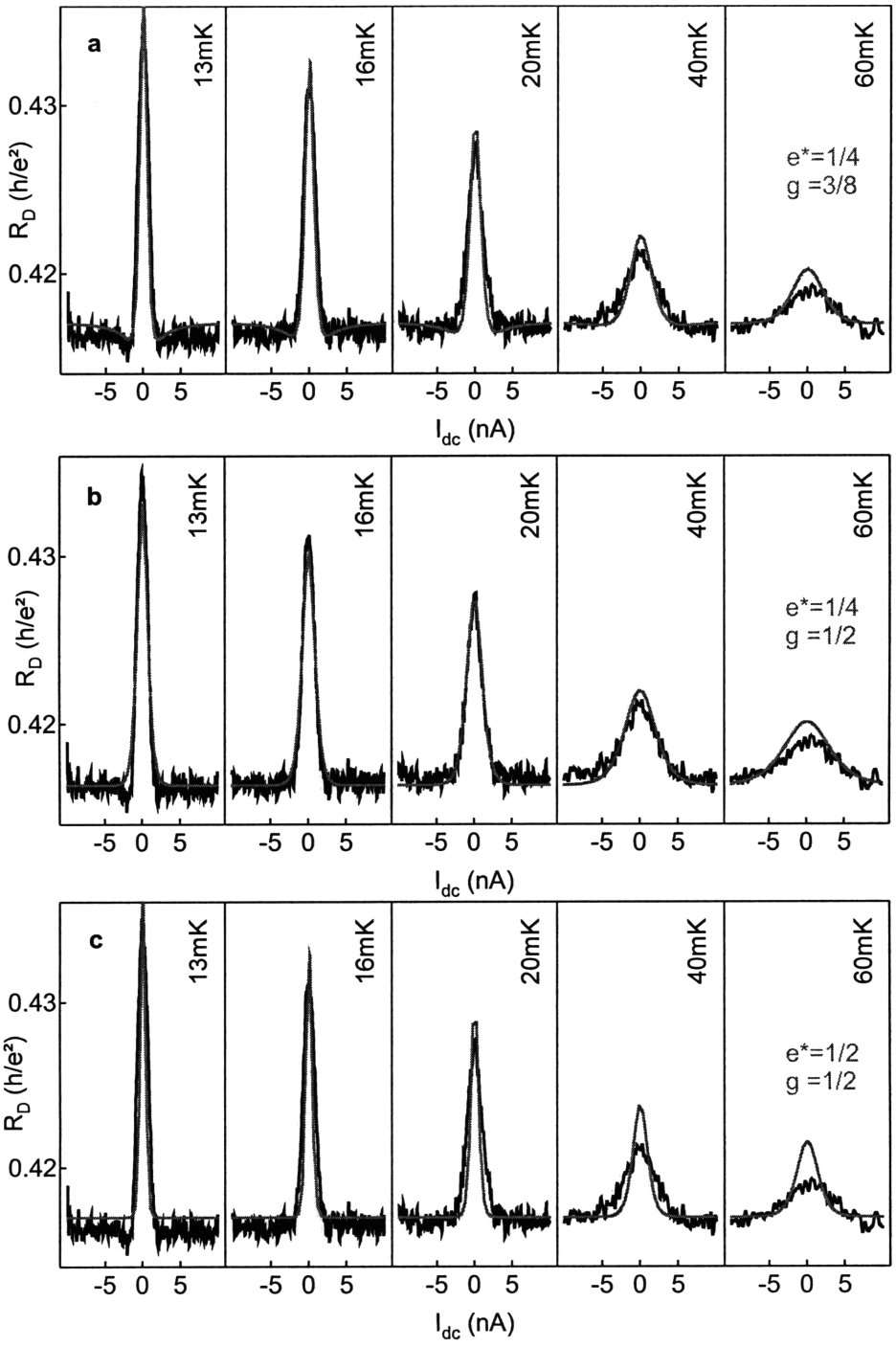

Figure 4-7: (a) Fit to the data holding $e^* = 1/4$ and $g = 3/8$ as predicted for the 331 state [34, 35]. (b) Fit to the data holding $e^* = 1/4$ and $g = 1/2$ as predicted for the Anti-Pfaffian [52, 51, 10] and the $U(1) \times SU_2(2)$ [92] states. (c) Fit to the data holding $e^* = 1/2$ and $g = 1/2$ as expected for composite fermions

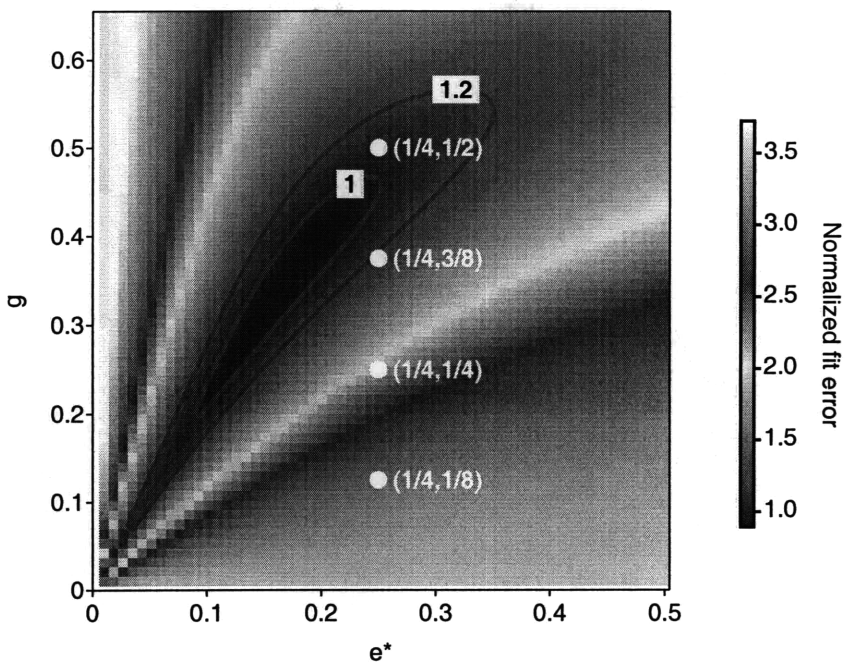

Figure 4-8: Map of the fit quality. Least squares fit of the data in Fig. 4-5 using the weak tunneling formula and holding pairs (e^*,g) fixed for each point of the map. The normalized fit error represents the residual per point divided by the noise of the measurement. Also marked on the map are proposed theoretical pairs (e^*,g).

constant-value contours, are shown in Fig. 4-8.

For clarity in comparing the quality of the fit with possible pairs (e^*, g), fits with the pairs highlighted in Fig. 4-8 are presented in Figures 4-6b and c and Figure 4-7. In Figs. 4-6b and c we present the fits with the fixed pair $e^* = 1/4$ and $g = 1/8$ corresponding to the K8 state [94] and the pair $e^* = 1/4$ and $g = 1/4$ corresponding to the Pfaffian state [60, 96]; Fig. 4-7a presents the fit with the fixed pairs $e^* = 1/4$ and $g = 3/8$ corresponding to the 331 state [34, 35]; Fig. 4-7b presents the fit with and the pair $e^* = 1/4$ and $g = 1/2$ corresponding to the Anti-Pfaffian [52, 51, 10] and the $U(1) \times SU_2(2)$ [92] states, respectively. Fig. 4-7c displays the fit with the fixed pair $e^* = 1/2$ and $g = 1/2$ as expected for the composite fermions. For all these fits, the only two free parameters are the amplitude A and R^∞. It is apparent from these figures that some of the fits work better than others. For example the fit with the pair (e^*,g)=(1/4,1/8) fails to reproduce not only the height of the peaks but also their width. The pair (e^*,g)=(1/4,1/4) works better but still underestimates the widths of

the peaks. The pair (e^*,g)=(1/4,3/8) tends to overestimate the height of the peaks especially at the higher temperatures. The pair (e^*,g)=(1/4,1/2) returns the best fit of all the theoretically predicted pairs, while the pair (e^*,g)=(1/2,1/2) corresponding to unpaired composite fermions fails to reproduce both the width and the height of the peaks.

4.7 Strong tunneling

The discussion so far has involved weak tunneling in the QPC. Although there are no exact theoretical predictions that apply to the strong tunneling limit or intermediate strength tunneling, for the states enumerated above, a set of qualitative theoretical expectations do exist [25] and qualitative cross-checks with strong tunneling data [73, 72, 74] and theoretical predictions for other states (such as $\nu = 1/3$) can be performed. Were we to extend the weak tunneling theory to the limit where either the temperature goes to zero or the coupling between the edges becomes large, we would find that the tunneling conductance diverges. However, as we have seen in Chapter 2, the weak tunneling theory is just a perturbation theory, where the highest term is a second order one. Since the perturbation diverges in the strong coupling limit, this can no longer apply. To gain intuition about the zero-bias conductance one begins by summing higher order perturbation terms. It has been shown that by doing so the singularity is lifted, and instead of a divergence at zero dc bias, the tunneling conductance saturates when the edge where the tunneling occurs is backscattered entirely by the tunneling across the QPC. The diagonal resistance in this case has the resistance of the underlying edge, and if $\nu = 5/2$ is the tunneling edge then the value of saturation R_D should be 3/7 h/e^2 (the underlying edge is $\nu = 7/3$).

In Fig. 4-9a we present dc bias dependence data from device 2 taken at several temperatures. The channel-like geometry of device 2 increases the likelihood of tunneling, at multiple sites which could be similar to strong tunneling. Comparing these data to those from the simple QPC device (Fig. 4-5), it is clear that qualitative differences are present at lower temperatures, while at higher temperatures the data

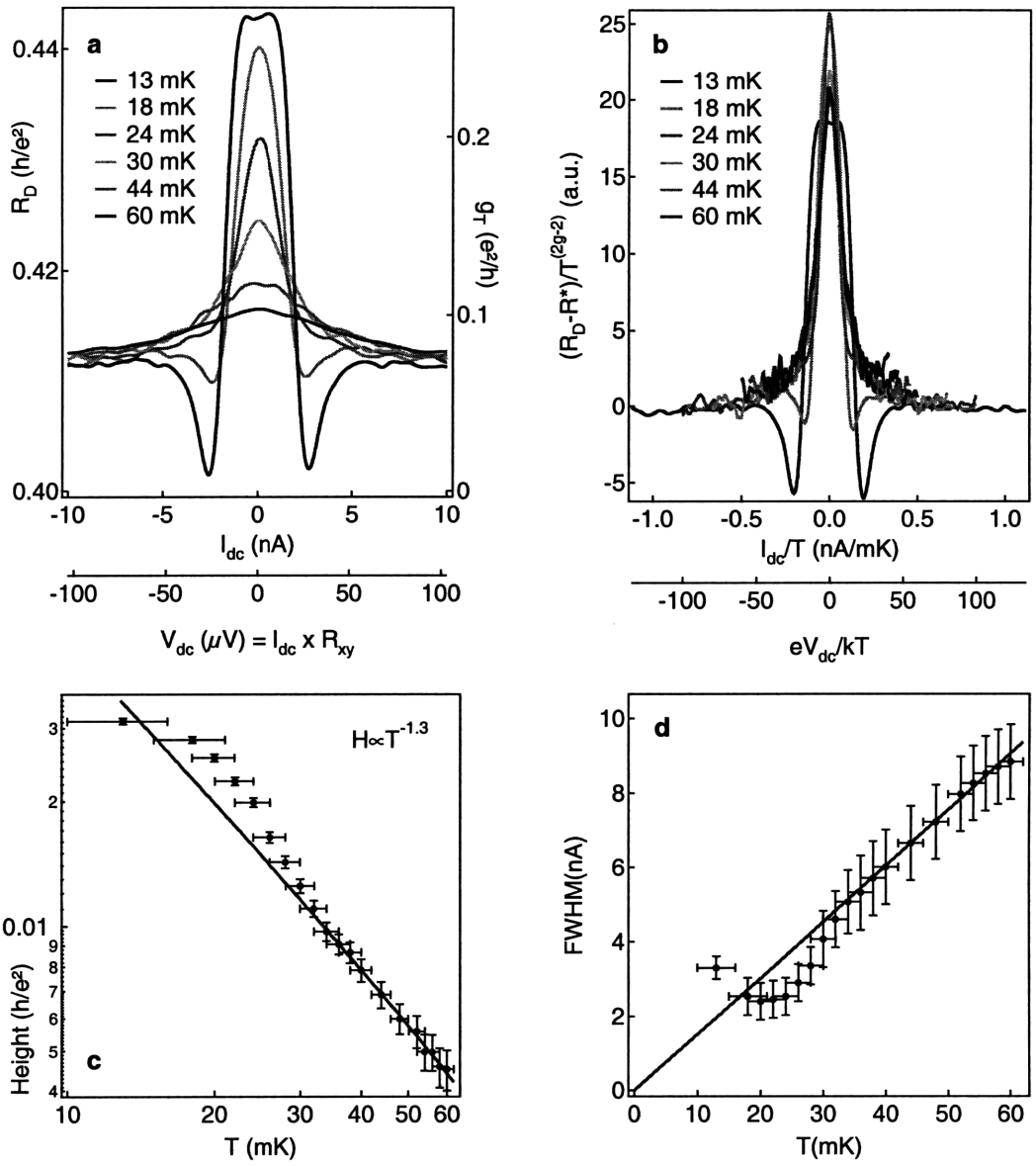

Figure 4-9: (a) R_D (device 2) as a function of dc bias at fixed magnetic field (B=4.31 T, middle of the $\nu = 5/2$ plateau) and fixed gate voltage (V_g= -2.4 V) at several temperatures. R_{xy} is independent of dc bias over this range of I_{dc} (not shown). At the lowest temperature, the peak develops a flat top at a value of resistance consistent with the resistance at $\nu = 7/3$. (b) Data collapsed using a power of -1.3. The data above ~30 mK collapses onto a single curve, while data at lower temperatures does not. (c) Zero-bias peak height as a function of temperature. The red line is the best fit with a power law with an exponent of -1.3. The peak height deviates from this power law below ~30 mK and saturates at the lowest temperatures. (d) The peak full width at half maximum (FWHM) as a function of temperature. The red line is best fit with a line going through zero. Note that below ~30 mK the peak width no longer follows this line.

from the two devices are similar. Specifically, the higher temperature peak heights measured from the common background at high dc bias R^{∞} (see Fig. 4-9c) follow a power law with the the exponent of -1.3, the same as for the weak tunneling data. The higher temperature FWHM increases with increasing temperature and follows a line that can be extrapolated to zero at zero temperature (see Fig. 4-9d). At lower temperatures, the peak height deviates from the power law and saturates at the lowest temperatures. The saturation value of R_D is consistent with the resistance at $\nu = 7/3$. (The actual resistance is higher than 3/7 h/e^2, although the value is the same as R^{∞} with the magnetic field above the $\nu = 7/3$ plateau). Also, at the lowest temperatures, the FWHM deviates from the line and even starts increasing with decreasing temperature. Finally, qualitative differences appear in R_D as a function of I_{dc} at low temperatures: the peak develops a flat top and strong side-dips at ~2.5 nA (Fig. 4-9a).

This behavior can be attributed to strong tunneling where the edges associated with the top fractional state ($\nu = 5/2$ in our case) are scattered almost entirely, and the tunneling of quasiparticles takes place in the direction along rather than across the QPC (see Chapter 2). When measuring the resistance in this case, one finds a value consistent with the underlying edge state ($\nu = 7/3$ if 5/2 is the top state). The strong side dips, much stronger than what the weak tunneling formula of Eq. 4.3 can produce, are probably created by the transition from tunneling along the QPC, with very little of the 5/2 edge state going through, to a state where the 5/2 edge state is virtually undeflected (around 2.5 nA) and then to the regime where tunneling across the QPC takes over again at higher dc bias.

As expected, when attempting to collapse the data from various temperatures onto a single curve (see Fig. 4-9b) we again encounter two situations: the higher temperature data can be collapsed, while those at lower temperatures (below ~30 mK) cannot be collapsed. To collapse the data we scale the left axis by $T^{-1.3}$ and the bottom axis by T.

Since the higher temperature data are similar to the weak tunneling data presented in Fig. 4-5, we can fit these data with the functional form given by weak tunneling

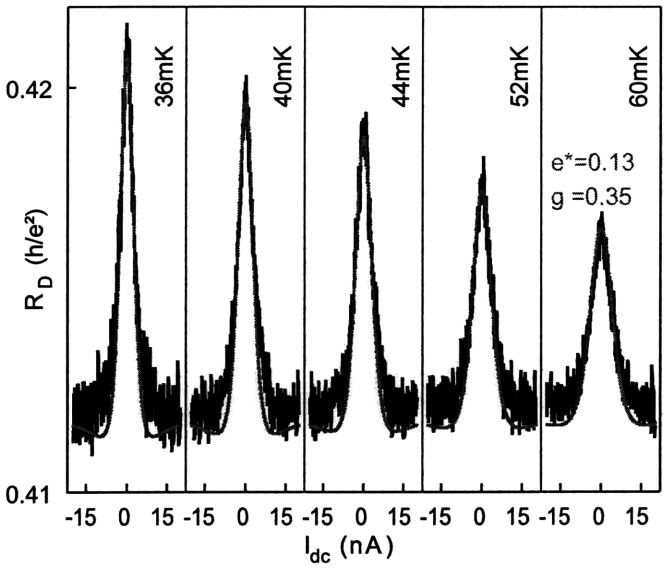

Figure 4-10: Best fit of all the data in 4-9**a** with the weak tunneling formula returns $e^* = 0.13$ and $g = 0.35$.

theory (Eq. 4.2). The best fit, shown in Fig. 4-10, returns values of of $e^* = 0.13$ and $g = 0.35$, consistent with the results from the weak tunneling data.

4.8 Conclusions

In this chapter, we have studied quasiparticle tunneling between edge states in a constriction at $\nu = 5/2$. By annealing the QPC at 4K and making the constriction short we have obtained the conditions for weak tunneling. We find quantitative agreement with theory for the temperature and current dependence of the zero-bias tunneling peak. We have estimated a quasiparticle charge e^* of 0.18, lower, but within error, than the predicted $e^* = 1/4$, and an interaction parameter g of 0.35. If we impose a charge of $e^* = 0.25$, then $g = 0.47$. Based on pairs (e^*, g), we have found that our data are most consistent with two proposed wavefunctions, the anti-Pfaffian [51, 52] and the $U(1) \times SU_2(2)$ [92], which happen to be both non-abelian. These two wavefunctions have both $e^* = 1/4$ and $g = 1/2$. However, we cannot exclude the abelian state 331 [34, 35] with $e^* = 1/4$ and $g = 3/8$. Our data are inconsistent with the leading candidate for describing the 5/2 state, the Pfaffian [60,

96]. The experiment presented here is the first realization of quasiparticle (rather than electron) tunneling between edge states and sets the foundation for quasiparticle braiding experiments which are required for topological quantum computing.

Chapter 5

Estimating Electron Temperature

For all the experiments described in this thesis, the electron temperature is a critical parameter. First, since all the states studied here are very fragile, the electron temperature needs to be very low so that the states can form. Second, a low base temperature allows the study of these states over a wider temperature range such that coefficients that characterize the states can be obtained. Last, the high sensitivity to temperature and the long times needed to acquire data at any fixed temperature, requires a high degree of control of the electron temperature. Low temperatures are obtained by cooling the samples in a dilution refrigerator and the temperature is measured and controlled with a resistor and a heater at the mixing chamber level. The heater current is provided by a PID controller.

Cooling the sample in a dilution refrigerator cools the GaAs crystal but does not guarantee low electron temperature. Attaining low electron temperatures needed in these experiments requires careful thermal anchoring of the electric wiring connecting the sample to the measurement instruments and extensive noise elimination to insure a quiet measurement set-up. Even with extreme care the noise in the measurement increases the effective electron temperature, such that at very low temperatures the electron and mixing chamber temperatures are no longer identical. It then becomes crucial to have a direct measure of the electron temperature. Quantum dots in the Coulomb blockade regime provide an absolute thermometer for electron temperature and can be used to identify when lattice (mixing chamber) and electron temperatures

no longer coincide. However, since part of the electron heating is caused by noise in the measurement set-up falling across the sample, it is expected that electron temperature will depend on sample resistance. Resistances in the Hall effect devices can be orders of magnitude lower than those of Coulomb blockaded dots, hence the electron temperature could be lower in the former for the same experimental setup. In this chapter we explain how electron temperature is measured using quantum dots and how we have used the temperature dependence of the Hall effect itself to estimate the electron temperatures in the Hall effect devices.

This chapter is divided in two sections, the first one covers temperature measurements using single electron quantum dots, while the second one focuses on electron temperature in the Hall regime.

5.1 Coulomb blockade as electron thermometer

Quantum dots are usually small islands in a semiconducting material defined by either electrostatic gating (lateral quantum dots) or by physical etching (either lateral or vertical quantum dots). Their size is typically of the order of a few hundred nm, and contain a few electrons that are not bound to the nuclei. The size of the dots is chosen such that it is comparable to the deBroglie wavelength of the electrons in the dot, allowing them to have quantized energy levels. For comprehensive introductions to the topic see, for example, refs. [42, 43, 28, 47, 48].

Typically, a dot has at least three terminals: a source and a drain which connect the dot to the measurement set-up and a third terminal which provides capacitive gating. The source and the drain provide only very weak coupling between the dot and the outside world via tunneling barriers, such that the number of electrons on the dot is a well defined integer. At discrete values of the electrochemical potential, an electron can be added or removed, and the conductance through the dot has a sharp peak. At other values of the electrochemical potential the conductance is small; therefore this is sometimes referred to as Coulomb oscillations.

Tunneling can take place only if the number of energy levels in the dot within

the interval between the Fermi energies of the two leads is not zero. There are three significant energy scales, which determine whether this condition is satisfied: the temperature of the electrons (k_BT_e), the energy level separation in the dot (ΔE) and the Coulomb charging energy (E_C). The charging energy is the energy needed to add to or remove one electron from the dot. This charging energy is analogous to the ionization energy from atomic physics.

In the limit of zero dc bias, depending on the interplay of these three energy scales, several regimes in transport can be identified:

1. If $E_C \ll k_BT_e$ then individual charging peaks cannot be observed. In this high temperature regime, the conductance is limited by the series resistance of the two tunneling barriers.

2. If $\Delta E \ll k_BT_e < E_C$ individual charge states can be identified, but several energy levels participate in the transport through the dot for each charge state. This is the Coulomb blockade observed in metallic quantum dots. In this regime the conductance has been shown to depend on temperature as [6]:

$$G = G_0 \cosh^{-2}\left(\frac{\varepsilon}{2.5k_BT_e}\right), \tag{5.1}$$

   where ε is the deviation of the electrochemical potential from the center of the Coulomb blockade peak.

3. If $k_BT_e \ll \Delta E < E_C$ only one energy level participates in transport. This is the quantum Coulomb blockade regime, and it is the one we use for measuring electron temperature. In this regime the conductance varies with temperature as [6]:

$$G = G_0 \frac{\Delta E}{4k_BT_e} \cosh^{-2}\left(\frac{\varepsilon}{2k_BT_e}\right) \tag{5.2}$$

In Eqs. 5.1 and 5.2 we have assumed that the quantum broadening of the energy levels, caused by tunneling to the leads is significantly smaller than the temperature broadening. In the opposite limit, when quantum fluctuations in the number of electrons on the dot is dominant, the conductance is given by the Breit-Wigner formula

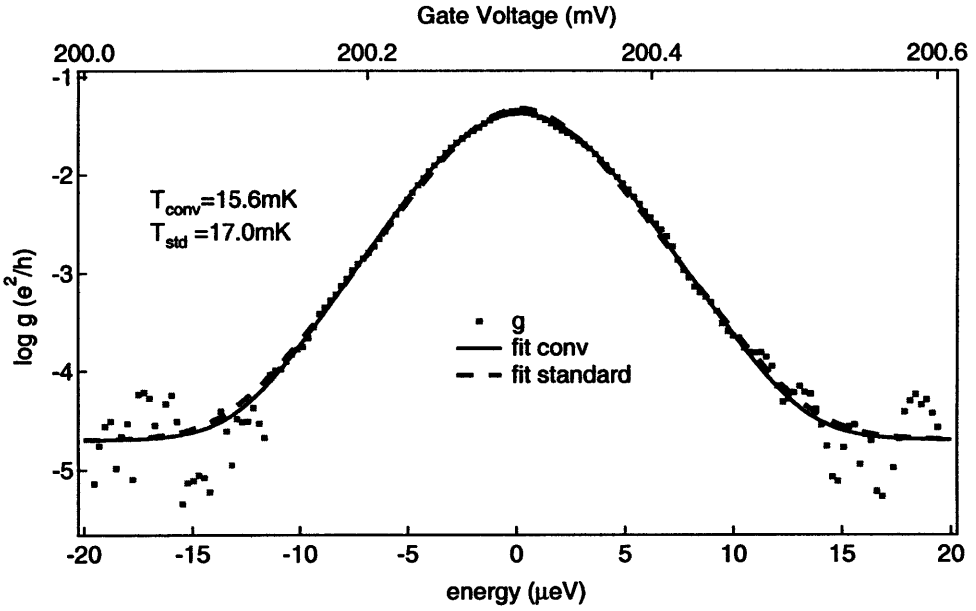

Figure 5-1: Coulomb blockade peak. Conductance (red squares) as a function of gate voltage (top scale) or energy (bottom scale) from the center of the peak for the first electron in a single-electron dot. The data has been fitted with formula 5.2 (green dashed line) giving an electron temperature of 17 mK when at base temperature. Fit of the data with a convolution of formula 5.2 and a Gaussian is also shown as blue solid line. This last method returns an electron temperature of 15.6 mK

[81] (in the limit $T = 0$):

$$G = \frac{2e^2}{h} \frac{(h\Gamma)^2}{(h\Gamma)^2 + (\varepsilon)^2} \tag{5.3}$$

This lineshape is called a Lorentzian.

Noise in the measurement system adds to the broadening of the Coulomb peaks. To account for this, we also attempt to fit the data with Eq. 5.2 convoluted with a Gaussian. Thermal noise is generated by the thermal agitation of the electrons in a resistor in the absence of an applied voltage. Its distribution follows a normal distribution and its signal amplitude has the shape of a Gaussian (bell curve):

$$G = \frac{1}{\sigma\sqrt{2\pi}} exp\left(-\frac{(x-a)^2}{2\sigma^2}\right) \tag{5.4}$$

When fitting data to extract electron temperature we present both versions: the simple fit with formula 5.2 as well the fit the convolution mentioned above.

The actual devices we have used to estimate electron temperature are lateral

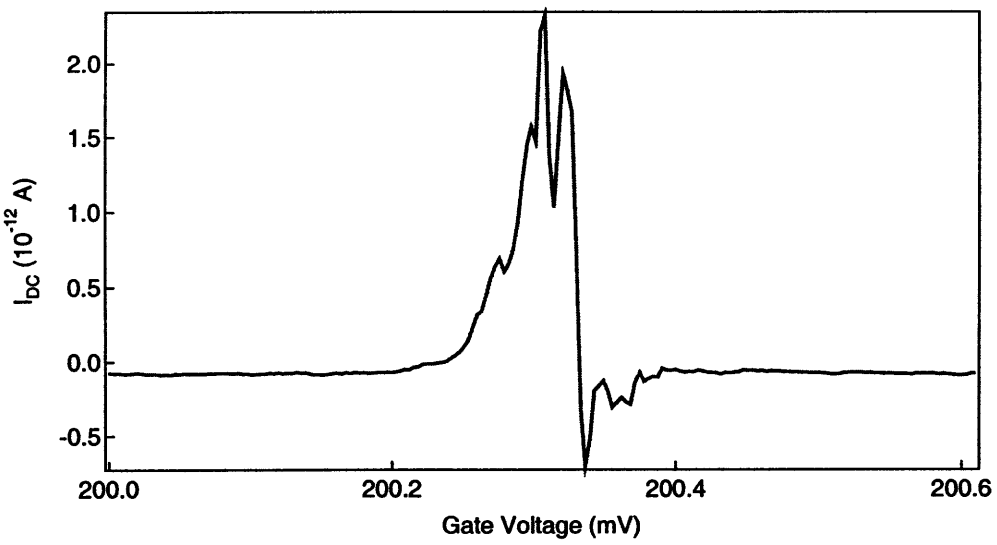

Figure 5-2: Dc current data acquired simultaneously with the data in Fig. 5-1. The current through the dot is mostly zero except in the vicinity of the peak and changes sign at the peak. This confirms that a negligible bias was applied to the device during the measurement.

quantum dots patterned on a GaAs/AlGaAs 2DEG. They have been fabricated by Ghislain Granger with a gate geometry that allows the dots to be completely emptied. Images and fabrication details can be found in Ref. [31]. To perform measurements, we apply a small ac voltage bias to the source and drain leads and measure differential conductance using a lock-in amplifier. Simultaneously, we acquire the dc current through the dot. For temperature measurements, these devices have been tuned to a regime where only one electron is present on the dot, and the tunneling rate is low enough that the quantum broadening is lower then the temperature broadening of the energy levels in the dot. To verify this, the line-shape of the Coulomb blockade peaks has been fit with both a Lorentzian and Eq. 5.2. If Eq. 5.2 does not fit better than the Lorentzian the gate voltages defining the dot are retunned to make the tunneling barriers become more opaque. Measurements are performed with an ac excitation that is smaller than k_BT and zero dc bias applied to the dot, while scanning the voltage on one of the gates controlling the size of the dot. An example of such a gate voltage scan is shown in Fig. 5-1. To insure that indeed there is no spurious dc

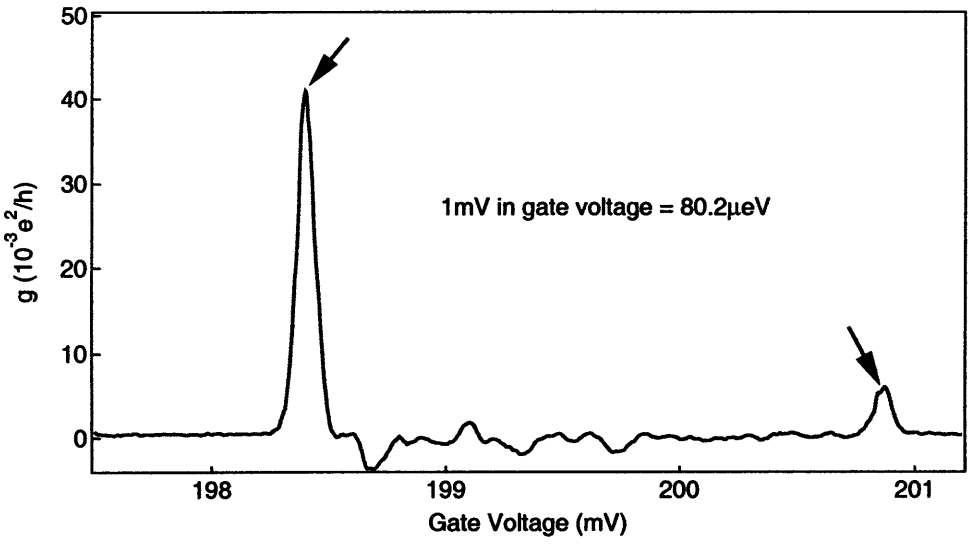

Figure 5-3: Example of conversion of gate voltage into energy. A dc bias of 0.2 mV is applied to the dot, resulting in a peak splitting of approximately 2.5 mV in gate voltage. We use this to convert gate voltage scans to energy. The position of the two peaks is marked by arrows.

bias[1] applied on the dot, the current through the dot is monitored simultaneously. A sample trace demonstrating zero dc bias is shown in Fig. 5-2. The current is zero everywhere except near the peak, positive on one side of the peak and negative on the other, going through zero at the peak.

To compare the data with the models, one has to convert gate voltage to energy using the capacitive coupling of the dot to the gates and leads. To perform this conversion, we apply a small dc bias (larger than the ac excitation) and sweep the gate voltage. The peak splits into two peaks separated by a gate voltage that corresponds to the applied dc bias, giving the capacitance ratio. This allows us to convert the change in gate voltage to a change in energy. We then fit the data with the above the two methods discussed above.

Using this approach, we have found that for temperatures higher than 21 mK, the mixing chamber and electron temperatures are equal within the error of the measurement. For temperatures below 21 mK, the electron temperature is higher than the mixing chamber temperature as electrons are cooled less efficiently than the

[1]The spurious dc bias has two sources: rectification of the ac excitation used to measure and small voltages that result from thermoelectric effects.

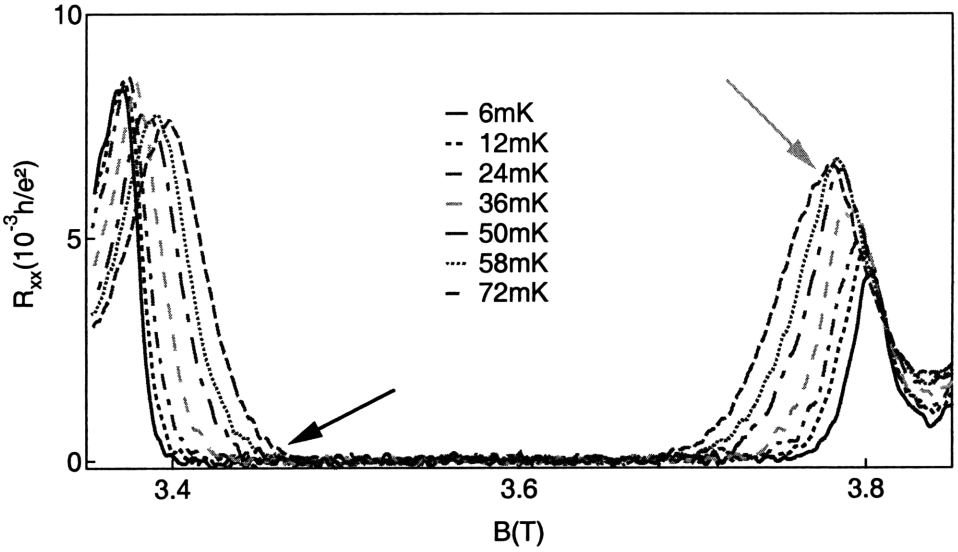

Figure 5-4: R_{xx} in the bulk of the sample as a function of magnetic field around the $\nu = 3$ plateau at several mixing chamber temperatures. The arrows mark the features used for estimating the electron temperature: the black arrow marks the low field edge of the $\nu = 3$ gap, while the yellow arrow marks the R_{xx} peak on the high field side of $\nu = 3$.

lattice and the noise at the sample level is not negligible. For these temperatures, we have performed the two fits explained above. At base mixing chamber temperature (less then 10 mK) we have consistently found the electron temperature (T_e) to be 17 mK using formula 5.2. Using the convolution method we found lower temperatures of approximately 16 mK. (See Fig. 5-1.)

5.2 Estimating temperature using the Hall effect

One of the major sources of electron heating is noise in the measurement circuit. The fraction of noise, and hence the amount of heating, at the sample is proportional to the ratio of the sample resistance to the overall resistance of the circuit. For a less resistive sample (if the resistance of the measurement leads is constant), a smaller fraction of the noise will fall across the sample. Samples in the quantum Hall effect at the filling numbers investigated in this thesis have a resistance lower than 25 kΩ, which is much smaller then the resistance of a quantum dot in the Coulomb blockade regime presented above. One would expect then that the electron temperature is

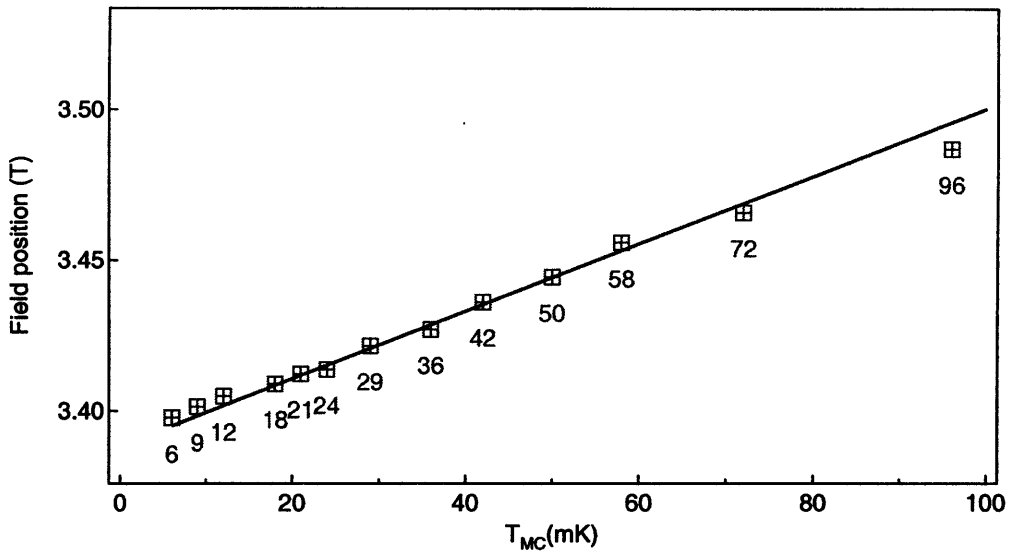

Figure 5-5: Dependence of the $\nu = 3$ gap low field corner position in R_{xx} on the mixing chamber temperature. The linear fit (solid line) was performed over a restricted range in temperature and extended to lower temperature where the data deviates from the line. This is used to estimate electron temperature below 20 mK.

lower in the Hall effect samples. We know of no absolute thermometers in the Hall effect, but since we can safely assume that the Coulomb blockade thermometer gives an upper bound on the temperature, we can develop an empirical extrapolation of the electron temperature for the Hall samples. To do so, we track several features that are present in the R_{xx} data around $\nu = 3$ in the bulk of the sample (Fig. 5-4). This most likely places a lower bound on the electron temperature, since the resistance in the bulk is smaller than in the quantum point contacts used for our measurements.

We have tracked two features of different nature in the bulk longitudinal resistance (R_{xx}): the position in magnetic field where R_{xx} becomes nonzero on the low field side of $\nu = 3$ plateau (marked with black arrow in Fig. 5-4) and the height (local maximum resistance) of the peak on the high field side of the plateau (yellow arrow in Fig. 5-4). To establish the position of the first feature we have chosen for each temperature the value of field where the resistance exceeds 5×10^{-4} h/e^2. This value of resistance is well above the noise of the measurement and allows for consistent identification of the feature. In Fig. 5-5 we show the plot of field position as a function of mixing chamber temperature (T_{MC}). The data is linear from 21 mK to 72 mK, and since we

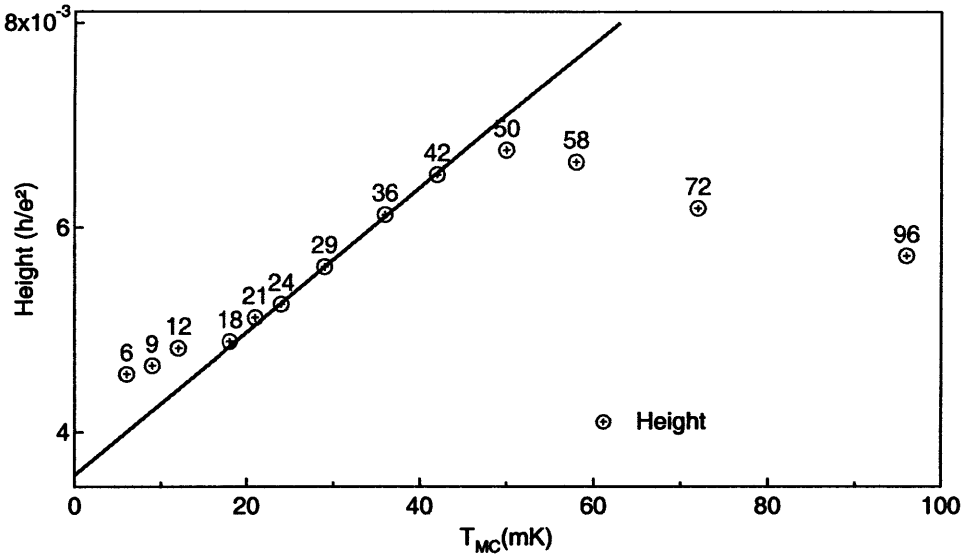

Figure 5-6: The dependence of the R_{xx} peak height on mixing chamber temperature. The linear fit (solid line) is performed over a restricted range in temperature and extended to lower temperature where the data deviates from the line. This is used to estimate electron temperature below 20 mK.

know from the Coulomb blockade measurements that for temperatures above 21 mK $T_{MC} = T_e$, we fit the data over this range. We use a linear fit and assume that below 21 mK data deviates from the line because the electrons are no longer cooled to the temperature of the mixing chamber. Extrapolating this fit to lower temperatures, we identify empirical electron temperatures below 21 mK. From this we estimate the base electron temperature to be ≈ 9.5 mK. Note that for this feature, the empirical electron temperature below 21 mK follows the mixing chamber temperature quite accurately.

The temperature dependence of the value of resistance at the peak on the high field side of $\nu = 3$ is presented in Fig. 5-6 as a function of mixing chamber temperature. The data have a linear dependence in the range 18 mK to 42 mK but deviates from linearity for temperatures below 18 mK and above 50 mK. Below 18 mK, the data deviates from linearity probably because the electrons can no longer be cooled as much as the mixing chamber. Above 50 mK, the data deviates from linearity presumably because the next higher field state gets destroyed with increasing temperature. Making the same assumption as above we fit this data range with a line and extend the fit below

18 mK. Using this method, the base electron temperature is estimated to be $\approx$ 13 mK, higher than the first empirical estimate. This is expected since the resistance for this feature is higher than the resistance of the first feature. However, the estimated base electron temperature is still lower than that obtained from Coulomb blockade measurements. Since this feature's resistance is almost equal to the one in the QPCs, we use the higher temperature in analyzing our QPC measurements. The error bars for temperature measurements encompass the results from all three methods at low temperature ($\leq$ 21 mK). At higher temperature, the error bars arise from fitting errors in the method using a lateral quantum dot as a thermometer.

5.3 Conclusion

The electron temperature can be measured using electron tunneling in a quantum dot, however the actual electron temperature can vary with the device resistance. For this reason we have not only measured electron temperature in a dot but also estimated temperature in Hall effect devices. The electron temperature above 21-22 mK follows mixing chamber temperature. For temperatures below 21 mK, when analyzing data, we have used the estimates obtained by extrapolating the temperature dependence of a peak in R_{xx} on the high field side of $\nu = 3$. With these estimates, the base electron temperature in the Hall effect devices around $nu = 5/2$ is 13 mK.

Appendix A

Fabrication of lateral quantum dots on GaAs

Over the course of my PhD I had the opportunity to use several cleanrooms, both here at MIT and at University of Washington in Seattle. I have learned most of my cleanroom skill from Yael Hanein, dear friend and mentor, who's support and confidence that I will succeed has brought me to MIT. My first experiences "fabbing" were in Si, making carbon nanotube devices. However this appendix covers only my experience at MIT, working in tandem with Dominik Zumbuhl, fabricating lateral quantum dots in GaAs. These devices have been used by my labmates Sami Amasha and Kenny Maclean for their real time measurements of electron tunneling [2, 1, 54]

These are dots where the last electron can be emptied, with quantum point contacts (QPCs) nearby. The purpose of these QPCs is to be used as listeners for observing in real time electrons tunneling in and out of the dot. Since the coupling of the listeners to the dot is capacitive, the main challenge for these dots was to decrease the width of the small metallic gates defining the dot to insure that the QPCs are very close to where the electrons are tunneling. To achieve this we have used a recipe where the developer used for the small gates is chilled on ice prior to using. We have done the work for these dots using the Raith e-beam writer at SEBL (Scanning Electron Beam Lithography Facility) and the EML (Exploratory Materials Laboratory) cleanroom which is part of MTL (Microsystems Technology Laboratory).

Three of the fabrication steps require metal lift-off. Traditionally, to achieve this it is recommended to use optical lithography with a negative resist or a positive resist and do "image reversal". Image reversal resists are usually very sensitive to environmental conditions. For this reason, in addition of the image reversal process, we have developed a recipe for the e-beam writer. Since we use it for lifting off a thick metal stack, we have developed a recipe where a stack of PMMA of different molecular weights is used. The lower molecular weight is placed at the bottom of the stack to create an undercut.

A.1 Mesa Isolation

The purpose of this step is to define and separate active regions in the heterostructure. We use baked resist as masking material for wet etching. The resist for this can be the standard cleanroom positive resist. For the actual samples, I have used AZ 5214E.

1. Sample cleaning: use Acetone, Methanol, and Isopropanol. Blow-dry with nitrogen. Short bake on hot plate to get rid of water.

2. Coat positive resist using standard clean room recipe (AZ5214 40s, 4000rpm), followed by pre-exposure bake (90°C, 30min.).

3. Expose the sample with appropriate mask (30-40s Hi-Res mask aligner).

4. Develop (2-4min).

5. Post-exposure bake to harden the resist somewhat (130°C, 15-20min). This is needed in order to use it as masking material for the subsequent etching step.

6. Wet etch: use mild Piranha (1:8:1000 Sulfuric Acid: Hydrogen Peroxide: Water for approx. 7 min giving 80nm depth). Rinse in water to remove the remnants of the etch solution.

7. Remove masking resist using Acetone followed by Methanol and Isopropanol. One should be very careful to remove all resist from this step as any residue will compromise the ohmic contacts and hence the sample.

8. Short ashing step performed to insure the removal of the resist.

A.2 Ohmic Contacts

The purpose of this step is to provide Ohmic contacts to the active regions defined in the first layer. I have developed two recipes for this step: a standard processing step using image reversal lithography followed by metal deposition and lift-off and a second recipe using the Raith e-beam writer with a stack of PMMA followed by metal deposition and lift-off. The features thus patterned were annealed to insure Ohmic contact to the active layer of the heterostructure.

A.2.1 Traditional Recipe

1. Sample cleaning: use Acetone, Methanol, and Isopropanol. Blow-dry with nitrogen. Bake on hot plate (130°C, 3 min).
2. Coat AZ5214E to be used as image reversal resist (40s at 4000rpm) using standard clean room recipe, followed by pre-exposure bake (90°C, 30min.).
3. Exposure with mask (10s).
4. Post-exposure bake (90°C, 30min.).
5. Flood exposure without mask (1min).
6. Develop (1min).
7. Evaluate under microscope. If needed develop more.
8. Short ashing step (1-2min).
9. Quick dip in a mix of ammonium hydroxide/water 1:3 for 3min to remove the oxide. This insures good adhesion of the metal stack and low contact resistance for the ohmics.
10. Metal deposition: Ni/Ge/Au stack (5/35/75nm).

11. Lift-off using Acetone followed by Methanol and Isopropanol.

12. Short ashing step.

13. Diffusion of the Ge in heterostructure. For this step I have used the Ashoori annealer with the following recipe: ramp to 200°C in 5min, hold for 0.5min, ramp to 415°C in 22s, ramp to 435°C in 12s, hold for 30s, then let cool with forming gas flowing.

A.2.2 E-beam writer recipe

1. Sample cleaning: use Acetone, Methanol, and Isopropanol. Blow-dry with nitrogen.

2. Bake chips for 2min at 180°C to remove water. PMMA doesn't like water very much.

3. Coat 2 layers of PMMA of different molecular weight (PMMA 495K C5 spun at 5000rpm, followed by hot plate bake at 180°C for 2min and PMMA 950K C3 spun at 3000rpm). This stack is approx. 600-700 nm thick.

4. Pre-exposure bake on a hotplate. (180°C, 2min.)

5. Expose using the pattern designed using the Raith (5kV, 120μm aperture, 200μm write field, step size 0.5, area dose 30μC/cm^2)

6. Develop (90s).

7. Evaluate under microscope. If needed develop more.

8. Short ashing step (60s).

9. Quick dip in a mix of hydrogen peroxide/ammonium hydroxide/water (2s)to remove the oxide. This insures good adhesion of the metal stack and low contact resistance for the ohmics. Although this is a water based step, I have found that it does not alter significantly the properties of the PMMA since the features

written in this step are fairly big. However this step is crucial to insure low contact resistance.

10. Metal deposition: Ni/Ge/Au stack (5/35/75nm).

11. Lift-off using Acetone followed by Methanol and Isopropanol.

12. Short ashing step (5min).

13. Diffusion of the Ge in heterostructure. For this step I have used the Ashoori annealer with the following recipe: ramp to 200°C in 5min, hold for 0.5min, ramp to 415°C in 22s, ramp to 435°C in 12s, hold for 30s, then let cool with forming gas flowing.

A.3 Small Gates

The purpose of this step is to provide small metallic gates, which will be used to deplete the carriers underneath define the quantum dots. I have used e-beam patterning followed by metal deposition and lift-off.

1. Sample cleaning: use Acetone, Methanol, and Isopropanol. Blow-dry with nitrogen.

2. Bake chips for 2min at 180°C to remove water. PMMA doesn't like water very much and for this step the quality of the resist is crucial for obtaining very small features.

3. Coat PMMA (950K A2 400rpm, 45s, double layer with 2min bake in between) to be used as resist for e-beam lithography patterning.

4. Pre-exposure bake on a hotplate (2min at 180°C).

5. The actual patterning was done in SEBL using clean-room compatible sample holders and tweezers (30kV, 120μm aperture, 100μm write field, step size area 6nm, area dose 250μC/cm^2, step size line 6nm, line dose 700pC/cm^2).

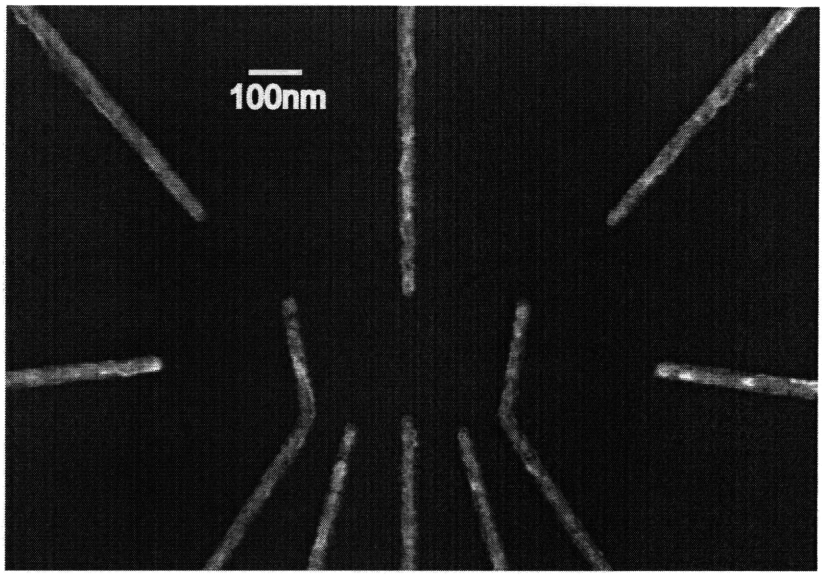

Figure A-1: Scanning electron micrograph of the small gates of a typical dot device fabricated using the present recipe. Scale bar is 100nm.

6. Develop using PMMA developer (MIBK:IPA 1:3) which has been chilled on ice for approx. 1 hour. Chilling the developer increases its selectivity so the lines written in this step will be narrower after developing in this manner (90s).

7. Metal deposition: Ti/Au 4/13nm.

8. Lift-off using Acetone followed by Methanol and Isopropanol.

9. Short ashing step.

An example of very small gates is presented in Fig. A-1

A.4 Large Gates

The purpose of this step is to provide large structure which one can bond to and at the same time connect with the small scale e-beam lithography features patterned in the previous step. Just like in the case of the Ohmic contacts, I have developed two recipes: a traditional one using optical lithography and image reversal and a second one using e-beam lithography. One important aspect to mind in this layer is the thickness of the metal stack. It has to be thicker than the height of the mesa.

A.4.1 Traditional Recipe

1. Sample cleaning: use Acetone, Methanol, and Isopropanol. Blow-dry with nitrogen. Bake on hot plate (130°C, 3 min).

2. Coat AZ5214E to be used as image reversal resist (40s at 4000rpm) using standard clean room recipe, followed by pre-exposure bake (90°C, 30min.).

3. Exposure with mask (10s).

4. Post-exposure bake (90°C, 30min.).

5. Flood exposure without mask (1min).

6. Develop (1min).

7. Evaluate under microscope. If needed develop more.

8. Short ashing step (1-2min).

9. Metal deposition: Ti/Au stack (40/80nm).

10. Lift-off using Acetone followed by Methanol and Isopropanol.

A.4.2 E-beam writer recipe

1. Sample cleaning: use Acetone, Methanol, and Isopropanol. Blow-dry with nitrogen.

2. Bake chips for 2min at 180°C to remove water. PMMA doesn't like water very much.

3. Coat 2 layers of PMMA of different molecular weight (PMMA 495K C5 spun at 5000rpm, followed by hot plate bake at 180°C for 2min and PMMA 950K C3 spun at 3000rpm). This stack is approx. 600-700 nm thick.

4. Pre-exposure bake on a hotplate. (180°C, 2min.)

5. Expose using the pattern designed using the Raith. (5kV, 120μm aperture, 200μm write field, step size 0.5, area dose 30μC/cm^2)

6. Develop (90s).

7. Evaluate under microscope. If needed develop more.

8. Short ashing step (60s).

9. Metal deposition: Ti/Au stack (40/80nm).

10. Lift-off using Acetone followed by Methanol and Isopropanol.

Done!

After this, one has to cleave the individual samples off the die (you can do this by hand, and this is how I did it, or you can you a diesaw). After diceing, we have mounted the samples on our chip carriers and bonded with Au wire.

Bibliography

[1] S. Amasha, K. MacLean, Iuliana P. Radu, D. M. Zumbühl, M. A. Kastner, M. P. Hanson, and A. C. Gossard. Electrical control of spin relaxation in a quantum dot. *Physical Review Letters*, 100(4):046803, 2008.

[2] S. Amasha, K. MacLean, Iuliana P. Radu, D. M. Zumbühl, M. A. Kastner, M. P. Hanson, and A. C. Gossard. Spin-dependent tunneling of single electrons into an empty quantum dot. *Physical Review B (Condensed Matter and Materials Physics)*, 78(4):041306, 2008.

[3] P. W. Anderson. More is different. *Science*, 177(4047):393–396, 1972.

[4] O. G. Balev, Sanderson Silva, and Nelson Studart. Many-body interactions in a quantum wire in the integer quantum Hall regime: Suppression of the exchange-enhanced g factor. *Physical Review B (Condensed Matter and Materials Physics)*, 72(8):085345, 2005.

[5] O. G. Balev and P. Vasilopoulos. Correlations, inhomogeneous screening, and suppression of spin splitting in quantum wires at strong magnetic fields. *Phys. Rev. B*, 56(11):6748–6757, Sep 1997.

[6] C. W. J. Beenakker. Theory of Coulomb-blockade oscillations in the conductance of a quantum dot. *Phys. Rev. B*, 44(4):1646–1656, Jul 1991.

[7] C. W. J. Beenakker and H. van Houten. Quantum transport in semiconductor nanostructures. *Solid State Physics*, 44:1, 1991.

[8] K.-F. Berggren, G. Roos, and H. van Houten. Characterization of very narrow quasi-one-dimensional quantum channels. *Phys. Rev. B*, 37(17):10118–10124, Jun 1988.

[9] K. F. Berggren, T. J. Thornton, D. J. Newson, and M. Pepper. Magnetic depopulation of 1D subbands in a narrow 2D electron gas in a GaAs:AlGaAs heterojunction. *Phys. Rev. Lett.*, 57(14):1769–1772, Oct 1986.

[10] Waheb Bishara and Chetan Nayak. Edge states and interferometers in the Pfaffian and anti-Pfaffian states of the ν =5/2 quantum Hall system. *Physical Review B (Condensed Matter and Materials Physics)*, 77(16):165302, 2008.

[11] Parsa Bonderson, Alexei Kitaev, and Kirill Shtengel. Detecting non-abelian statistics in the $\nu = 5/2$ fractional quantum Hall state. *Phys. Rev. Lett.*, 96(1):016803, 2006.

[12] M. Büttiker. Four-terminal phase-coherent conductance. *Phys. Rev. Lett.*, 57(14):1761–1764, Oct 1986.

[13] M. Büttiker. Quantized transmission of a saddle-point constriction. *Phys. Rev. B*, 41(11):7906–7909, Apr 1990.

[14] F. E. Camino, Wei Zhou, and V. J. Goldman. Realization of a Laughlin quasiparticle interferometer: Observation of fractional statistics. *Physical Review B (Condensed Matter and Materials Physics)*, 72(7):075342, 2005.

[15] F. E. Camino, Wei Zhou, and V. J. Goldman. e/3 Laughlin quasiparticle primary-filling $\nu = 1/3$ interferometer. *Phys. Rev. Lett.*, 98(7):076805, 2007.

[16] T. Chakraborty and P. Pietilainen, editors. *The Quantum Hall Effects*. Springer Verlag, 1995.

[17] D. B. Chklovskii, K. A. Matveev, and B. I. Shklovskii. Ballistic conductance of interacting electrons in the quantum Hall regime. *Phys. Rev. B*, 47(19):12605–12617, May 1993.

[18] S. Das Sarma, M. Freedman, and C. Nayak. Topologically protected qubits from a possible non-abelian fractional quantum Hall state. *Phys. Rev. Lett.*, 94(16):166802, 2005.

[19] R. de Picciotto, M. Reznikov, M. Heiblum, V. Umansky, G. Bunin, and D. Mahalu. Direct observation of a fractional charge. *Nature*, 389:162, 1997.

[20] O. E. Dial, R. C. Ashoori, L. N. Pfeiffer, and K. W. West. High-resolution spectroscopy of two-dimensional electron systems. *Nature*, 448:176, 2007.

[21] M. Dolev, M. Heiblum, V. Umansky, A. Stern, and D. Mahalu. Observation of a quarter of an electron charge at the $\nu = 5/2$ quantum Hall state. *Nature*, 452, 2008.

[22] J. P. Eisenstein, R. Willett, H. L. Stormer, D. C. Tsui, A. C. Gossard, and J. H. English. Collapse of the even-denominator fractional quantum Hall effect in tilted fields. *Phys. Rev. Lett.*, 61(8):997, Aug 1988.

[23] F. F. Fang and P. J. Stiles. Effects of a tilted magnetic field on a two-dimensional electron gas. *Phys. Rev.*, 174(3):823–828, Oct 1968.

[24] D. E. Feldman and A. Kitaev. Detecting non-abelian statistics with an electronic Mach-Zender interferometer. *Phys. Rev. Lett.*, 97:186803, 2006.

[25] P. Fendley, A. W. W. Ludwig, and H. Saleur. Exact nonequilibrium transport through point contacts in quantum wires and fractional quantum Hall devices. *Phys. Rev. B*, 52(12):8934–8950, Sep 1995.

[26] Paul Fendley, Matthew P. A. Fisher, and Chetan Nayak. Dynamical disentanglement across a point contact in a non-abelian quantum Hall state. *Phys. Rev. Lett.*, 97(3):036801, 2006.

[27] H. A. Fertig and B. I. Halperin. Transmission coefficient of an electron through a saddle-point potential in a magnetic field. *Phys. Rev. B*, 36(15):7969–7976, Nov 1987.

[28] E. B. Foxman. *Single Electron Charging and Quantum Effects in Semiconductor Nanostructures.* PhD dissertation, Massachusetts Institute of Technology, Department of Physics, August 1993.

[29] L. I. Glazman and I. A. Larkin. Lateral position control of an electron channel in a slit-gate device. *Semicond. Sci. Technol.*, 6:32–35, 1991.

[30] V. J. Goldman and B. Su. Resonant tunneling in the quantum Hall regime: Measurement of fractional charge. *Science*, 267:076805, 1995.

[31] Ghislain Granger. *Spin effects in Single Electron Transistors.* PhD dissertation, Massachusetts Institute of Technology, 2005.

[32] F. D. M. Haldane and E. H. Rezayi. Spin-singlet wave function for the half-integral quantum Hall effect. *Phys. Rev. Lett.*, 60(10):956–959, Mar 1988.

[33] B. I. Halperin. Quantized Hall conductance, current-carrying edge states, and the existence of extended states in a two-dimensional disordered potential. *Phys. Rev. B*, 25(4):2185–2190, Feb 1982.

[34] B. I. Halperin. Theory of the quantized Hall conductance. *Helvetica Physica Acta*, 56(1-3):75–102, 1983.

[35] B. I. Halperin, Patrick A. Lee, and Nicholas Read. Theory of the half-filled Landau level. *Phys. Rev. B*, 47(12):7312–7343, Mar 1993.

[36] Chang-Yu Hou and Claudio Chamon. "Wormhole" geometry for entrapping topologically protected qubits in non-abelian quantum Hall states and probing them with voltage and noise measurements. *Phys. Rev. Lett.*, 97(14):146802, 2006.

[37] S. Ihnatsenka and I. V. Zozoulenko. Spatial spin polarization and suppression of compressible edge channels in the integer quantum Hall regime. *Physical Review B (Condensed Matter and Materials Physics)*, 73(15):155314, 2006.

[38] S. Ihnatsenka and I. V. Zozoulenko. Spin polarization of edge states and the magnetosubband structure in quantum wires. *Physical Review B (Condensed Matter and Materials Physics)*, 73(7):075331, 2006.

[39] S. Ihnatsenka and I. V. Zozoulenko. Magnetoconductance of interacting electrons in quantum wires: Spin density functional theory study. *Physical Review B (Condensed Matter and Materials Physics)*, 78(3):035340, 2008.

[40] J. K. Jain. Composite-fermion approach for the fractional quantum Hall effect. *Phys. Rev. Lett.*, 63(2):199–202, Jul 1989.

[41] J. F. Janak. g factor of the two-dimensional interacting electron gas. *Phys. Rev.*, 178(3):1416–1418, Feb 1969.

[42] M. A. Kastner. The single-electron transistor. *Reviews of Modern Physics*, 64(3):849, 1992.

[43] M. A. Kastner. Artificial atoms. *Physics Today*, 46:24, 1993.

[44] M. A. Kastner, S. B. Field, J. C. Licini, and S. L. Park. Anomalous magnetoresistance of the electron gas in a restricted geometry. *Phys. Rev. Lett.*, 60(24):2535–2538, Jun 1988.

[45] Jari M. Kinaret and Patrick A. Lee. Exchange interaction in a quantum wire in a strong magnetic field. *Phys. Rev. B*, 42(18):11768–11773, Dec 1990.

[46] A. Yu. Kitaev. Fault-tolerant quantum computation by anyons. *Annals Phys.*, 303:3, 2003.

[47] L. Kouwenhoven and C. Marcus. Quantum dots. *Physics World*, 11:35, 1998.

[48] L. P. Kouwenhoven, C. M. Marcus, P. L. McEuen, S. Tarucha, R. M. Westervelt, and N. S. Wingreen. Electron transport in quantum dots. In L. L. Sohn, L. P. Kouwenhoven, and G. Schön, editors, *Mesoscopic Electron Transport*, volume 345 of *NATO ASI Series E*, pages 105–214. Kluwer, Dordrecht, 1997.

[49] R. B. Laughlin. Anomalous quantum Hall effect: An incompressible quantum fluid with fractionally charged excitations. *Phys. Rev. Lett.*, 50(18):1395–1398, May 1983.

[50] D. R. Leadley, R. J. Nicholas, J. J. Harris, and C. T. Foxon. Critical collapse of the exchange-enhanced spin splitting in two-dimensional systems. *Phys. Rev. B*, 58(19):13036–13046, Nov 1998.

[51] Sung-Sik Lee, Shinsei Ryu, Chetan Nayak, and Matthew P. A. Fisher. Particle-hole symmetry and the ν=5/2 quantum Hall state. *Phys. Rev. Lett.*, 99(23):236807, 2007.

[52] Michael Levin, Bertrand I. Halperin, and Bernd Rosenow. Particle-hole symmetry and the Pfaffian state. *Phys. Rev. Lett.*, 99(23):236806, 2007.

[53] D. R. Luhman, W. Pan, D. C. Tsui, L. N. Pfeiffer, K. W. Baldwin, and K. W. West. Observation of a fractional quantum Hall state at $\nu = 1/4$ in a wide GaAs quantum well. arXiv:0810.2274.

[54] K. MacLean, S. Amasha, Iuliana P. Radu, D. M. Zumbühl, M. A. Kastner, M. P. Hanson, and A. C. Gossard. Energy-dependent tunneling in a quantum dot. *Physical Review Letters*, 98(3):036802, 2007.

[55] L. Martin-Moreno, J. T. Nicholls, N. K. Patel, and M. Pepper. Non-lineal conductance of a saddle-point constriction. *J. Phys.: Condens. MAtter*, 4:1323–1333, 1992.

[56] J. B. Miller, Iuliana P. Radu, D. M. Zumbuhl, E. Levenson-Falk, M. A. Kastner, C. M. Marcus, L. N. Pfeiffer, and K. W. West. Fractional quantum Hall effect in a quantum point contact at filling fraction 5/2. *Nature Physics*, 3(6):561 – 565, 2007.

[57] Jeffrey B. Miller. *Electron Transport in GaAs heterostructures at various magnetic field strengths.* PhD dissertation, Harvard University, 2007.

[58] C. P. Milliken, C. P. Umbach, and R. A. Webb. Indications of a Luttinger liquid in the fractional quantum Hall regime. *Solid State Comm.*, 97:309–313, 1995.

[59] M. Milovanović and N. Read. Edge excitations of paired fractional quantum Hall states. *Phys. Rev. B*, 53(20):13559–13582, May 1996.

[60] Gregory Moore and Nicholas Read. Nonabelions in the fractional quantum Hall effect. *Nuclear Phys. B*, 360(2-3):362, 1991.

[61] R. H. Morf. Transition from quantum Hall to compressible states in the second Landau level: New light on the $\nu = 5/2$ enigma. *Phys. Rev. Lett.*, 80(7):1505–1508, Feb 1998.

[62] R. Mottahedeh, M. Pepper, R. Newbury, J. A. A. J. Perenboom, and K. F. Berggren. Absence of valley splitting and quantum interference effects in the quantum Hall regime of a narrow two dimensional electron gas in Si.

[63] Chetan Nayak, Steven H. Simon, Ady Stern, Michael Freedman, and Sankar Das Sarma. Non-abelian anyons and topological quantum computation. *Reviews of Modern Physics*, 80(3):1083, 2008.

[64] Bas Jorn Overbosch. *Edge tunneling and transport in non-abelian fractional quantum Hall systems.* PhD dissertation, MIT, 2008.

[65] I. Pallecchi, Ch. Heyn, J. Lohse, B. Kramer, and W. Hansen. Magnetocapacitance of quantum wires: Effect of confining potential on one-dimensional subbands and suppression of exchange enhanced g factor. *Physical Review B (Condensed Matter and Materials Physics)*, 65(12):125303, 2002.

[66] W. Pan, J.-S. Xia, V. Shvarts, D. E. Adams, H. L. Stormer, D. C. Tsui, L. N. Pfeiffer, K. W. Baldwin, and K. W. West. Exact quantization of the even-denominator fractional quantum Hall state at $\nu = 5/2$ Landau level filling factor. *Phys. Rev. Lett.*, 83(17):3530–3533, Oct 1999.

[67] W. Pan, J. S. Xia, H. L. Stormer, D. C. Tsui, C. Vicente, E. D. Adams, N. S. Sullivan, L. N. Pfeiffer, K. W. Baldwin, and K. W. West. Experimental studies of the fractional quantum Hall effect in the first excited Landau level. *Physical Review B (Condensed Matter and Materials Physics)*, 77(7):075307, 2008.

[68] R. E. Prange and S. M. Girvin, editors. *The Quantum Hall Effect.* Springer Verlag, 1990.

[69] Iuliana P. Radu, J. B. Miller, C. M. Marcus, M. A. Kastner, L. N. Pfeiffer, and K. W. West. Quasi-particle properties from tunneling in the ν=5/2 fractional quantum Hall state. *Science*, 320(5878):899–902, May 2008.

[70] N. Read and Dmitry Green. Paired states of fermions in two dimensions with breaking of parity and time-reversal symmetries and the fractional quantum Hall effect. *Phys. Rev. B*, 61(15):10267–10297, Apr 2000.

[71] E. H. Rezayi and F. D. M. Haldane. Incompressible paired Hall state, stripe order, and the composite fermion liquid phase in half-filled Landau levels. *Phys. Rev. Lett.*, 84(20):4685–4688, May 2000.

[72] Stefano Roddaro, Vittorio Pellegrini, Fabio Beltram, Giorgio Biasiol, and Lucia Sorba. Interedge strong-to-weak scattering evolution at a constriction in the fractional quantum Hall regime. *Phys. Rev. Lett.*, 93(4):046801, Jul 2004.

[73] Stefano Roddaro, Vittorio Pellegrini, Fabio Beltram, Giorgio Biasiol, Lucia Sorba, Roberto Raimondi, and Giovanni Vignale. Nonlinear quasiparticle tunneling between fractional quantum Hall edges. *Phys. Rev. Lett.*, 90(4):046805, Jan 2003.

[74] Stefano Roddaro, Vittorio Pellegrini, Fabio Beltram, Loren N. Pfeiffer, and Ken W. West. Particle-hole symmetric Luttinger liquids in a quantum Hall circuit. *Phys. Rev. Lett.*, 95(15):156804, 2005.

[75] L. Saminadayar, D. C. Glattli, Y. Jin, and B. Etienne. Observation of the $e/3$ fractionally charged Laughlin quasiparticle. *Phys. Rev. Lett.*, 79(13):2526–2529, Sep 1997.

[76] S. Das Sarma and A. Pinczuk, editors. *Perspectives in Quantum Hall Effects: novel quantum liquids in low-dimensional semiconductor structures.* Wiley, 1996.

[77] Yu. V. Sharvin. *Zh. Eksp. Teor. Fiz.*, 48:984–988, Nov 1965.

[78] K. Shepard. Antiscreening and exchange-enhanced spin splitting in quantum wires. *Phys. Rev. B*, 45(23):13431–13437, Jun 1992.

[79] Ady Stern. Anyons and the quantum Hall effect—a pedagogical review. *Annals of Physics*, 323:204–249, 2008.

[80] Ady Stern and Bertrand I. Halperin. Proposed experiments to probe the non-abelian $\nu = 5/2$ quantum Hall state. *Physical Review Letters*, 96(1):016802, 2006.

[81] A. Douglas Stone and P. A. Lee. Effect of inelastic processes on resonant tunneling in one dimension. *Phys. Rev. Lett.*, 54(11):1196–1199, Mar 1985.

[82] Horst L. Stormer. Nobel lecture: The fractional quantum Hall effect. *Rev. Mod. Phys.*, 71(4):875–889, Jul 1999.

[83] Alexander Struck, Siawoosh Mohammadi, Stefan Kettemann, and Bernhard Kramer. Confinement-induced depletion of the enhanced g-factor in quantum wires. *Physical Review B (Condensed Matter and Materials Physics)*, 72(24):245317, 2005.

[84] K. J. Thomas, J. T. Nicholls, N. J. Appleyard, M. Y. Simmons, M. Pepper, D. R. Mace, W. R. Tribe, and D. A. Ritchie. Interaction effects in a one-dimensional constriction. *Physical Review B (Condensed Matter and Materials Physics)*, 58(8):4846–4852, 1998.

[85] K. J. Thomas, J. T. Nicholls, M. Y. Simmons, M. Pepper, D. R. Mace, and D. A. Ritchie. Possible spin polarization in a one-dimensional electron gas. *Phys. Rev. Lett.*, 77(1):135–138, Jul 1996.

[86] K. J. Thomas, M. Y. Simmons, J. T. Nicholls, D. R. Mace, M. Pepper, and D. A. Ritchie. Ballistic transport in one-dimensional constrictions formed in deep two-dimensional electron gases. *Applied Physics Letters*, 67(1):109–111, 1995.

[87] D. C. Tsui, H. L. Stormer, and A. C. Gossard. Two-dimensional magnetotransport in the extreme quantum limit. *Phys. Rev. Lett.*, 48(22):1559–1562, May 1982.

[88] K. v. Klitzing, G. Dorda, and M. Pepper. New method for high-accuracy determination of the fine-structure constant based on quantized Hall resistance. *Physical Review Letters*, 45(6):494–497, 1980.

[89] H. van Houten, C. W. J. Beenakker, P. H. M. van Loosdrecht, T. J. Thornton, H. Ahmed, M. Pepper, C. T. Foxon, and J. J. Harris. Four-terminal magnetoresistance of a two-dimensional electron-gas constriction in the ballistic regime. *Physical Review B (Condensed Matter)*, 37(14):8534–8536, 1988.

[90] B. J. van Wees, H. van Houten, C. W. J. Beenakker, J. G. Williamson, L. P. Kouwenhoven, D. van der Marel, and C. T. Foxon. Quantized conductance of point contacts in a two-dimensional electron gas. *Phys. Rev. Lett.*, 60(9):848–850, Feb 1988.

[91] X. G. Wen. Electrodynamical properties of gapless edge excitations in the fractional quantum Hall states. *Phys. Rev. Lett.*, 64(18):2206–2209, Apr 1990.

[92] X. G. Wen. Non-abelian statistics in the fractional quantum Hall states. *Phys. Rev. Lett.*, 66(6):802–805, Feb 1991.

[93] X.-G. Wen. Topological orders and edge excitations in FQH states. *Advances in Physics*, 44:445, 1995.

[94] X. G. Wen and Q. Niu. Ground-state degeneracy of the fractional quantum Hall states in the presence of a random potential and on high-genus Riemann surfaces. *Phys. Rev. B*, 41(13):9377–9396, May 1990.

[95] Xiao-Gang Wen. Edge transport properties of the fractional quantum Hall states and weak-impurity scattering of a one-dimensional charge-density wave. *Phys. Rev. B*, 44(11):5708–5719, Sep 1991.

[96] Xiao-Gang Wen. Topological order and edge structure of $\nu = 1/2$ quantum Hall state. *Phys. Rev. Lett.*, 70(3):355–358, Jan 1993.

[97] Frank Wilczek. Quantum mechanics of fractional-spin particles. *Phys. Rev. Lett.*, 49(14):957–959, Oct 1982.

[98] R. Willett, J. P. Eisenstein, H. L. Störmer, D. C. Tsui, A. C. Gossard, and J. H. English. Observation of an even-denominator quantum number in the fractional quantum Hall effect. *Phys. Rev. Lett.*, 59(15):1776–1779, Oct 1987.

[99] L. W. Wong, H. W. Jiang, E. Palm, and W. J. Schaff. Termination of the spin-resolved integer quantum Hall effect. *Phys. Rev. B*, 55(12):R7343–R7346, Mar 1997.

[100] J. Wróbel, T. Dietl, K. Regiński, and M. Bugajski. Transport and tunneling within a compressible electron liquid in wires and rings of GaAs/$Al_xGa_{1-x}As$ heterostructures. *Phys. Rev. B*, 58(24):16252–16261, Dec 1998.

[101] J. S. Xia, W. Pan, C. L. Vicente, E. D. Adams, N. S. Sullivan, H. L. Störmer, D. C. Tsui, L. N. Pfeiffer, K. W. Baldwin, and K. W. West. Electron correlation in the second Landau level: A competition between many nearly degenerate quantum phases. *Phys. Rev. Lett.*, 93(17):176809, 2004.

[102] Zhongxi Zhang and P. Vasilopoulos. Screening and electronic correlations in quantum wires in strong magnetic fields: Filling factor dependence. *Phys. Rev. B*, 66(20):205322, Nov 2002.

[103] I. V. Zozoulenko. private comunication.